Nanoparticle Enhanced Solders for High Temperature Reliability

Mokhtari Amirmajdi, Omid-Ahmad

Awarding institution:
King's College London

Nanoparticle Enhanced Solders for High Temperature Reliability

Omid Ahmad Mokhtari Amirmajdi

Doctor of Philosophy

Mechanical Engineering
King's College London

2015

Acknowledgements

I would like to express my sincere gratitude to my supervisor, Prof. Samjid Mannan who has given me the opportunity to pursue this PhD study. His patience, expertise and valuable guidance have been always helpful in my study. Thanks are also given to my second supervisor, Dr. Michael Clode, who was always very helpful.

I am also grateful to my parents for their strong support to finish my PhD.

Thanks are also given to Dr. Hiren R. Kotadia for his guidance has greatly helpful to overcome technical obstacles during my research.

Abstract

This thesis is focused on high temperature electronics and how the reliability of solder can be improved for high temperature applications using nanoparticles. Therefore this thesis first investigates a method of using cross-section polishing (CSP) based on argon ion milling to cross section the sample without damaging it. This research will show that this method is very effective in cross-sectioning the delicate samples and allowing embedded nanoparticles to be detected.

Once this method of detecting nanoparticles is established, the thesis reports on an investigation into nano-composite solders. This part of the thesis will show that passive Silica (SiO_2) nanoparticles can be added to solder to improve room temperature creep resistance of the solder. Compression tests at room temperature and elevated temperature were performed to compare the mechanical characteristics of normal solder and nano-enhanced solder. Compressed samples were cross-sectioned to investigate their microstructure. Results show that while nanoparticles are effective in improving creep resistance of the solder at room temperature, the efficiency of nanoparticles decreases with increasing the temperature.

Finally the thesis reports on attempts to combine solders with highly reactive nanoparticles, focussing on the fundamental property of dissolution of thin aluminium layers in solder. As aluminium is highly reactive with oxygen, the main thrust of this chapter is to generate a method to avoid the oxidation of aluminium prior to introducing molten tin to it. After introducing molten tin to aluminium thin films, samples were cross-sectioned by CSP to examine the thickness of the remaining aluminium layer by scanning electron microscopy (SEM). Results did not allow accurate determination of the dissolution rate of aluminium in molten tin and the likely reasons for this are discussed.

Table of Contents:

List of Figures

List of Tables

1. Introduction

During operation, electronic packages are usually subjected to a wide range of temperatures, especially in aerospace, automotive and oil and gas industry applications. These components may experience temperature changes from −40 °C to 150 °C or even higher [1]. The reliability of the electronic device which is operating in high temperature environment is highly dependent on the structural integrity of the electronic package. Electronics manufacturer have come under pressure to assemble components with high solder joint integrity meet customer expectations for high temperature applications [1]. This thesis is focused on the high temperature electronics and how the reliability of solder improves for high temperature applications.

This thesis has six chapters in the sequence: Chapter 1 Introduction; Chapter 2 Literature Review; Chapter 3 Cross-Section Preparation for Solder Joints Using Argon Ion Beam Milling; Chapter 4 Nano-composite solders; Chapter 5 Dissolution of Al in Sn; and Chapter 6 Conclusions.

1.2 Literature Review

Chapter 2 introduces the theories that underpin the following chapters. Chapter 2 thus reviews theories and previous research predating the original results of this thesis. First it introduces and explains basic concepts in solder technology, including a brief review about solder joints, solder microstructure and reliability and mechanical properties of the solder. After this, it briefly reviews nanoparticles and their associated safety issues. This chapter also describes possible methods for cross-section preparation methods. The final topic of this chapter is the dissolution of Al in Sn.

1.3 Cross-Section Preparation for Solder Joints Using Argon Ion Beam Milling

Chapter three is about a method of cross-section preparation for solder joints. In this chapter the relatively new instrument termed Cross-Section Polisher (CSP) which works by polishing with an Argon ion beam is described, and some new applications of the technique presented. The advantages and disadvantages of this method are illustrated and this method also is compared with the traditional method of mechanical polishing.

1.3.1 Research questions

Chapter three tries to answer a series of research questions and explains the potential of CSP for various studies. Below is the list of questions.

1.3.1.1 Finding a suitable method for detecting nanoparticles embedded in solder in relation to grain boundaries

Observation of nanoparticles inside a solder requires a highly smooth and abrasive-free cross-section since it is challenging for a SEM observation to distinguish between nanoparticles and embedded abrasive. Therefore, a new polishing method and equipment is desired to provide an abrasive-free cross-section for the SEM observation of nanoparticles-contain solders.

1.3.1.2 Finding a suitable method for polishing cross-sections of delicate and brittle samples for SEM observation

Mechanical grinding and polishing is commonly used for SEM sample preparation because of its ease of preparation and low cost of use. However, this method can distort delicate structures

such as thin membrane. Mechanical polishing can also distort samples which contain voids and cracks or very hard and very soft constituents. The abrasive particles such as silicon carbide or diamond can become embedded in any soft material. Therefore, a new polishing method and equipment is needed in order to provide smooth and polished cross-sections for delicate and brittle materials for SEM observation.

1.3.1.3 Finding a suitable solution for polishing solder alloys for SEM observation of microstructural detail

For in depth microstructural analysis of a solder joint clear SEM images are needed which represent the detail of solder matrix, interfacial IMCs and IMCs within the bulk solder. Mechanical grinding and polishing cannot provide a detailed image of the solder including grain boundaries, particulate additives and IMCs simultaneously. Therefore, a new polishing method is requires to provide a smooth and clear image of a detail of the solder joint microstructure.

1.3.2 Contributions

Chapter three shows a series of results and discussions which present a new method of cross-sectioning by CSP.

- Using CSP provided ultra-smooth images taken by SEM. Images clearly represented details of a Ag_3Sn plate in solder (see Figs. 3.7 and 3.8).

- CSP proved to be able to provide abrasive-free images which are crucial in the case of detection of nanoparticles inside a solder matrix. Two images in chapter four represent the liability of CSP in order to provide these abrasive-free images (see Fig. 4.7).

1.4 Nano-composite solders

Chapter four is about nano-composite solders. This chapter explains how nanoparticles were added to Sn-Ag-Cu solder to improve its reliability for high temperature applications. The fabrication of the nano-composite solders is explained. Mechanical testing results performed both at room temperature and at elevated temperatures are presented. A comparison of unmodified and nanoparticle enhanced microstructures both before and after tests using scanning electron microscopy (SEM) and optical microscopy images is given and related to the mechanical test results. Theoretical analysis is provided that explains the experimental results at the end of this chapter.

1.4.1 Research questions

Chapter four tries to answer a series of research questions and explains the effectiveness of nanoparticles in reducing creep in solders at high temperatures.

1.4.1.1 Effectiveness of nanoparticles in reducing creep in solders as a function of temperature

Electronic packages working at high temperature applications are subjected a wide range of temperatures as high as 150 °C or even higher. It is well-established that nanoparticles can be effective in pinning the grain boundary movements at low temperatures. However, it is desired to understand the effectiveness of nanoparticles in pinning grain boundary movement at higher temperature.

1.4.1.2 Finding a mathematical model to explain the pinning behaviour of nanoparticles at elevated temperatures

There are various sizes of nanoparticles which can be used to decrease the grain boundary movement at high temperatures. However, it is required to investigate the optimum size of nanoparticles which can have the largest effect for a desired working temperature.

1.4.2 Contributions

Chapter four shows a series of results and discussions which represents the efficiency of nanoparticles in limitation of grain boundary movements in solder at high temperatures.

- SiO_2 nanoparticles proved to be effective in suppressing the grain boundary movement and dynamic grain growth during compression at low homologous temperatures (see Fig. 4.9).

- At higher homologous temperatures, the pinning effects of nanoparticles decreased rapidly as a result of thermal fluctuations in the position of grain boundary (see Fig. 4.10).

- Considering the diameter of SiO_2 nanoparticles, 100 nm, the analysis of thermally activated grain boundary movement indicated that the fluctuations of the grain boundaries at temperature under 100 °C are less than the particle diameter, which resulted in effective pinning. However, at temperature above 100 °C, the fluctuations of grain boundaries become larger than the particle diameter which resulted in unpinning of the grain boundaries (see section 4.4).

- A mathematical model was developed in order to investigate the optimum diameter of nanoparticles for 150 °C and was predicted to be 274 nm (see Eq. 4.8).

1.5 Dissolution of Al in Sn

Chapter five is about the dissolution of Al in Sn; this work is related to attempts to modify solders chemically by adding highly reactive elements in the form of nanoparticles that dissolve in the solder during reflow. As Al in highly reactive with oxygen, the main thrust of this chapter is to generate a method to avoid the oxidation of Al prior to introducing molten Sn to it. All the methods in this chapter are concerned with coating Al with another element such as Sn or Au to avoid the possibility of O reacting with Al prior to and during soldering.

1.5.1 Research questions

Chapter five tries to answer a series of research questions and investigates a method to prevent the oxidation of Al prior to introducing Sn in order to measure Al dissolution in Sn.

1.5.1.1 Finding a method of measuring Al dissolution and diffusion parameters in liquid solder

As was mentioned earlier, the aim of this chapter is to modify solders chemically by the addition of Al nanoparticles that dissolve in the solder during the reflow. The solubility of Sn in (Al) is a maximum of approximately 0.026 at.% Sn dissolving at 625 ± 20 °C. However, the determination of the solubility of Al in (Sn) is still unclear whereas the occurrence of the eutectic at 3.3 ± 0.5 °C below the melting point of Sn suggests that some solubility exists. Therefore, the solubility of Al in Sn and diffusion parameters in liquid solder is desired for an in depth investigation of addition of reactive Al nanoparticles to the solder.

1.5.1.2 Finding a suitable method to prevent the oxidation of Al prior to introduce to Sn

Al is highly reactive to Oxygen and easily forms Aluminium Oxide, Al_2O_3, upon exposing to air. Once the oxide layer is formed it becomes difficult to be removed. Therefore, it is crucial to find a method to prevent the oxidation of Al prior to introducing the Sn.

1.5.2 Contributions

Chapter four represents a series of results which attempted to prevent the oxidation of Al prior to introducing to Sn. However, there was no method which could generate reproducible results.

- Various experiments proved to be not effective while one of the methods showed a potential to represent the solubility of Al in Sn (see Fig. 5.27). However, it needs refinement and repetition for further investigation as future work.

1.6 Conclusion

Chapter six is the summary and conclusion of the thesis. In this chapter the results of other chapters are reviewed and the main advances that this body of work makes to the field of solder technology, particularly with regard to high temperature applications described. In addition, possible future work for each chapter has been explained.

2. Literature Review

2.1 Microelectronics packaging

Microelectronics packaging is about how to connect the circuitry on a Si chip to the outside world. There are two major ways to connect the chip circuitry to the outside circuitry. The first is by wire bonding and the second is by solder bumping [2, 3]. In modern electronic devices, wire bonding is used to connect the circuits on a Si chip to the leadframe substrate. Solder joints (surface mount solder) are then used to join legs of the leadframe to the circuit board. Leadframe legs are placed on solder paste which is printed on the circuit board. The next step is moving the assembly through an oven (tube furnace) with various heating zones to ramp the temperature up and down in a controlled manner. Fig. 2.1 shows a schematic diagram of the solder joint between the leg and the substrate [1].

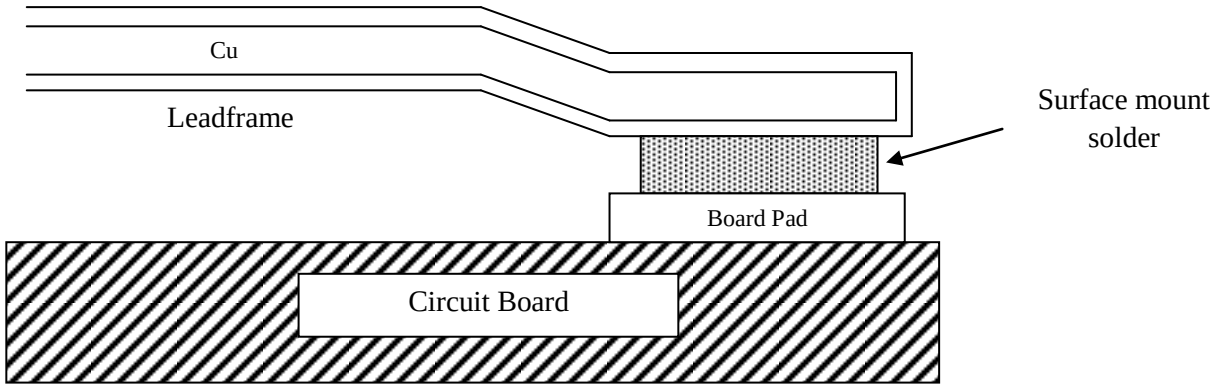

Figure 2-1 - A schematic diagram of the solder joint between the leg and the substrate [1].

In mainframe computers, interconnections between Si chips and substrates are more complicated. For example, wiring on a very-large-scale-integration (VLSI) needs a very long wire for only a 1 cm^2 chip area. Also these wires need several thousand input/output (I/O) pads

on the chip surface. The best practical method for such high density of I/O pads is, as was mentioned earlier, using the second way of interconnection which is array of solder bumps.

Solder balls with diameter of 50 μm with a spacing of 50 μm between them gives the pitch of 100 μm. So by placing 100 of them along 1 cm or 10,000 of them on an area of 1 cm^2 would result in 10,000 solder balls on a chip or 10,000 I/O. Because of the expected use of such small size of solder balls, the 1999 International Technology Roadmap for Semiconductor (ITRS) has identified "flip chip technology" to be in important subject of study concerning its yield in manufacturing and its reliability in use [3]. Controlled Collapse Chip Connection known as C-4 Flip Chip Technology is a method of electrical connections between a Si chip and a printed circuit board. In this method the Si chip which has an area array of solder bumps is flipped and faced down on the circuit on the substrate [1].

One of the main differences between wire bonding and flip chip connections is that in wire bonding wire connections are made at the periphery of the chip, however, in flip chip connections an area array of solder bumps cover a large part of the surface of the chip. The main advantages of flip chip technology are large I/O count, smaller packaging size and higher performance [1]. Fig. 2.2 shows a schematic diagram of a flip chip package.

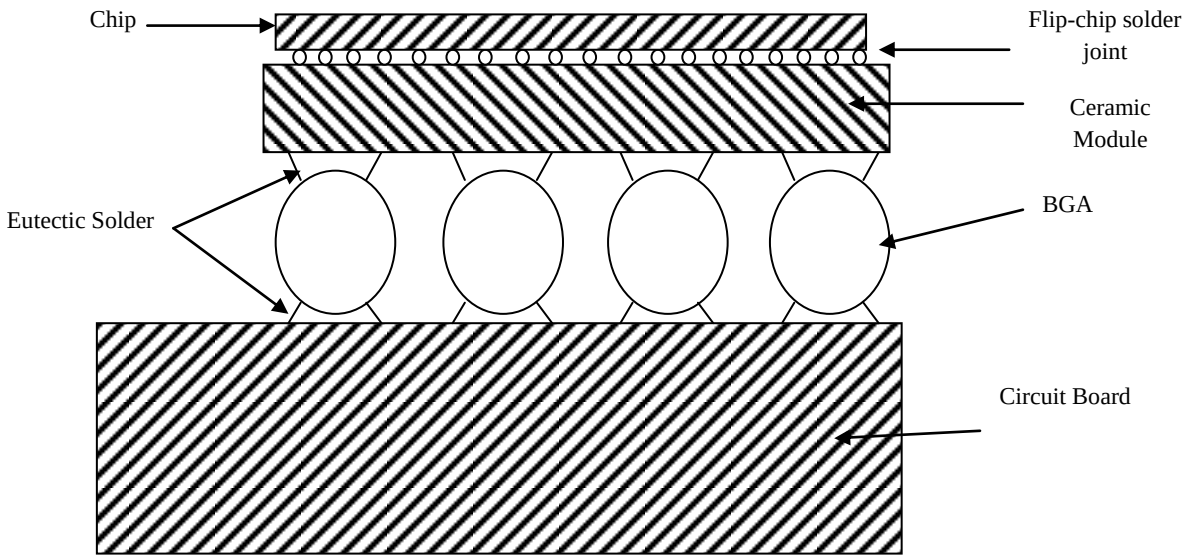

Figure 2-2 - Schematic diagram of a flip chip package [1].

Modern developments in packaging materials and processes have allowed flip chip technology to be used in more mainstream applications [2, 3].

2.2 Solder joint

Soldering is a metallurgical joining method by using a filler metal which relies on wetting for the bond formation. The physical wetting of the molten solder generates the joining interface. The solidification of the molten solder after wetting results in a permanent bond. There are at least two such bonds in each solder joint [1, 4].

Solder is typically used as a low melting point eutectic composition alloy [5-12]. It is generally preferred to have a eutectic composition. Firstly because eutectic alloys have a lower melting point than the two other components individually and secondly, eutectic composition allows solder to have a single melting point rather than a melting range. Hence both of its interfaces are joined at the same time, when the temperature reaches the eutectic point. When hundreds of solder balls as interconnections are placed on a silicon chip, all of them must melt and join at the

same time. This is achieved through a simple process of heating which is called “reflow”, allowing a large number of solder joints between the substrate and chip to form simultaneously. In a “reflow” process the solder joint is exposed to a temperature cycle. During one part of this temperature cycle, temperature increases to a temperature above the melting point of the solder for about half a minute and subsequently samples are cooled down to room temperature.

The purpose of alloying Pb with Sn was to decrease the melting point of the solder and to enhance ductility. Eutectic tin-lead has a melting point of 183°C. The typical temperature of solder joint application is from room temperature to working temperatures of around 100 °C or even higher. Those applications above military specifications (+125 °C) [13] are classed as high temperature applications. At such high temperatures, there are thermally activated processes such as atomic diffusion and creep which are accelerated [1].

Under standard conditions, both the base metal and the solder have a thin film of contamination, or oxide, on the surface, which interferes with the formation of the interfaces between them. Such non-metallic thin films act as a barrier to the formation of metallic bonding and must be removed. Fluxes are one of the main elements of solder systems and needed in most soldering processes to prepare the surface of the substrate as they remove these films [3, 10, 14]. This contamination can act as a barrier for dissolution of one metal into another metal (e.g. Al in molten Sn). Further explanation is given in chapter 5.

The reaction between the molten solder and the metallic substrate forms intermetallic compounds (IMCs) whose nucleation and growth play a key role in the reliability of the solder joint [1]. As the chemical reactions of Sn with the metallic substrate, specifically Cu and Ni, are an important reliability issue in lead-free solder applications, many studies have focused on this topic [1, 7, 15, 16]. These chemical reactions form IMCs such as Cu_3Sn, Cu_6Sn_5 and Ni_3Sn_4 by heterogeneous nucleation and growth at the solder-substrate interface (Fig. 2.3) [1].

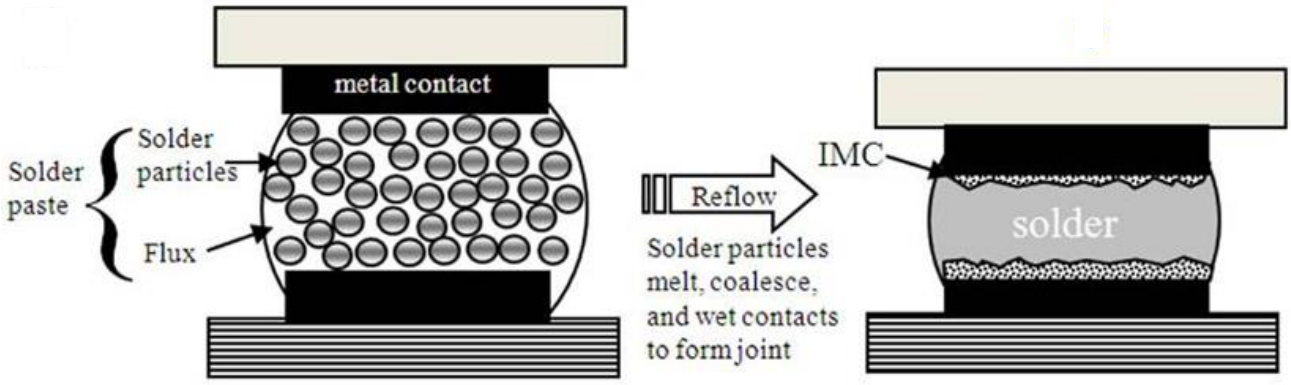

Figure 2-3 – A schematic view of the solder joint and the formation of the IMC at the interface between solder and substrate

After the reflow process, solid-state reactions still take place and can eventually lead to joint failure. These solid-state reactions, which are investigated in aging tests, thermal cycling tests and damp heat tests, are to test the device reliability, e.g. at 150°C for 1000 hr. The aging test is of special interest for applications at quite high temperature, such as experienced in automobile, aerospace and oil and gas industry [1]. One of the most widely used tests is thermal cycling. Cyclic parameters vary widely and should be customized to specific material sets and product applications. In this test, temperature-cycle profiles are unique to specific applications [17]. The damp heat test is usually performed in humidity chambers where the joints are exposed to temperature and humidity for various amounts of time. Cleanliness can be checked by silver nitrate for halides or black light for rosin [11].

2.2.1 Lead-free solders

Near-eutectic SnPb alloys such as 60Sn40Pb, 63Sn37Pb and Ag-bearing 62Sn36Pb2Ag have traditionally been the most widely used solder alloys for electronic manufacturing [18]. However, due to environmental concerns of lead toxicity, international laws have been proposed to limit the use of Pb in manufactured products. Interest in Pb-free solders was stimulated by the

introduction of a bill in the US Congress in 1990 that proposed the banning of Pb from a wide range of uses, including electronic solders [19]. The European Union instruction on Waste Electrical and Electronic Equipment (WEEE) pronounced that products sold in the EU must be lead-free from July 1, 2016 [20, 21]. In Japan and South Korea, major firms also moved forward to develop products with alternative alloys ranging from handhelds, such as calculators to white goods including consumer applications such as washing machines [18]. Thus, the issue of the lead-free soldering received a great deal of interest in the electronics assembly industry. However, there has been some resistance to change from the leaded to lead-free solders. The reasons for this resistance may be divided into cost and reliability concerns [22].

Lead is one of the least expensive elements on earth which means that any replacement for lead implies an increase of price. There is also an additional cost of educating and training company personnel in the use of lead-free solder [22].

Reliability issues are the greatest concern in the lead-free solder issue. Although many lead-free alloys have exhibited good reliability characteristics, providing the level of security offered from thirty years of tin-lead solder usage and data would not be easy [22].

In response to these concerns, the new elemental additions to Sn-based system should fulfil the following basic requirements [23, 24]:

1. Reduce the surface tension of pure Sn to improve the wettability;
2. Sufficient joint strength and thermal fatigue resistance;
3. Enable fast, but not overly rapid formation of IMCs between the solder and substrate by diffusion;
4. Adequate quantities of base materials available now and in the future;

5. No current or future negative environmental impact;
6. Similar melting temperature to leaded solder;
7. Prevent the transformation of β-Sn to α-Sn, which causes unwanted change and degrades structural integrity and reliability of solder;
8. Compatibility with existing parts and processes;
9. Easily repaired;
10. Prevent the occurrence of excessive tin whisker growth.

The Pb-free solder alloys which can fulfil these requirements are more likely to be multi-component alloys rather than a binary composition. Accordingly, SAC solders have emerged as the front runner for the replacement of Sn-Pb solders. However, the high-Sn-content alloys have shown problematic behaviours such as large undercooling during solidification, void formation, overly rapid IMC formation and spalling of interfacial IMCs during high temperature storage [25]. A wide variety of alloys are available as shown in Table 2-1 [18].

Table 2-1 - Solder alloys

Alloy system	Nominal composition of selected alloys	Melting range		Application remarks	ref
		Solidus (°C)	Liquidus (°C)		
SnPb	63Sn37Pb (e)	183	183	Primary joining alloys for electronic assembly	[26-29]
	60Sn40Pb	183	191		[30-32]
	62Sn36Pb2Ag (e)	179	179		[33, 34]
PbSn	95Pb-5Sn	308	312	High-temperature solders for die attach	[35, 36]
	90Pb-10Sn	268	301		[37, 38]
PbSnAg	97.5Pb1.0Sn1.5Ag (e)	305	305		[18]
	82.5Pb15Sn2.5Ag	275	280		[18]
SnAg	96.5Sn3.5Ag (e)	221	221	Primary replacement candidates for near-eutectic SnPb solder alloys with high melting point	[39-41]
SnAgCu	95.5Sn3.8Ag0.7Cu (e)	217	217		[42, 43]
	Sn3.9Ag0.6Cu	~217	~217		[44-46]
SnBi	42Sn-58Bi (e)	138	138	Low melting point eutectic with potential segregation problems	[47-49]
SnCu	99.3Sn0.7Cu (e)	227	227	Low cost with poor mechanical properties	[50]

Eutectic (Sn3.8Ag0.7Cu) or near eutectic (Sn3.0Ag0.5Cu and Sn4.0Ag0.5Cu) SnAgCu (SAC) has become the most recommended lead-free soldering alloy to substitute for Sn-Pb eutectic solder [51, 52]. Other common lead-free solders are eutectic SnCu and SnAg which have melting points in the range of 221-227°C [51, 53]. This higher melting temperature increases the dissolution rate and solubility of Cu and Ni contact metallization in molten solder. Also it increases the rate of IMC formation with Cu and Ni under-bump metallisation [1].

2.2.2 Reflow soldering

Reflow soldering is a process in which the PCB and the solder paste are heated so that the solder paste melts, kinetically wets and then forms the solder joint after solidification. Various heat-

transfer modes can be used for soldering, such as conduction, convection, vapour condensation, hot gas, induction and laser beam (see section 4.2.2 Reflow soldering of solder paste). Each of these methods has advantages and limitations which are listed in Table 4.2. Many of the alternative Pb-free solders require higher soldering temperatures than eutectic Sn-Pb. Thus, board materials and components must be compatible with the higher temperature to avoid damage. The reflow profile must be determined for the solder paste since each process and application has its own characteristics of heat transfer. The soldering process can be divided to two major processes; pre-heating and soldering.

2.2.2.1 Pre-heating

This important step fulfils a large number of needs depending on the process. Pre-heating ramp rates during ramp-up to peak temperature are between 1-3 ℃ per min to provide high throughput with low defect rates and without damage. Pre-heating has direct effects on flux and solder joints:

Effect on flux

1. Evaporate all volatiles, such as thinners and solvents
2. Melt any solid flux ingredients, to facilitate flux wetting
3. Activate the milder fluxes such as rosin formulations

Effect on solder joints

1. Shortens the dwell time at the peak wetting temperatures where heat damage to the assembly can happen

2. Eliminates the stress due to heat shock which may result in micro-cracks inside ceramics, glass-to-metal seals and the like

3. Eliminates the uneven heating stresses which can be due to temperature differences from side to side or top to bottom.

2.2.2.2 Soldering

Soldering is a heating step to fuse the solder alloy, by raising its temperature above the melting point of the solder alloy. The temperature increment (dT) is a function of several factors, for instance:

- The cohesive force of the solder alloy as a function of temperature.
- The internal friction (viscosity) of the solder as a function of temperature.
- The type and the strength of the flux used [54].

2.2.3 Intermetallic compound (IMC)

When a pure metallic element solidifies, the atoms arrange themselves in a well ordered lattice. But if a second element is introduced in solution, then as the solution solidifies there are two locations that the second element can occupy. If the size of the foreign atom is similar to the size of the parent atom, it will replace an atom of the parent metal in the lattice and form a substitutional solid solution. But if the foreign atom is smaller, it may slip into the interstitial spaces and form an interstitial solid solution. In soldering, all metallic atoms which are of interest in the formation of IMCs are of the substitutional type. Furthermore, there are two possibilities for lattice arrangement during the solidification of the solution. In the first one, the

substitutional atoms in the lattice arrange in a haphazard way. In contrast, in the second one, there is a long-range order in the lattice. The latter one is called a superlattice. In a superlattice, when two metals with mutual solubility solidify, with the right concentration, a new crystalline phase is formed. This superlattice phase is called an IMC [11], and is characterised by a well-defined ratio between the participating elements. During the soldering process, the formation of interfacial IMCs is one of the mechanisms for establishing the bond between the solder and the substrate [55].

IMCs have a different lattice structure from that of the parent metals which gives them non-metallic properties. The conductivity of IMCs is greatly reduced and also they have smaller ductility and greater hardness and brittleness [11, 55, 56]. Fig. 2.4 shows Cu_6Sn_5 IMCs at the interface between solder and a Cu conductor and also Ag_3Sn IMCs inside the bulk solder. IMCs' of Sn and Cu also form in the molten solder. These IMCs have a much higher melting point than the solder, for example, the melting points of Cu_3Sn and Cu_6Sn_5 are 670°C and 415°C respectively. The ideal location for IMCs to grow is at the interface as the Cu surface is an endless supply of Cu atoms but IMCs tend to float away from the surface. This is one of the reasons which cause IMCs to be found throughout the joint. Some IMCs also form as the solder solidifies and can be distinguished due to their dendritic structure.

As Cu atoms diffuse into the liquid solder, scallop shaped η-Cu_6Sn_5 IMCs form at the solder/Cu interface. The very thin layer of ε-Cu_3Sn IMCs also form between the η-Cu_6Sn_5 and the substrate. The formation of specific Cu-Sn compounds depends on the availability of Sn and Cu. Thus, Cu-rich Cu_3Sn can be found closer to the Cu substrate, while the Sn-rich Cu_6Sn_5 forms near to the liquid solder [8, 11, 53, 55, 57-61]. The morphology and thickness of the reaction layer is highly depended on the dissolution rate of Cu into the liquid solder. As the reaction between the Sn-based solder and the Cu substrate goes on, the Cu_6Sn_5 IMC layer becomes

thermodynamically unstable which leads to the formation of the thin IMC layer of Cu_3Sn by consuming the Cu_6Sn_5 IMC layer. The Cu_3Sn layer is too thin to be observed experimentally immediately after reflow, however, during ageing this layer grows significantly between the Cu_6Sn_5 IMC layer and the Cu substrate. Over time, voids can form inside the Cu_3Sn IMC layer which is either by the Kirkendall effect or solute segregation. Therefore, the Cu_3Sn layer plays a key role in determining the reliability of the solder joints [1].

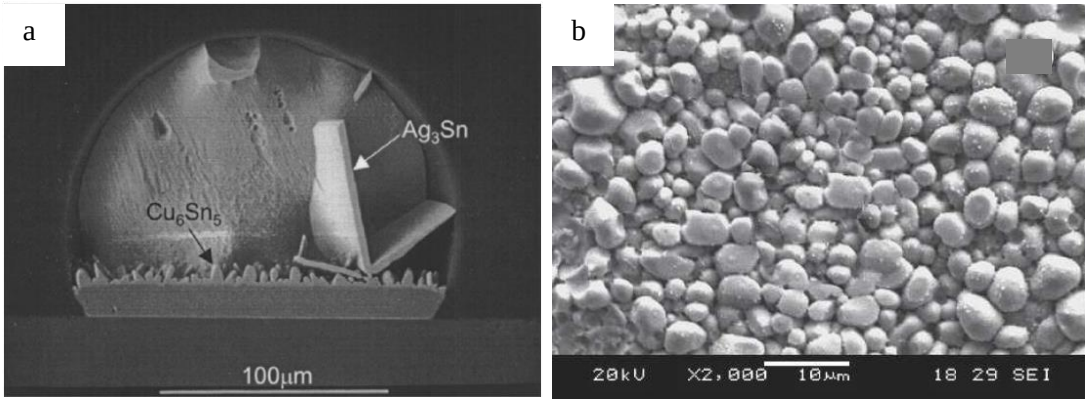

Figure 2-4 - IMCs in SAC: (a) SEM image of Cu_6Sn_5 and Ag_3Sn platelet in SAC solder joint [1], (b) The scallop-type Cu_6Sn_5 generated at the SAC/Cu reaction couple during solder reflow after etching the solder away

The formation of bulk platelike Ag_3Sn IMCs in the SAC solders might severely influence the mechanical properties of solder joint as large platelike Ag_3Sn IMCs may show brittle behaviour under stressed conditions [62-66]. It is also reported that cracks can initiate at the interface between the Ag_3Sn plate and the solder and can propagate along this interface [8, 63, 64, 67, 68]. However, it is suggested that the formation of bulk Ag_3Sn IMC plate could be decreased by an applied cooling rate or reducing the Ag content in the solder [62, 66]. Ag_3Sn IMCs can form during decreasing temperature and in the middle of the cooling stage rather than at the beginning. Because as the temperature decreases, Cu_6Sn_5 IMCs form at the interface, which consumes both Cu and Sn, resulting in increasing of the Ag content at the local area near the

interface between the solder and the substrate. Thus, Ag_3Sn IMCs begin to form when the composition reaches a particular value. Therefore, Ag_3Sn IMCs nucleate mainly at the solder/interface [67, 69, 70].

Another substrate which can be used in Printed Circuit Boards (PCBs) in the microelectronics industry is Au/Ni (P)/Cu or Electroless Ni Immersion Gold (ENIG). The advantage of this substrate over the Cu substrate is that the Ni layer slows down the interfacial reactions between the molten solder and the under bump metallization layers of the substrate. By reaction between the molten solder and the ENIG substrate, first the Ni_3Sn_4 IMC nucleates and grows [15]. The rate of the dissolution of Ni (which is the first element to dissolve) into the molten solder is much less than Au and Cu [71]. Additional to the Ni_3Sn_4 IMC layer, Ni_3Sn_2 and Ni_3Sn are the other IMC layers which form at the interface during the reaction between the liquid solder and the ENIG substrate. The electroless Ni(P) substrate has a slower reaction rate with solders than pure Ni substrate. Thus, the addition of other elements can be highly advantageous to the reaction between Ni and Sn [1, 15]. By adding P to the Ni substrate, a stable layer of Ni_3P forms between the substrate and the Ni-Sn IMC layers. This layer can act as barrier to Ni diffusion into the solder and other IMC layers, resulting in suppressing the growth of the Ni_3Sn_4 [72-74].

2.2.4 Geometry of solder and the "edge effect"

The effect of geometry and size of joints on the microstructure and reliability are becoming important as the miniaturization of solder joints are continuing in high-density packaging [75-76]. As solder joint geometries are becoming smaller toward a microscopic scale, the microstructural features such as grain size and IMCs which govern the mechanical and electrical performance, can become equivalent in scale to the size of the joint [77]. Solder bump geometry can influence the dissolution kinetics of the pad metal into the solder [78]. Schaefer *et al.* [79], reported that the ratio (V/A) of solder volume to contacted area controls the dissolution rate of

the Cu substrate into the solder. They explained that as the value of V/A increases, the diffusion distance for Cu to saturate the molten solder becomes longer. Their results are consistent with other studies which were previously reported which reported that the amount of dissolved Cu controls the IMC layer growth [80].

In addition, the diffusion of Cu flux along the Cu/liquid solder interface is not the same [81]. The difference in interfacial IMC sizes between the bump edge and bump center of the solder joint is called "edge effect". The diffusion and IMC formation kinetics at the solder bump edge are faster than in the middle [81, 82]. The difference in the thickness of IMCs at the bump edge and bump middle can also be attributed to the high saturation level of Cu content at the bump edges which results in providing the sufficient amount of Cu for the formation of Sn-Cu IMCs [81]. The edge effect is more visible in the solder joints with smaller volume of solder indicating that the possibility of the saturation of Cu at the bump edge appears faster in the small solder volume than the one with larger solder volume. It is also reported that the Cu_3Sn phase formed first in the Cu balls which were plated with smaller volume of Sn [83]. The schematic illustration of the edge effect is shown in Fig. 2-5.

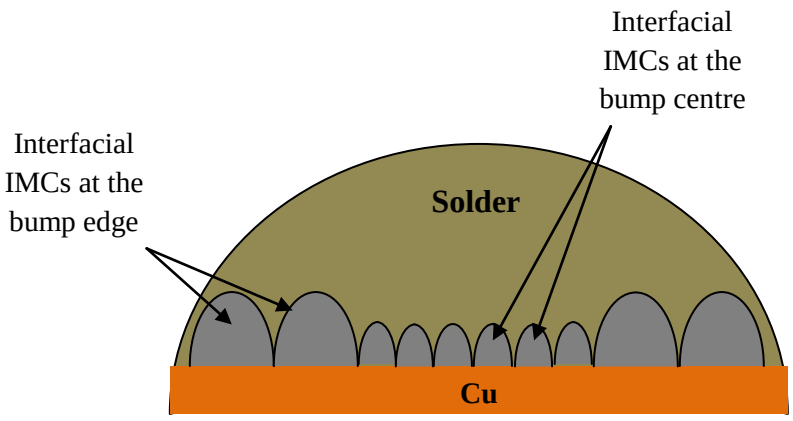

Figure 2-5 - The schematic illustration of the edge effect

2.2.5 Reliability

If an electronic system fails to provide its required function, there is a lack of reliability. Failure in everyday electronic products such as TV, radio and mobile phone would not necessarily be catastrophic. However, in cases such as medical diagnostic systems and air-traffic control systems, reliability is a vital issue and failure can be life threatening. Environment-related reliability is an important issue in electronic industry. Environmental stimuli such as extreme temperature, electromagnetic fields and mechanical shock and vibration can cause failures of electronic packaging. The research in this thesis is focused on high temperature effects on microelectronic interconnects. In this case, two types of high temperature exposure can have an affect, one is during the process of manufacturing which is often high in temperature but few in number of occasions. The second happens during operation, which is lower in temperature but greater in frequency. This research is about the latter which assumes that the structure has survived manufacturing. If the structure is unable to tolerate the high temperature, it will fracture prematurely [17]. High temperature can affect both the IMC at the interface between the solder and the substrate and the solder itself. Elevated temperature increases the thickness of IMC at the interface between the solder joint and the substrate. The presence of IMC in solder joints provides good bonding between the solder and the substrate; however, because of the brittle nature of IMCs, critical thicknesses raise concerns for long term service life reliability [84-96].

The useful lifetime of a device is the ultimate concern in thermal-cycle reliability. The failure of metals under alternating stresses is called fatigue. A fatigue fracture always starts as a small crack but under repeated applications of the stress, grows in size. By expansion of the crack, the cross-section of the specimen which carries the load decreases. This results in increasing the stress on this section. Ultimately, the cross-section will not be strong enough to carry the load. In recent years, the interest in fatigue tests has increased, especially, when failures occur after a

small number of cycles. Fatigue studies which involve fewer than 10^4 cycles are called *low-cycle fatigue* (LCF), while those which require more than 10^4 cycles are grouped in the *high-cycled fatigue* (HCF) classification [17, 97].

Temperature cycling is an environmental test where the sample is subjected to several temperature changes from a low to a high temperature and both over a period of time [17].

Some of thermal strain which is caused by the temperature change and any thermal expansion mismatch in electronic package is consumed by elastic displacement. There is also a plastic strain of the solder joint. But instead, this plastic strain is determined by thermal and mechanical properties of the electronic assembly and the rate and magnitude of the temperature cycle [98].

An electronic assembly consists of a substrate and components which are joined by solder joints. The temperature of the electronic package can change because of either the external environment or internal power variations. This temperature change causes thermal expansion differences between the component and the substrate which are taken up by elastic displacement in the component and the substrate and by plastic displacement in the solder joint [98].

2.2.6 Grains and grain boundaries

Most crystalline solids are composed of many small crystals or grains. These materials are called polycrystalline. In the initial stage of solidification of a polycrystalline material small nuclei or grains form at various positions. The small grains grow by addition of surrounding liquid atoms to the structure. Their crystallographic orientation is completely random and varies from grain to grain. The atomic mismatch where two grains meet is called a grain boundary. There is a crystallographic misalignment between adjacent grains which meet at grain boundary [52]. A schematic top view of grain and grain boundary is shown in Fig. 2.6. [11]:

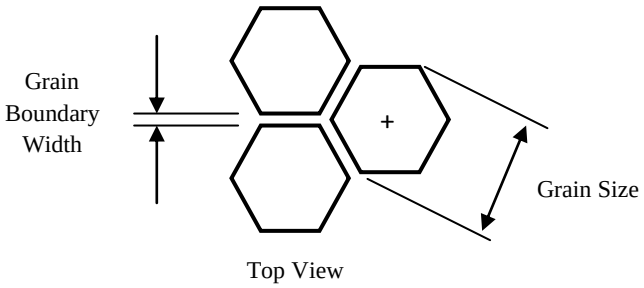

Figure 2-6 - Schematic top view of grain and grain boundary [11]

Grain boundaries play an important role in the mechanical properties of materials [97]. At high temperatures under slow strain rates, grain boundaries lose their strength faster than grains. After solidification grains may continue to grow, especially if they experience high homologous temperature. Increase of grain size results in a decrease of total boundary area. This will reduce the total energy which is a driving force for grain growth. Grain growth is the result of the migration of grain boundaries. Some grains grow and some grains shrink. Thus, the growing grains consume small ones. Fine-grained metals have higher strength and toughness than coarse-grained ones [99].

Therefore, stabilizing the initial fine microstructure is an important topic that will be discussed further in chapter 4.

It is hard to see the granular structure and detect grain boundaries of metals by microscopy after polishing the polycrystalline materials. It is possible to detect grain boundaries of some metals which have several grains with different colours but this does not apply to pure metals and SAC alloys which are predominantly Sn. Various grain size measurements are discussed later (see section 4.2.5 Grain size measurements techniques).

2.2.7 Creep properties of solders

When a material is loaded at a high homologous temperature, it undergoes creep; a continuously increasing and permanent deformation at a stress that is less than the stress that would be needed to cause any permanent deformation at room temperature. There are two mechanisms of creep: dislocation creep and diffusional creep. In dislocation creep, the stress results in plastic deformation, by movement of dislocations. Their movement is resisted by (a) the intrinsic lattice resistance and (b) the obstructing effect by obstacles. Diffusion of atoms, which would be increased by increasing temperature, can "unlock" dislocations from obstacles in their path. Applied stress would make these unlocked dislocations move which would lead to dislocation creep. Fig. 2.7 and 2.8 show what happens during the creep at the atomic level [5].

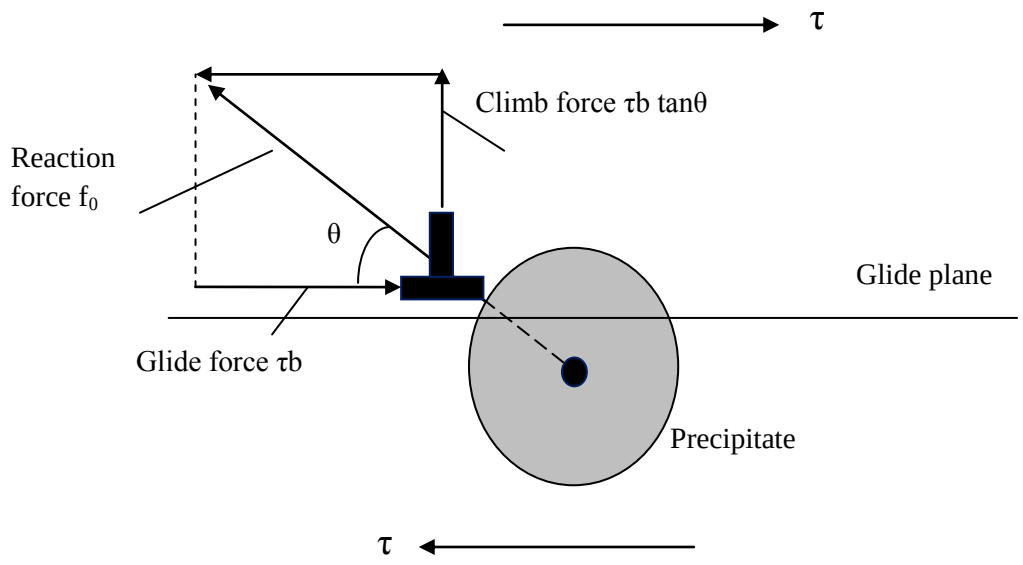

Figure 2-7 – The climb force on a dislocation [5]

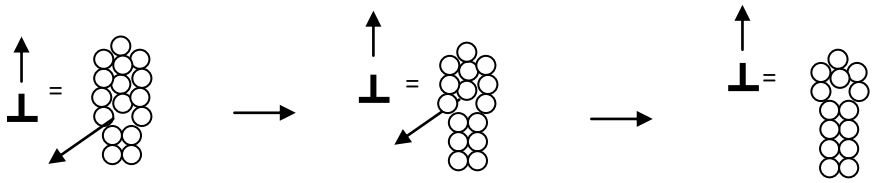

Figure 2-8 – How diffusion leads to climb (atoms diffuse away from the bottom of the half plane) [5]

As can be seen in Fig. 2.7, the glide force τb (where τ is shear stress and b is the unit of slip or the Burgers vector) is in balance with the reaction f_0 from the precipitate. But there is another force, $\tau b \tan\theta$, which pushes the dislocation out of its slip plane. This process is called "climb", and since it needs diffusion, it happens only when the temperature is above $0.3T_M$. The diffusion coefficient in Fick's law of diffusion,

$$D=D_0e^{-Q/RT} \qquad (2.1)$$

explains the dependence of diffusion on temperature. When this dislocation unlocks from this precipitate, it continues to glide and reaches another obstacle and this cycle repeats explaining why creep is progressive and continuous. Fig. 2.9 shows this process of climb and glide [5].

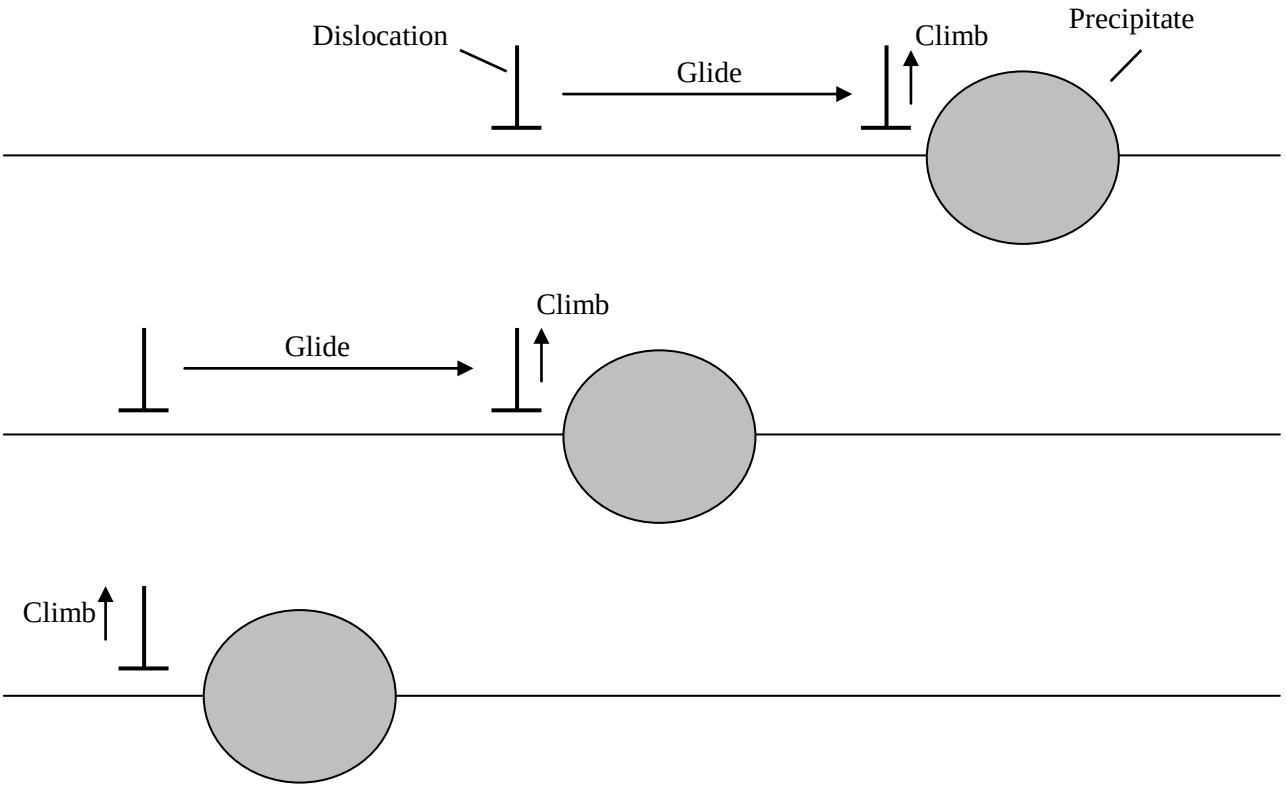

Figure 2-9 – How the climb-glide process leads to creep [5]

As the applied stress σ increases, the climb force, $\tau b \tan \theta$, increases. That is why the creep rate depends on the applied stress. The higher σ leads to the higher climb force leading to more unlocked dislocations occurring per second. More dislocation gliding per second results in higher strain rate [5]. Creep, which occurs in solders, is this type of creep [5].

Another type of creep is diffusion creep. In this type, there is no dislocation. As the stress is reduced, the creep does not stop; instead, an alternative mechanism takes over. In this case, the polycrystalline material extends in response to the applied stress, σ, by grain elongation. In this type of creep, atoms diffuse from one set of the grain faces to the other [5].

One of the common equations which is used by design engineers to investigate the relation between the stress and temperature dependence of creep strain rate, especially in electronics, is the Norton power law [100, 101]:

$$\dot{\varepsilon} = A\sigma^n \exp(\frac{-Q}{RT}) \qquad (2.2)$$

where $\dot{\varepsilon}$ is the steady state creep strain rate, A is a constant, σ is the stress, n is the stress exponent, Q is the activation energy, R is the universal gas constant, and T is the absolute temperature. Thermally activated plastic flow mechanisms are characterized by stress exponents and activation energies. The creep mechanisms which are caused by dislocation climb are characterized by a stress exponent of 6-7 and an activation energy corresponding to self-diffusion, those that are caused by viscous dislocation glide are characterized by a stress exponent of 3-4 and the one which is caused by grain boundary sliding are characterized by a stress exponent of 2-3 and an activation energy corresponding to grain-boundary diffusion [100]. However, there are significant differences among the available values of stress exponents and activation energies. These disagreements can be attributed to the differences in the specimen (bulk solder or solder joint), the specimen geometry (dimension ratio and shape, etc.) and the boundary and test conditions. These variables make the analysis of the creep behaviour of solder joints complicated [102, 103].

Creep is the most important deformation mechanism in typical electronic conditions, which are between 25°C to 125°C [51]. One of the best methods to increase the creep resistance is dispersion and precipitate strengthening. This method is an effective way to impede dislocations by dispersing small and strong particles with a high melting point [5, 104-109]. However, IMCs inside the SAC solder can also act as barriers to impede dislocations movement. The two IMCs inside the SAC solder matrix, Ag_3Sn and Cu_6Sn_5, are two significant phases which have much

higher deformation resistance than Sn matrix, thus they form hard particles in the comparatively soft Sn matrix. The movement of dislocations is slowed down or arrested at these particles [110]. It is reported that the creep life of SAC solder is almost 70 times greater than Sn-Cu which is attributable to a smaller volume fraction of the precipitate phase (1.79 vol. %) compared with SAC (5.9 vol. %) [102].

In general, SAC solders, as well as Sn-37Pb, exhibit typical creep curves with stages of primary, steady-state, and tertiary creep. The primary stage is usually shorter under a lower applied stress or at a higher temperature. The Pb-free solder alloys show well-defined steady-state creep behaviour and the steady-state creep deformation process is about 15-40% of the total creep life [102].

2.2.8 Zener pinning

The microstructure of materials is normally made of multiple grains with different crystallographic orientations [111]. Grain growth is a phenomenon in which the mean grain size increases with time. In some cases, grain sizes grow at a similar rate, however, in a small number of cases, grains grow at a significantly faster rate than the other grains [112]. The stagnation of grain growth by a dispersed second phase is crucial for grain size control in materials. Grain size plays an important role in controlling the mechanical properties of the materials, including their creep resistance, tensile strength and low cycle fatigue life [113-115]. Dispersions of second phase particles can inhibit grain growth by generating pinning force on the migrating grain boundaries during thermal treatment [114, 115]. The mechanism of grain growth limitation by second phase particles is called Zener pinning. Zener pinning concerns the limiting of grain growth which is caused by heat treatment without the effect of stress. The Zener pinning effect has been analysed by a variety of theoretical approaches. But most of the

approaches predict relationships between limiting grain size, λ_g, particle size, λ_p, and the volume fraction, *f*, which can be generalized as follows:

$$\frac{\lambda g}{\lambda p} = \alpha \frac{1}{f n} \tag{2.3}$$

Where α and n are constants [116].

2.2.9 Creep activation energy

The activation energy, Q, is the energy barrier above which an atom can move from a higher energy location to a lower energy location [117]. So a larger creep activation energy value provides higher creep resistance [118].

It has been suggested that fine particles segregate preferentially at boundary dislocations, which causes a pinning effect at boundaries. The interaction between fine particles and dislocations can change the threshold stress τ_0 which is the stress that should be exceeded before boundary dislocations can break away to produce sliding [119]. The relationship between τ_0 and Q_0 is expressed by equation 2.4:

$$\frac{\tau_0}{G} = B_0 \exp(Q_0 / RT) \tag{2.4}$$

Where τ_0 is the threshold stress, G is shear modulus, B_0 is a constant, Q_0 is activation energy, R is Boltzmann's constant and T is the absolute temperature [119-126].

2.2.10 Nano-composite solders

A nanoparticle is defined as a small object in the range of 1 nm to 100 nm. Various types of nano-sized reinforcements have been used to change the microstructure of solder matrices thereby helping to improve the mechanical properties of nano-composite solders [105]. Nanoparticles decrease the size of grains of solder matrices and these fine grains increase the strength of the solder alloy [127]. Another reason for choosing nano-sized reinforcements in composite solders is their effectiveness in improving the creep resistance by limiting the grain boundary sliding. These reinforcements also hinder large IMC formation and grain growth [105, 127, 128].

Using nano-sized reinforcements has further beneficial effects beyond creep resistance, which include increasing the hardness, tensile strength and shear strength. For example, the addition of ceramic nano-sized reinforcements, such as ZrO_2, SiC, Al_2O_3 and TiO_2 considerably enhances the hardness and tensile strength [127]. Hardness is a key parameter of the mechanical property of metal materials. The hardness value provides an indication of resistance to deformation, densification and cracking [105]. According to the literature, the enhancement of the strength of composite solders is because of the presence of fine strong particles within the matrices and at the grain boundaries of solder matrices, which changes the deformation characteristics of solder alloys by slowing down grain boundary sliding. Fine nanoparticles are more effective obstacles to dislocation movement in solder matrices [105, 107, 127, 128].

2.2.10.1 Safety

The safety of nanoparticles is an issue which environmental organizations and governments are concerned about. The potential negative side effects of nanotechnology are still not clear. According to the 3rd International Symposium on Nanotechnology Occupational and Environmental Health which was held on 2007 in Taiwan, some research in various fields of

safety in nanotechnology have been undertaken to discover any negative influence of nanotechnology on human life, such as, emission control and exposure protection, international standards and nanotoxicity and environmental applications of nanotechnology. For example, papers by Yu et al. demonstrate that amorphous silica (silicon dioxide, SiO_2) nanoparticles smaller than 100 nm induces cytotoxicity in mouse keratinocytes and the nanoparticle size is found to be a crucial factor [129, 130].

The dissolution rates of nanoparticles are very important from a hazards point of view. This is because when the dissolution rate is slower, nanoparticles generate less toxic response due to slower release of individual molecules. Hence, not only the composition and dose of the material can influence toxicity, but the size and the shape of the material are important too. Larger particles may be trapped at the upper part of the respiratory parts, but small particles can penetrate deep into the more sensitive parts of the lung [131]. The silica nanoparticles used in this study are 100 nm in diameter. Based on present-day knowledge it cannot be ruled out that SiO_2 nanoparticles might have possible negative physiological effects. Henkel Loctite Adhesives Ltd. recommended to avoid direct skin contact by wearing suitable gloves (butyl rubber) while working with this type of product [132].

2.3 Cross–section polishing review

Detection of nanoparticles in solder cross sections is challenging due to the small size of the nanoparticles; hence this section reviews the techniques used to produce high quality cross sections. Mechanical grinding and polishing is routinely used for SEM sample preparation due to ease of preparation and low cost of use. The basic principle is that successively finer grades of abrasive powders on rotary polishing cloths are used to produce extremely flat, high quality samples. A lubricant is also used to minimize sample damage. However this method can distort delicate structures such as thin membranes, and also samples containing voids, cracks and samples containing both very hard and very soft constituents. The abrasive particles (e.g. silicon carbide or diamond) can also become embedded in any soft phases present. In order to overcome these problems, a new polishing method and equipment based on the use of a beam of argon ions directed at the sample has been developed by Jeol Ltd [133-135]. An argon ion beam is used in the JEOL SM-9010 Cross Section Polisher (CSP). The beam is produced and directed towards the sample and shield plate to mill the unshielded part of the sample. This result in a sample cross section that is of the order of 1mm in width and which is produced perpendicular to the plane of the shield plate as shown in Fig. 2.14.

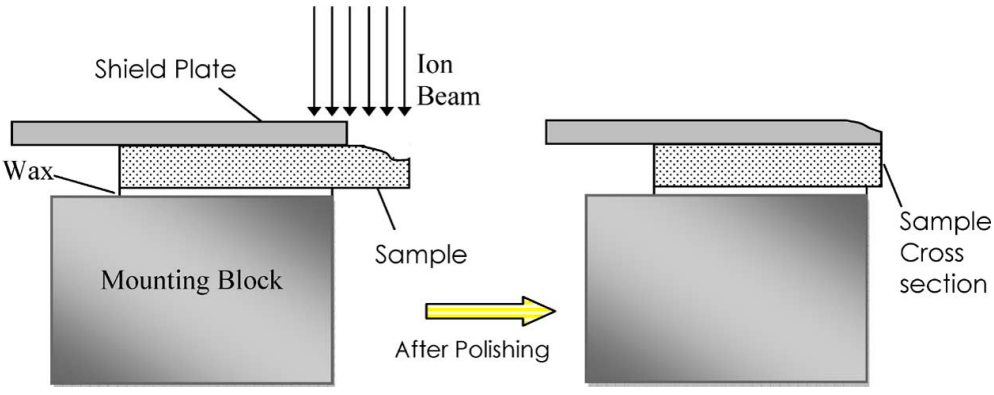

Figure 2-10 - Schematic of CSP operation for cross-section preparation [9]

The argon ion beam also provides an excellent method of etching in order to increase the contrast between phases, in a similar way to chemical etching with dilute acid (see Fig. 4.5). In order to achieve this, the shield plate was removed and the mounting block rotated through 90 degrees, as shown in Fig. 2.11.

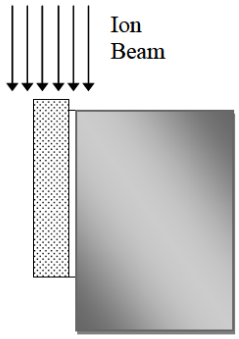

Figure 2-11 - Schematic of CSP operation for etching [9]

For normal cross section preparation, targeting of particular features by aligning them against the shield is possible with the aid of a loupe to an accuracy of approximately 10 microns. Because of the near zero incident angle of the ion beam, the quantity of implanted ions into the cross section region is very small and deposition of the elements from the shield plate is also minimized [133]. Focused Ion Beam (FIB) milling is a similar technique, but the size of the polished surface is of the order of tens of square micrometers. Thus, FIB is applicable only when long preparation times are acceptable. Additionally, concerns have been raised that Ga ions can be implanted in the sample [136]. However, the positional accuracy of a polishing cross section

by CSP is about 10 μm which is more than one order of magnitude poorer than the one by the FIB method [133-135, 137].

2.4 Dissolution rate of Al in Sn-based solders

In contrast to adding passive nanoparticles to solders, chemically active nanoparticles composed of highly reactive metals such as Al and Zn are also of interest. At King's College London, a programme of work investigating the use of nanoparticles of Al in solders is underway. The effect of Al addition to solder baths in suppressing Cu_6Sn_5 interfacial IMC growth has been reported in previous studies [138-140]. However, the use of Al in solder is generally avoided because of excessive oxidation of solder particles leading to poor wetting [141]. The present research tries to extend these previous researches by considering the effects of the additives to smaller solder volumes for reflow soldering rather than solder baths. The aims of this study are to by addition and complete dissolution of Al in solder, form Al-Cu IMCs at the solder/Sn-Cu IMC interface. This study tries to suppress the Cu_6Sn_5 IMC growth by the formation of Al-Cu IMCs. The schematic illustration of this study is shown in Fig. 2.12.

As was mentioned earlier in this chapter, at King's College London, a programme of work investigating the use of nanoparticles of Al in solders is underway. Aluminium soldering is a challenging task since aluminium as a metal has a hard oxide layer which forms easily upon expose to air and is extremely difficult to remove. However, the addition of Al into solder has been tried and some examples are represented in Table 2.2.

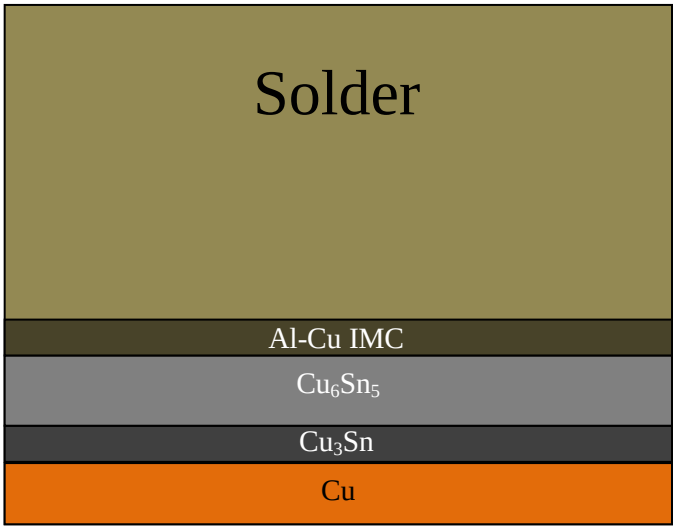

Figure 2-12 - The schematic illustration of suppression of the Cu_6Sn_5 IMC growth by the formation of Al-Cu IMCs

Table 2-2 –Examples of the addition of Al into solder

	Substrate	Atmosphere during reflow	Results	Ref.
Sn-Bi-1-2wt.%Al	Cu	Air	Al migration to the surface, followed by oxidation, depleted Al from the solder bulk and no Al containing IMC was formed	[142]
Sn-3.5Ag-0.5-2wt.%Al	Cu	Air	Al from the solder reacted with Cu from the substrate to form Al-Cu intermetallics which however, spalled away from the substrate during reflow. Normal interfacial IMCs of Cu_6Sn_5 and Cu_3Sn are observed.	[141]
Sn-3.5Ag-0.5-2wt.%Al	ENIG	Air	Al_3Ni_2 IMC particles are observed as a discontinuous layer around 5 µm away from the Ni(P) substrate rather than at the substrate interface.	[141]

			The location of the layer suggests that the IMC was first formed at the solder/substrate interface before being replaces by Ni_3Sn_4.	
Sn-3.0Ag-0.1-2wt.%Al	Cu	—	When the aluminium content is less than 0.5 wt.%, the interfacial IMCs are Cu_6Sn_5 and Cu_3Sn. For the case of 0.5 wt.%, a continuous $CuAl_2$ layer is spalled off into the bulk solder. However, a thin flat layer of $CuAl_2$ was observed for the case of 1.0 wt.% aluminium addition.	[143]
Sn-3.0Ag-0.1-2wt.%Al	ENIG	—	When the aluminium content is less than 0.1 wt.%, Ni_3Sn_4 and P-rich layer are formed at the interface while spalling Ni_3Sn_4 particles are also observed in the bulk solder near the interface. When the aluminium concentration is high (0.5 wt.% and 1.0 wt.%), a planar AuAl layer is formed at the interface. Relatively high aluminium content also suppressed the P-rich layer and spalling.	[143]

There are various method to fabricate Al-containing solder, for instance, Kotadia H.R. et al., compressed Sn-Ag ingots and Al foil, mechanically, and placed in a quartz tube sealed into an electric resistance furnace with vacuum (10^{-5} Torr) [141]. The aluminium oxide is a refractory material with a chemically inert behaviour. Thus, for soldering operation, strong flux is needed in order to clean the surfaces and maintain cleanliness. Only specific fluxes which are designed

for aluminium soldering are effective; they contain either organic- or inorganic-acid compounds. Also, mechanical abrasion or ultrasonics can break through the oxide layer [54]. However, the aim is to design nanoparticles to release Al into the solder at the optimum time in the solder reflow process so as to maximize Al reactions with the substrate while minimizing interference with solder wetting reactions. In order to achieve this, the dissolution rate of Al in liquid solder is an important parameter and hence fits into the overall aim of this thesis in developing nanoparticle enhanced solders.

2.4.1 Dissolution of Al in Sn

Al-Sn is a simple eutectic system with limited solid solubilities in the two terminal solid solutions. The binary phase diagram of Al-Sn is shown in Fig. 2.13 [144]. As can be seen in Fig.2.13, the eutectic temperature appears at 228.5 ± 0.5 °C and the eutectic composition appears to fall at 97.6 ± 0.2 at.% Sn. The solubility of Sn in (Al) is a maximum of approximately 0.026 at.% Sn dissolving at 625 ± 20 °C. However, the determination of the solubility of Al in (Sn) is still unclear whereas the occurrence of the eutectic at 3.3 ± 0.5 °C below the melting point of Sn suggests that some solubility exists [144].

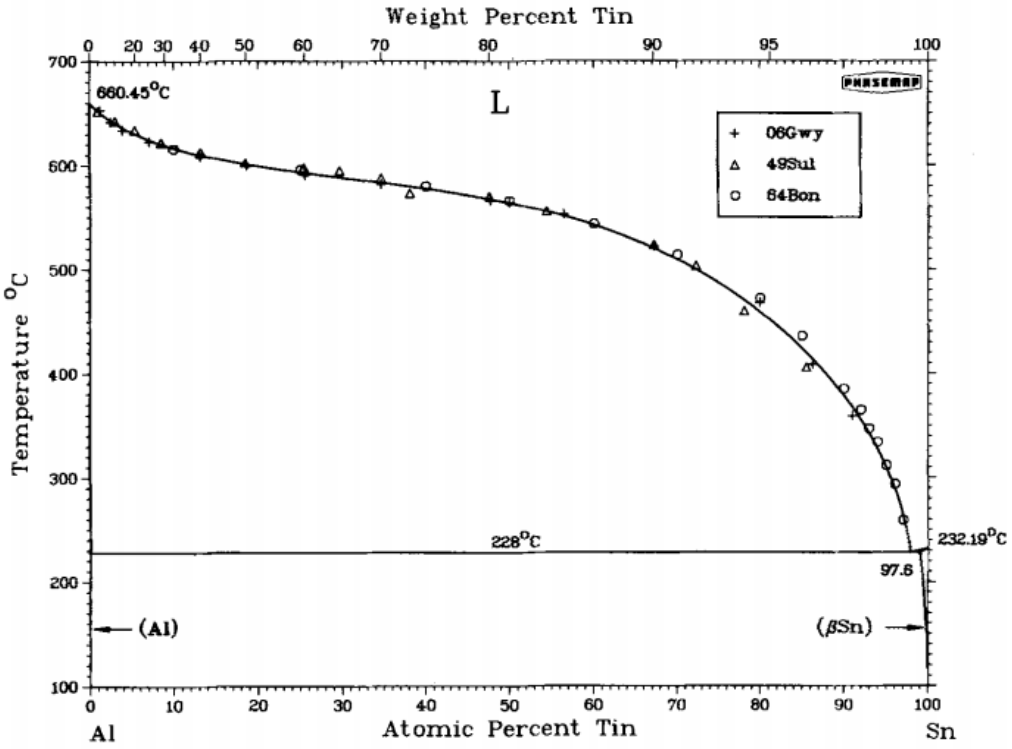

Figure 2-13 - The binary phase diagram of Al-Sn

Al Nanoparticles must be designed to be released into the solder at the optimum time in the solder reflow process so as to maximize Al reactions with the substrate while minimizing interference with solder wetting reactions. One of the key parameters is the rate at which these Al nanoparticles dissolve in liquid solder and hence this section reviews the relevant techniques. The components of a reaction couple usually have different melting points. There is a particular temperature range in which one of the components is in the liquid state and the other one in solid. In this case, the solid substance can dissolve in the liquid phase. It will be assumed that substance A has a higher melting point than substance B. If the solubility of component A in the liquid B at the temperature T is c_s, kg/m^3 (or mol/m^3), and if at a particular time of the experiment the concentration c of A in B is less than c_s, A will dissolve in B. The dissolution rate of a solid material in a liquid can be described by the following equation:

$$\frac{dc}{dt} = k\frac{S}{\nu}(c_s - c) \qquad (2.5)$$

where c_s is the metastable saturation concentration, c is concentration of the dissolved component in the liquid at the time t, S is the surface area of the dissolving component, *k* is the dissolution rate constant and ν is the volume of the liquid [145, 146].

The dissolution of a solid material in a liquid metal generally occurs in two stages. The first is migration of atoms or molecules of the solid material into the liquid metal and the second stage is mass transport of dissolved material inside the liquid metal. These two stages are called the kinetic and diffusion stages of the dissolution process respectively. If the kinetic stage timescale is longer than that of the diffusion stage, the dissolution process would be kinetic controlled and if the diffusion stage timescale was longer, the dissolution process would be diffusion controlled [147].

There are various methods to measure the dissolution rate of solid materials in liquid metals and some of the most common are listed below:

a. The first method is to measure the dissolution rate by investigating changes in weight or dimensions of the specimen. This method is very simple and is widely used. The problem with this method is that it is hard to obtain accurate results. Firstly, because the specimen needs to be removed from the melt periodically, interrupting the steady-state dissolution conditions, especially, for short-term experiments. Secondly, in some cases, an intermediate layer of intermetallic forms at the solid/liquid interface. In these cases, it is very hard to measure the dissolved layer as this intermetallic layer may be included.

b. The second method is to measure the dissolution rate by investigating changes in concentration of the solute material in the liquid metal. This method is the most widely used method.

c. The third method is to measure the dissolution rate by investigating changes in electrical resistance of the liquid metal. The advantage of this method is that the measurement can be developed continuously.

d. Another method is to measure the dissolution rate by investigating changes in liquid metal density. The accuracy of this method is estimated to be about 0.001% of the change in density of the liquid metal.

e. The fifth method is to measure the dissolution rate by investigating the degree of absorption of x-rays by the liquid metal. This experiment needs a resistance furnace with a heating element, an x-ray source (200 kV, 5mA), a cassette with film and a cassette shift mechanism. By evaluating the film density it can be found out that the concentration of metal which has passed into the solution. Photometry should be always developed at the same point on the crucible axis, as changing the angle and location of camera does affect the accuracy of results [147].

2.4.2 The mathematics of diffusion

The dissolution or consumption of a solid metal into a liquid metal is the consequence of the continuous atomic diffusion through the liquid metal/solid metal interfaces. The mathematical theory of diffusion of a metal such as Al in Sn is based on the hypothesis that the rate of diffusion of Al through a unit area of the interfacial section is proportional to the concentration gradient measured normal to the section area [148, 149]:

$$F = -D(\frac{\partial C}{\partial x}) \tag{2.6}$$

where F is the transfer rate per unit area of the interfacial section, D is the diffusion coefficient, C is the concentration of diffusion substance and x is the space coordinate measured normal to the interfacial section. In this thesis, it is assumed that the diffusion is one dimensional and the gradient of concentration is only along the x-axis, the fundamental differential equation of diffusion for time t could be rewritten as

$$\frac{\partial C}{\partial t} = D\frac{\partial^2 C}{\partial x^2} \tag{2.7}$$

Equations (2.6) and (2.7) can be referred to as Fick's first and second laws of diffusion.

2.4.3 The addition of Zn to the SAC solder as an alternative to Al

The method which has been explained in this study for supressing the Cu_6Sn_5 interfacial IMCs can be also applied to other elements with similar properties. For example, Zn can also have a similar effect on suppressing the intermetallic layers at the solder/IMC interface. Zn is one of the inexpensive metals to be used in solder alloys and has many advantages for soldering [16]. However, Zn is also reactive with Oxygen and is generally avoided in solder since as with Al, excessive oxidation of solder particles leads to poor wetting [141] even though the rate of reaction is much less than one between Al and O.

The effects of Zn addition on properties such as tensile [150, 151], drop [152] and creep resistance [153, 154] have been reported in Sn-Zn and Sn-Cu-Zn reflow soldering systems.

Zn can also be added to the solder [155-157] or Cu substrate [158] in order to form a Cu-Zn IMC layer, which acts as a diffusion barrier to decrease Cu consumption between the Sn-Cu IMC layers and the Cu substrate.

2.5 Conclusion

This chapter reviewed the main topics of this research which are nano-composite solders, cross-section polishing method and the dissolution of solid metals in liquid metals. During the nano-composite solder review, solders, nanoparticles and experimental techniques used for the fabrication of nano-composite solder were explained in detail. The creep properties of solders and the theory behind the creep were also investigated. As the efficiency of the nanoparticles in improving the creep properties of solders depends on the interaction between grain boundaries and nanoparticles, the grains and grain boundaries were explained in detail. Also different methods for observation of grains were shown. As IMCs in solders play an important role in defining the microstructure of solders, their characteristics were also investigated.

In the cross-section polishing section, the necessity and needs for this technique were explained. A brief detail of this method along with schematic pictures of the action of the CSP instrument was also shown. Also this section included alternatives to the CSP method. The advantages and disadvantages of this method were also illustrated.

In order to review the dissolution of metals in liquid metals, a brief review of the measuring methods for dissolution rate of a solid metal in a liquid metal was demonstrated. Theory and mathematical background of dissolution were also reviewed in this chapter.

3 Cross-Section Preparation for Solder Joints Using Argon Ion Beam Milling

3.1 Introduction

Mechanical grinding and polishing has been used for sample preparation for SEM because of its low cost of use as well as ease of preparation. However, mechanical polishing can distort and damage delicate samples. This chapter is about a method of using CSP based on argon ion milling to cross section the sample without damaging it. In this method the argon ion beam is produced and directed towards the sample and shield plate to mill the unshielded part of the sample. In this chapter, the interaction between solder and Cu substrate, ENIG, and inert (glass) substrates was investigated with both methods of polishing i.e. mechanical polishing and CSP, and the results of both methods were compared. In this chapter, the emphasis will be on studying IMC structures and grain boundaries, and on the use of the argon ion beam as an alternative to mechanical polishing. Lead-free solder paste SAC samples were prepared on Cu substrate, ENIG, and inert (glass) substrates. In Chapter 4 the CSP method used for detecting nanoparticles in solders is reported.

3.2 Experimental procedure

For observation of SAC solder on the inert substrate, a small amount of solder paste was placed on a microscope slide which was then placed inside a bench-top oven (Benz Ltd MRO 160). The paste was preheated for 150 s at 140 °C and soldered for 60 s at 260 °C. Immediately after the soldering stage, while the solder was molten, a heated metal weight (also placed inside the oven during the reflow) was placed on the solder to reduce the solder thickness down to 0.410 mm

(thickness controlled by spacers). Although the CSP can accommodate samples up to 2 mm thick, thinner samples reduced the preparation time.

For the SAC solder on Cu substrates, 0.8 cm x 0.8 cm x 0.25 mm copper foils were used. SAC solder paste weighing 0.05g was placed on the Cu foil supported by a glass side and reflowed using the method described above for glass. ENIG pads were used for the SAC solder on Ni substrates. The metal pad and top layers of the printed circuit board (PCB) were peeled off the glass fiber reinforced PCB, leaving a substrate thickness of 0.25 mm.

Cross sections of these samples were prepared using the CSP and mechanical polishing. For the CSP, the samples were attached onto the mounting block using a thin layer of wax heated to 100 °C. The block was then positioned with the sample jutting out approximately 50 μm from the shield plate (see Fig. 3.1) and the milling chamber was filled with low pressure Ar gas. The accelerating voltage (typically 5.0–5.5 kV) of the ion beam and milling time (typically 24–35 h) were set and the CSP was allowed to operate without further intervention. The optimum settings for the CSP were established by using the CSP manual and also trial and error. Using the CSP polishing for less than 24 hours for a metallic sample was not sufficient and longer than 35 hours was unnecessary. Also 5.0 kV was the lowest accelerating voltage of ion beam for effective cross-sectioning of a metallic sample. Further details on the operation of the CSP can be found in [9]. After the cross sections were formed, the samples were etched using 4 kV for 30s (see Fig. 3.2).

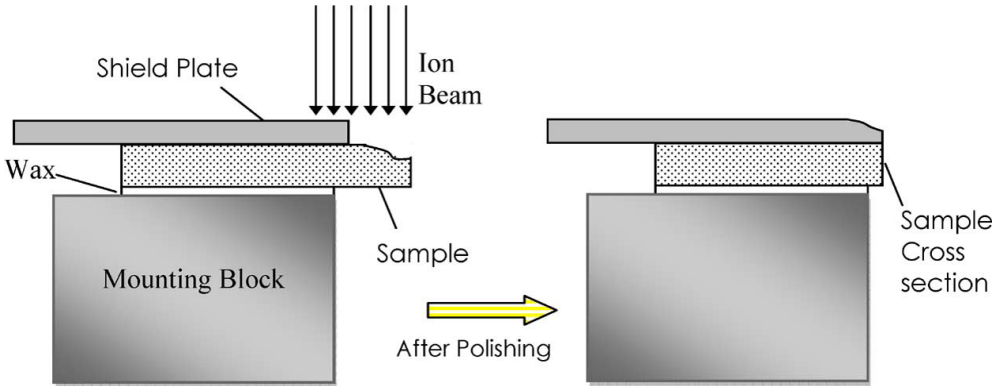

Figure 3-1 - Schematic of CSP operation for cross-section preparation [9].

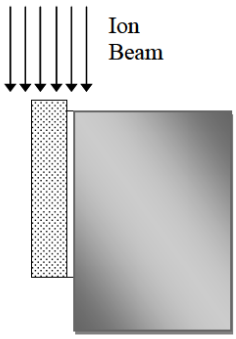

Figure 3-2 - Schematic of CSP operation for etching [9].

Mechanically polished samples were soldered following the same procedure as the CSP samples (including the use of a weight to reduce sample thickness). They were then cold mounted in a standard epoxy potting compound. The mounted SAC samples were then polished using P240-, P600-, and P1200- grit silicon carbide papers for about 5 minutes for each paper (Fig. 3.3). Next, the samples were polished using diamond suspensions of 3 μm and finally 0.25 μm. Finally, the cross sections were etched in a solution of 2% nitric acid in water for 10 s.

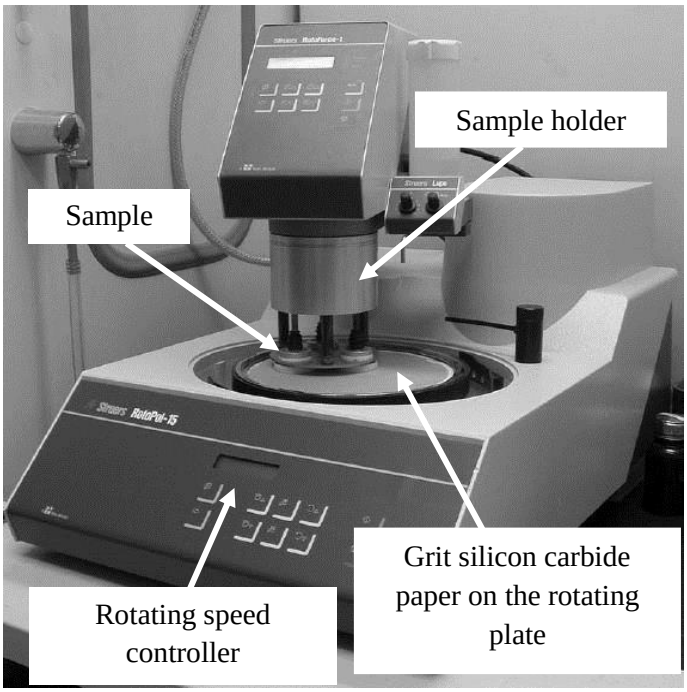

Figure 3-3 - Mechanical polisher

3.3 Results and discussion

CSP works in this chapter were performed by an MSc student, Yunqi Wang, under my supervision. My contribution to this chapter was to teach the MSc student the instruction of using the CSP and also monitoring the process of cross-sectioning by reviewing the pictures taken by SEM after polishing by the MSc student. In order to compare the mechanically polished and CSP images, the same settings such as magnification and voltage were applied in taking pictures by SEM. Fig. 3.4 presents images of the bulk solder samples (solder on inert substrate). Although these are taken from different areas, both are representative examples of the bulk microstructure. While both methods show the IMC structures in detail, only the CSP prepared image simultaneously shows details of the β-Sn phase as the etching has removed details of this phase from the mechanically polished sample.

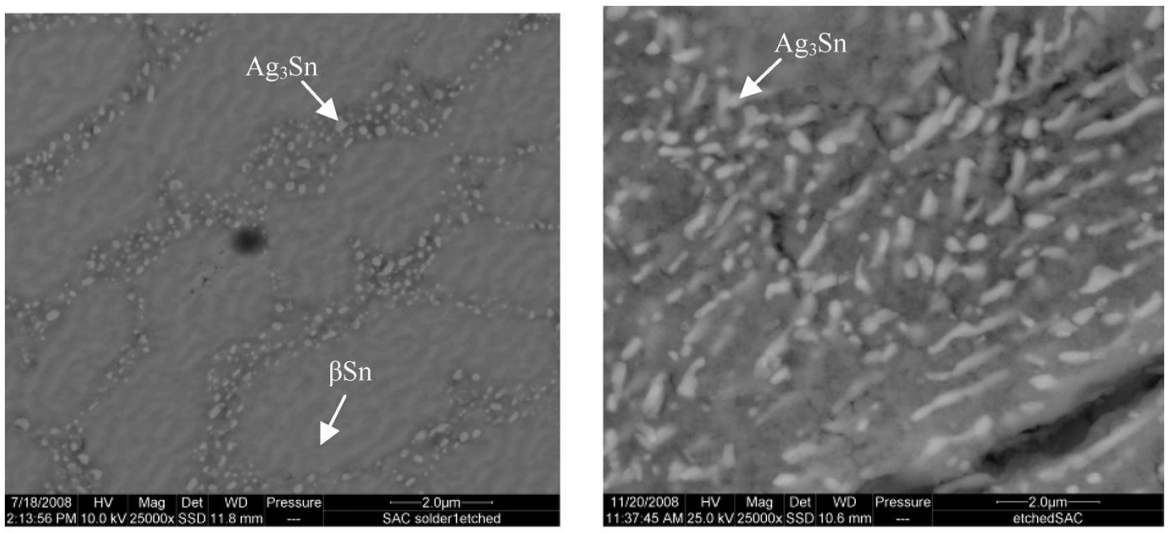

Figure 3-4 - SEM cross-sectional views of SAC bulk. (a) SAC solder sample was polished and etched using CSP, (b) SAC solder sample was mechanically polished and chemically etched

Comparison of the SAC on Cu samples is shown in Fig. 3.5(a) (CSP) and 3.5(b) (mechanically polished). There appears to be a large difference in size between the two samples even though they were prepared under identical conditions. The discrepancy may be caused by the fact that for sample 3.4(a) the cross section was taken 75 μm from the edge of the substrate while for 3.4(b), the grinding and polishing operations resulted in a section further in towards the center. The diffusion and IMC formation kinetics at the solder bump edge are faster than in the middle due to the "edge effect" (see section 2.2.4 Geometry of solder and the "edge effect"). It is also clear that the mechanical polishing resulted in scratches and embedded particles (both Silicon carbide and diamond).

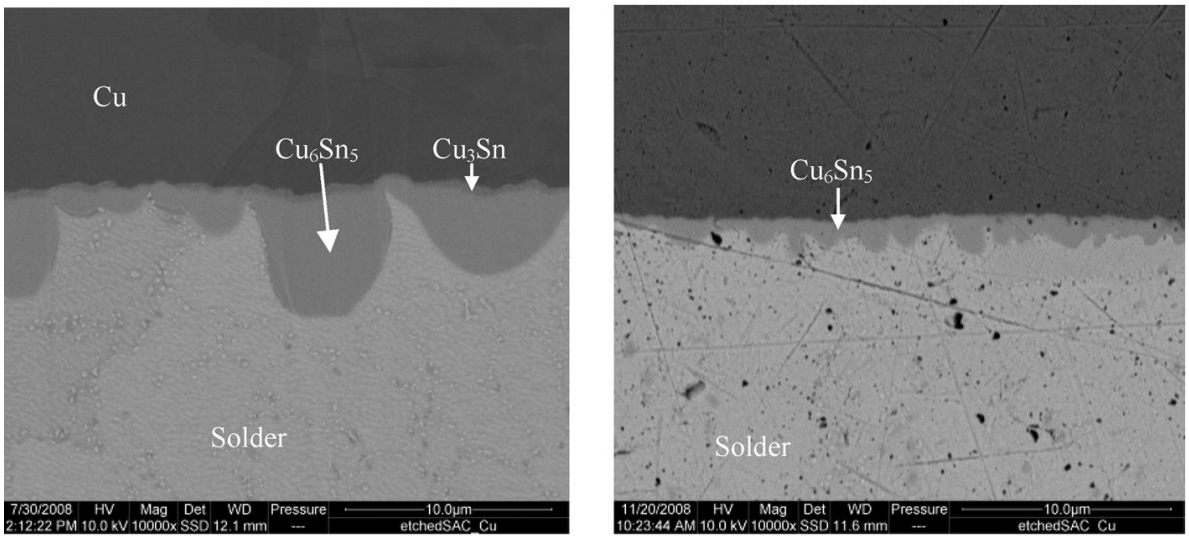

Figure 3-5 - SEM cross-sectional views of IMC in SAC on Cu substrate. (a) SAC on Cu substrate polished and etched by ion beam miller. (b) SAC on Cu substrate polished mechanically and chemically etched.

Fig. 3.5 also shows that the CSP method was able to simultaneously define the crystalline structure of the Cu substrate and both the Sn and Ag-Sn phases in the solder while the mechanically polished sample was unable to show details of the Cu substrate or the bulk solder. Although the CSP method shows a Cu_3Sn IMC layer that is not present in the mechanically polished sample, this may be due to the smaller IMC layers present in the latter.

Next, SAC on Ni samples were examined and are shown in Fig. 3.6. Again, the limitation of the CSP only being able to image samples 75 microns from the edge of the sample is apparent as the solder is only a few microns thick at the edge of the pad Fig. 3.6(a). These result in a markedly different microstructure from the mechanically polished sample sectioned through the middle of the pad Fig. 3.6(b). Of course, the sample could first have been cut through the middle of a pad with a diamond saw, but the saw can induce cracks or other features artificially. One way of avoiding this problem might be to mill away 75 micron slices of the sample sequentially but this

would be time consuming. An additional artefact induced by the CSP was the vertical striations caused by the ion beam. These can be eliminated by increasing beam voltage and decreasing milling time. Superior quality mechanically polished samples can be viewed in refs. [1], [4], [10], but results suggest that the CSP is able to image more aspects of the microstructure than mechanical polishing. However since only one comparison has been made for each case (Fig. 3.4 - 3.6), further comparison could be done as a future work.

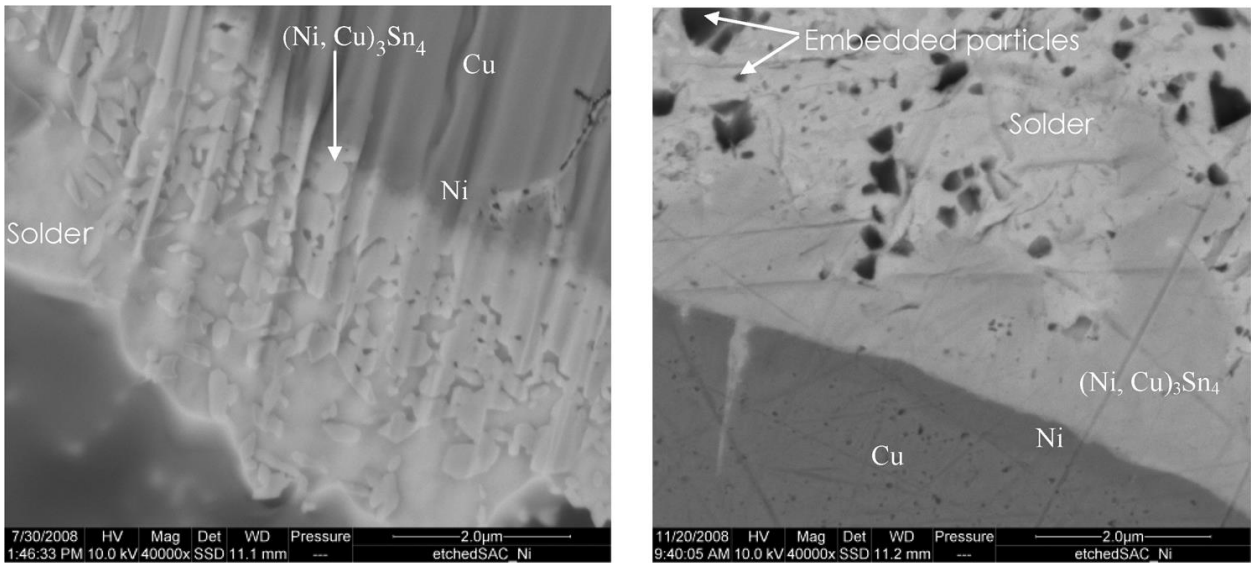

Figure 3-6 - SEM cross-sectional views of IMC in SAC on Ni substrate. (a) SAC on Ni substrate polished and etched by ion beam miller (b) SAC on Ni substrate polished by mechanical polishing and etched chemically

To investigate further details of SAC solder morphology, more images of SAC which were revealed with the CSP and were not generally observed with mechanical polishing have been studied. The CSP method reveals variations in composition inside IMC structures as shown in Fig. 3.7 where it can be seen that the core of the Ag_3Sn IMCs contains dark spots which were found by SEM equipped with an energy-dispersive x-ray spectroscopy (EDX) to have depleted levels of Ag. Fig. 3.8 shows a large Ag_3Sn plate IMC with detailed internal platelet like structures. K.S. Kim *et al.* [63] have also shown a detail microstructure of Ag_3Sn IMCs in a

SAC solder matrix after polishing with 0.05 µm Al_2O_3 powders and deeply etching with 5%HCl-95%C_2H_5OH solution for several seconds. In the represented images, it is clear that the large Ag_3Sn are platelets with a similar structure as Fig. 3.8.

Fig. 3.9 shows primary Ag_3Sn and Cu_6Sn_5 IMCs dispersed within bulk SAC solder and reveals that each Cu_6Sn_5 crystal is in contact with a Ag_3Sn crystal. Other researchers have also reported similar dispersed Ag_3Sn IMCs within bulk SAC solder but Cu_6Sn_5 IMCs in contact with Ag_3Sn were not represented in their results. However, they have used different experimental procedures. For example, Takamatsu *et al.* [159, 160] have grounded cross section of solders using SiC papers (180 to 4000 grit) or alumina slurry followed by polishing with colloidal silica and if necessary with the addition of slight etching for *β*-Sn. In addition, F. Ochoa *et al.* [161] polished the cross sections to a final finish of 0.05-µm colloidal silica solution followed by etching in a solution of 10 vol.% hydrochloric acid.

While grain boundaries in SAC solders can be observed using optical microscopy, or revealed using selective chemical etching, the CSP method reveals both grain boundaries and IMC location. Fig. 3.10 reveals a Cu_6Sn_5 IMC at the intersection of three Sn grains.

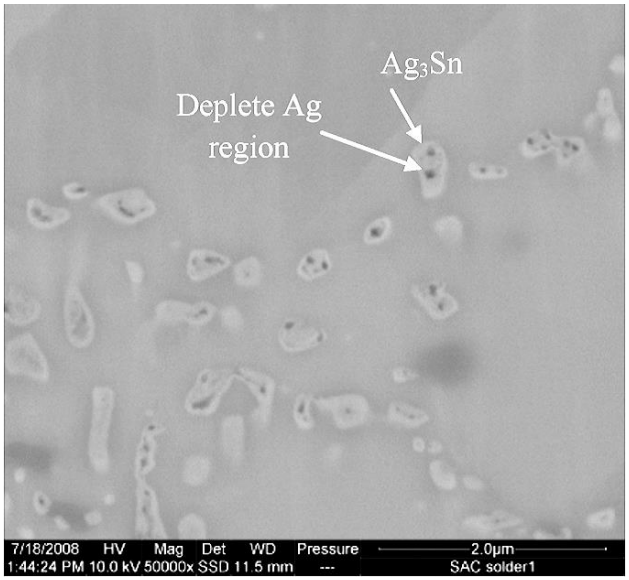

Figure 3-7 - Bulk SAC solder prepared by CSP showing detail of primary Ag_3Sn

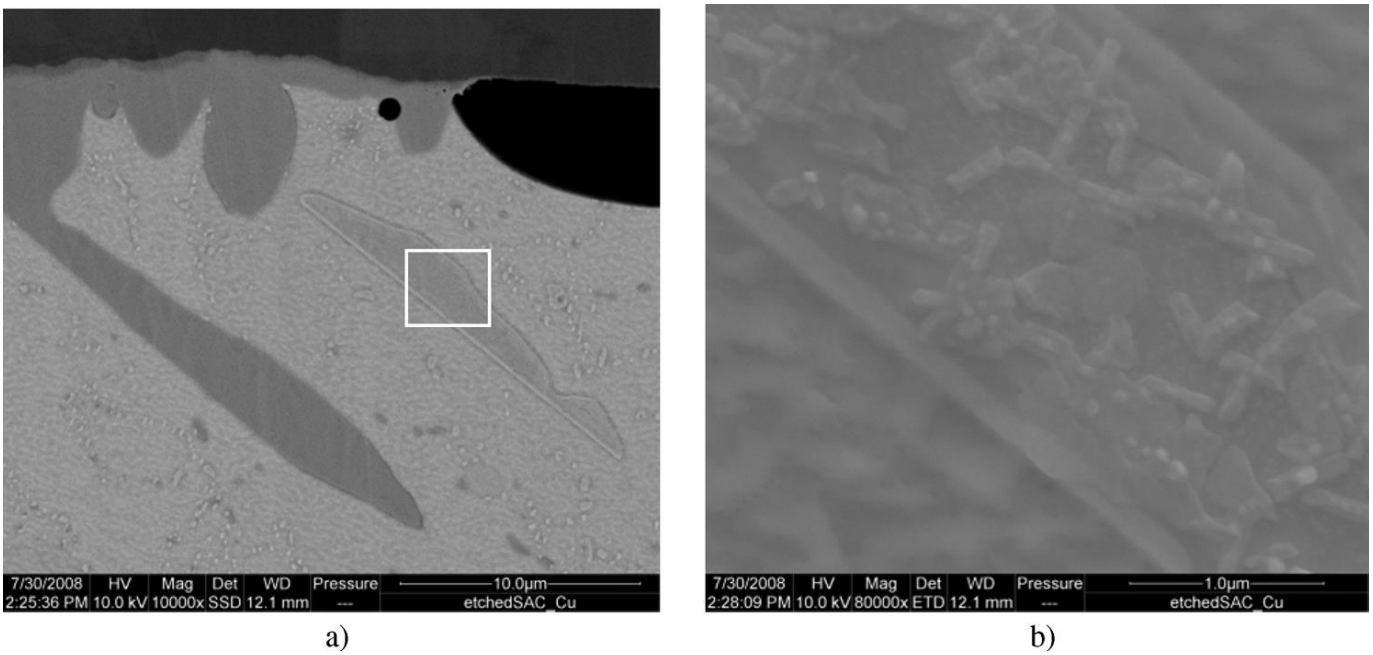

Figure 3-8 - (a) Large Ag Sn plate in SAC on Cu sample prepared by CSP and high magnification of inset in (b)

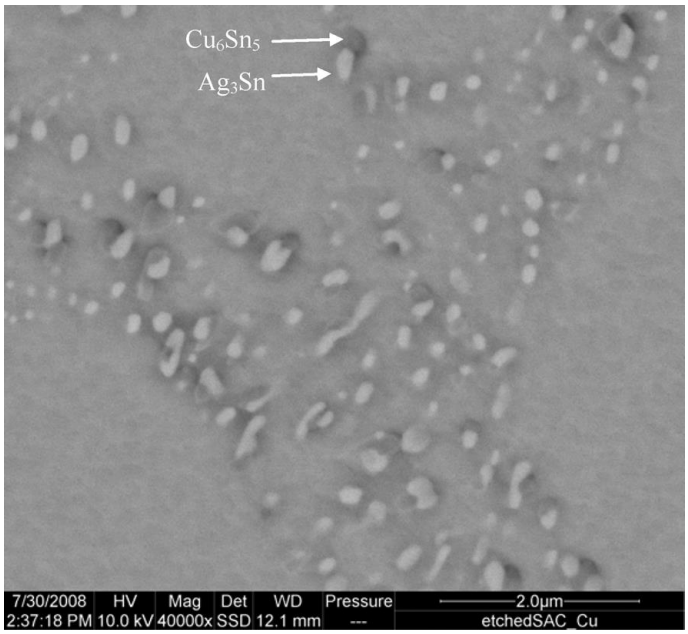

Figure 3-9 - Bright Ag_3Sn and darker Cu_6Sn_5 IMCs dispersed in SAC solder

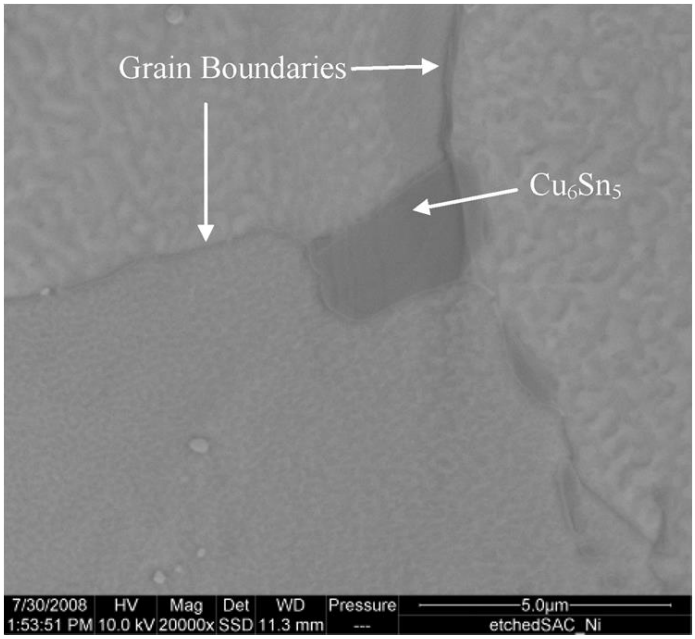

Figure 3-10 - Backscattered cross-sectional image of bulk SAC (from SAC on Ni sample)

3.4 Conclusion

This chapter presented a new method of using Cross-Section Polishing by argon ion beam to cross-section the sample. While mechanical polishing remains the quickest and cheapest method of obtaining cross sections suitable for SEM imaging, the CSP has benefits in a number of scenarios. First, when the sample is composed of delicate or brittle structures, mechanical polishing may not be an easy option [9]. Second, the CSP is easier to mechanical polishing when the system contains structures encompassing a large range of hardness. The third benefit will be of particular value for failure analysis when the nature of the problem will not *a priori* be known. Certainly more specialized techniques such as transmission electron microscopy (TEM) or FIB could be used to focus on individual features, but the CSP is able to deliver a detailed overview. CSP has disadvantages as well. One disadvantage of CSP is the limitation in mounting a sample inside the CSP chamber for polishing. Polishing further than 75 μm from the edge of the sample is impossible as 75 μm is the maximum length which can be jutted out from the shield plate to be polished. This problem can be avoided by milling away 75 micron slices, however, this would be time consuming.

4 Nano-Composite Solders

4.1 Introduction

Due to environmental concerns, traditional eutectic tin-lead solder is gradually being replaced by “lead-free” solders (see section 2.2.1 Lead-free solders). During this transition, nanoparticle technology is also being investigated in order to explore the possibility of making major improvements in joint reliability for harsh environments such as high impact loading and high temperature situations [162].

Potential replacements for tin-lead include SAC, SnAg, SnCu, SnZn, SnBiAg and SnInAg [51]. While these alloys have proven suitable for application temperatures up to 125 °C, many electronics applications in the aerospace, automotive and oil and gas drilling sectors require application temperatures in excess of 150 °C. Deformation in these high temperature environments due to creep is one of the main problem with these alloys [163]. SAC is generally the most recommended lead-free soldering alloy for reflow soldering because of its mechanical strength, low-melting point, adequate wetting properties and good availability [51, 164, 165]. Hence this SAC solder is used as the base solder for this chapter, to which nanoparticles have been added.

Metals and alloys can be strengthened by the presence of fine second-phase particles, e.g. foreign dispersoid particles. The particles also increase fatigue resistance and creep strength by retarding grain boundary sliding [162] (see section 2.2.8 Zener Pinning). The dispersed particles can serve as obstacles to grain growth and coarsening of the solder microstructure by exerting a pinning force on migrating grain boundaries. While traditionally the dispersed particles are in the micron size range, theoretically the maximum benefit is obtained with the smallest particles

[166]. These should also be uniformly sized and homogenously distributed within the solder in order to impede grain boundary sliding and dislocation movement [107, 114, 115].

The ultimate aim of the research reported in this chapter is to reduce fatigue and solder joint failure in electronic packaging industry by increasing creep resistance. Hence the mechanical properties of nano-enhanced solder are investigated at elevated temperatures to study its capability for high temperature applications. Nanoparticles were added to the solder to limit the grain growth and grain boundary migration during a hot compression test. The purpose of using nanoparticles is thus to first limit grain growth which happens during solidification and second, to limit grain boundary movement which happens after solidification, driven by thermo-mechanical effects. As a result of the experiments and calculations reported in this chapter, only the second limiting effect is predicted to occur. As the efficiency of the pinning effect of nanoparticles is dependent on the degree of grain boundary-particle contact [116], only nanoparticles which are located at grain boundaries can effectively pin the grain and limit their movement. Fig. 4.1 illustrates the nanoparticle role in limiting grain boundary movement during hot compression.

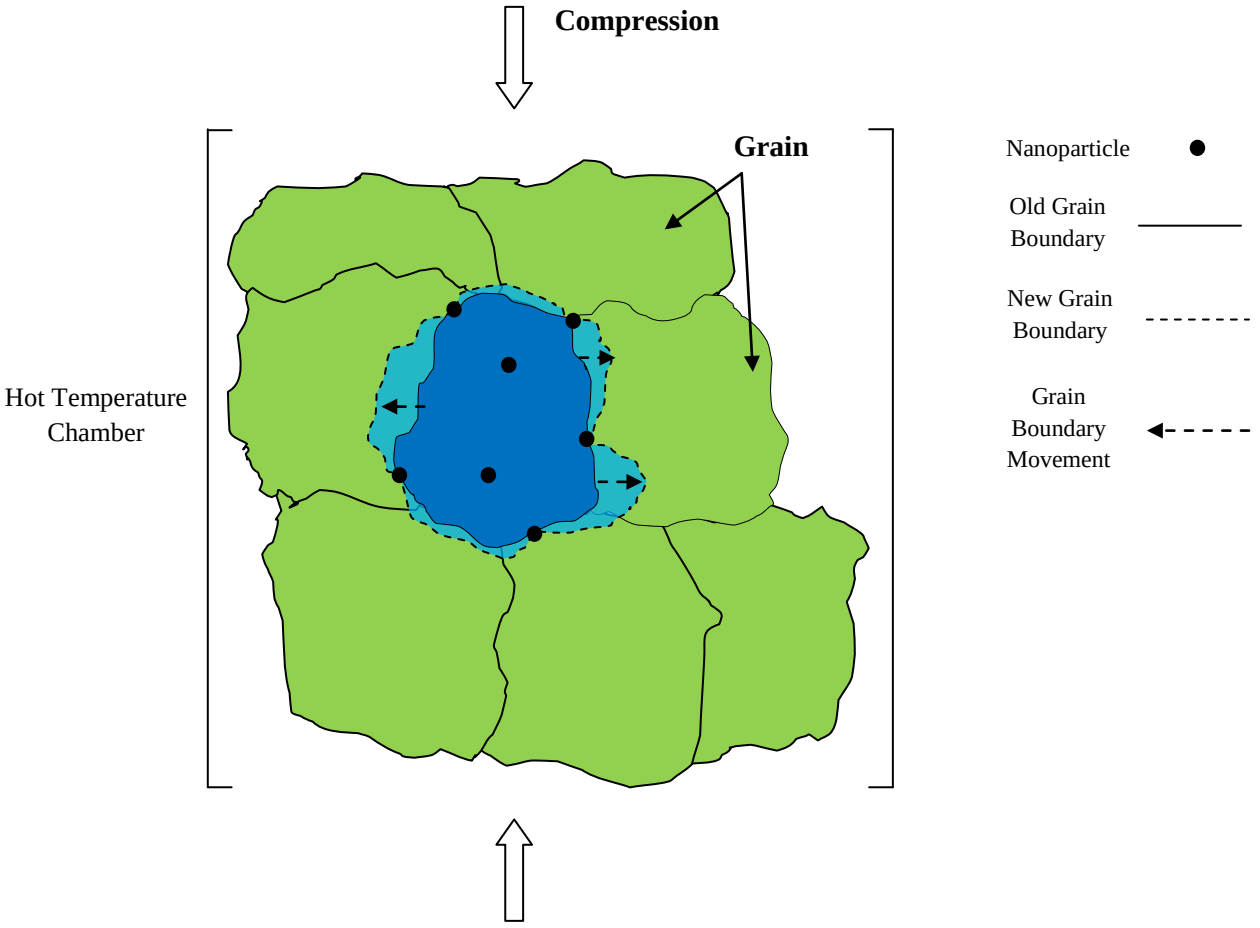

Figure 4-1 - A schematic image of nano-composite solder after reflow and during hot compression test, assuming effective pinning.

There are various methods of adding nanoparticles to the solder in order to enhance the mechanical properties [108, 127] (see section 4.2.1.1 The fabrication of nano-composite solders). In this research 100 nm silica nanoparticles were added to the solder to improve the mechanical properties. Parallel to this, 250 nm silica particles were added to the solder to ease the particle identification in the solder. Nanoparticles were mixed with solder paste and only incorporated with the solder during the reflow soldering. To ensure solder wettability,

nanoparticles were composed of a silica core and Au metallic shell. Synthesis of the nanoparticles was carried out by Dr. Roya Ashayer [167] whereas my main contributions concerned specimen preparation for observation of nanoparticles embedded in solder, mechanical testing of the composite and standard solders, and analysis of the resulting microstructure and stress-strain data. Table 4-1, shows a brief overview of the steps required for this research.

Table 4-1 - Research covered by this chapter step by step

4.3.1	SAC paste and nanoparticle enhanced SAC paste preparation
4.3.1	Nanoparticle observation within solder matrix
4.3.2	Soldering (reflow)
4.4	Compression test at room temperature
4.4	Hot compression test
4.4	Microstructure analysis of SAC and SAC with nanoparticles before and after hot compression
4.4	Generating mathematical model for relationship between the variation of thermal displacement of the grain boundary, d, and temperature, T
4.4.1	Generating mathematical model for relationship between activation energy and threshold stress

4.2 Methodology

4.2.1 Nanoparticle enhanced solder paste preparation

The fabrication of nanostructures which are made of a dielectric core and metallic shell, called "nano shells", is a subject of an extensive research due to their unique applications in many areas [168-171]. As these types of nanoparticles are stable and their preparation is easy and well-established, they have received a particular attention. Silica was chosen as a core because of its availability and ease of production. In order to the incorporate the nanoparticles into the solder a wettable coating of e.g. Au was required. The detail of the preparation of the nanocomposite solder has given elsewhere [167].

4.2.1.1 The fabrication of nano-composite solders

According to the literature, there are two popular methods to prepare nano-composite solders which are the mechanical mixing method and the in-situ method [127]. Well-dispersed reinforcements can be obstacles to crack growth, grain growth, dislocation motion, and also can strengthen the solder against creep and fatigue deformation [172].

4.2.1.1.1 Mechanical mixing method

The mechanical mixing method is based on adding nanoparticles into solder matrices. Different mechanical mixing methods for nano-composite preparation [127] are outlined in the following sections.

4.2.1.1.2 Mixing solder powders with nanoparticles

There are two methods of mixing solder powders with nano-sized reinforced particles. The first uses solder alloy powders and the second one is mixing pure Sn or Ag powder. In the first method, nano-sized particles are added to standard solder alloy (e.g. SnCu or SnCuAg powder)

to prepare the nano-composite. Once solder powders are blended, flux is added to form the blended nano-composite solder paste. The mixture is stirred to provide homogeneous distribution of nanoparticles inside the paste. The second method is using nano-sized particles added to a pure Sn (-100 mesh, purity 99.85 wt. %) or pure Ag (5–8 mm, 99.9 wt. %) powder. Flux is then added to the mixture, and mixed until a uniform mixture is achieved [56, 127, 173].

4.2.1.1.3 Mixing solder pastes with nanoparticles

This method has proven to be the simplest method to prepare nano-composite solder paste. To prepare the nano-composite, nanoparticles are added to the solder paste directly. Once nanoparticles are added to the paste, the mixture is mechanically mixed in a ceramic crucible for at least 15 minutes to ensure homogenous distribution of nanoparticles within the solder paste [127].

4.2.1.1.4 Mixing molten solder alloy with nanoparticles

In this method, the solder alloy ingot and the precise amount of nanoparticles are put inside the crucible. The crucible is placed in a chamber, chamber was vacuumed and the desired pressure was achieved. High-purity argon is imported inside the chamber. A temperature-controlled arc generator is used to melt the mixture. An electromagnetic stirrer is used to mechanically stir the mixture for at least 15 min to ensure uniform distribution of the reinforcement particles has been achieved [127]. This method can be used to make nano-composite solder for testing.

4.2.1.1.5 In-situ method

The in-situ method is based on forming the reinforced nanoparticle phases, during the processing of the bulk solder alloys. One popular in-situ method is using rapid solidification technology. In this method which was used by Shen et al. [174], which is a rapid solidification technique, a Sn-3.5Ag composite solder was prepared from bulk rods of pure Sn and Ag. The

melting process was carried out in a vacuum arc furnace under a high purity argon atmosphere. In order to prepare a homogeneous composition, the alloy was remelted four times in order to get a homogenous composition within the ingot. After this, the molten alloy was cast into a water-cooled copper mould. The rapid cooling rate promotes the nucleation of Ag_3Sn IMC particles and leads to rapid heat dissipation during solidification which makes the long-range diffusion of Sn and Ag atoms impossible. Using this method the nucleation of Ag_3Sn IMC particles was greatly increased but their growth in the eutectic matrix was suppressed [127]. The disadvantage of this method is that unlike ceramic particles, the nanoparticles are not chemically inert and their size and composition may change over time.

4.2.2 Reflow soldering of solder paste

The reflow soldering process heats the PCB and the solder paste so that solder paste melts, kinetically wets and finally solidifies to form the desired solder joints (see section 2.2.2 Reflow soldering). Soldering can be achieved through different heat-transfer modes, which each has advantages and limitations in performances, cost, and operational efficiency depending on materials and product volume. Table 4.2 shows a comparison between various types of reflow methods [18].

Table 4-2 - Reflow methods [18].

Reflow method	Advantages	Limitations
Conduction	• Low equipment capital • Rapid temperature change • Visibility during reflow	• Planar surface and single-side attachment required • Limited surface area
Nonfocused infrared	• High throughput • Versatile temperature profiling and processing	• Mass and geometry dependency

	parameter	
Vapour-phase condensation	• Uniform temperature • Geometry independence • High throughput	• Difficult to change temperature • Temperature limitation • Relatively high cost
Hot gas	• Low cost • Fast heating rate • Localized heating	• Temperature control • Low throughput
Convection	• High throughput	• Slow heating
Induction	• Fast heating • High temperature capability	• Applicability to nonmagnetic metal parts only
Laser	• Localized heating with high intensity • Short reflow time • Packaging crack prevention • Superior solder joint	• High equipment capital • Specialized paste requirement • Limit in mass soldering

According to the literature, the most common reflow method is convection and temperature for Sn-Ag-Cu solders is in the range of 250-260˚C so in this research the reflow temperature is set at 260˚C [175]. In the current study, the solder paste was preheated for 150 s at 140°C and ('reflowed') for 60 s at 260°C.

The addition of nanoparticles did not change the soldering temperature. Since only 0.1 vol.% of the added nanoparticles stay in the solder during the reflow (see section 4.3.2) and 4 vol.% of each nanoparticle is Au, therefore, the addition of Au to the solder matrix is around 4×10^{-5} by

volume. Accordingly, the effect of adding Au to the melting point of the new solder is negligible. Moreover, the reflow profile was modified to the shortest possible soldering time to prevent nanoparticles being expelled from the solder during the reflow (see section 4.3.2).

4.2.3 High temperature test protocols

As it has been mentioned before, the objective of this research is to provide a solder composite for high temperature applications. There are several test methods for investigation of the solder reliability during a life of the product at high temperature operational situation. One of them is applying humidity, pressure and heat over a long period of time (autoclave test). Another is to apply temperature cycling. Also, another method to investigate the strength of the product under force and temperature is the hot compression test. In this case the force and temperature are applied to the product for a short time. In this research, this last method was chosen for the investigation of the reliability of the samples for high temperature applications. This method was chosen taking account of the available facilities at King's College London and at the collaborating institution Sharif University of Technology in Iran.

4.2.4 Compression test

Creep testing can be carried out with a constant load at elevated temperature by either tension or compression [176, 177]. Until recently, a number of studies on Sn-Ag-based solders at strain rate from 10^{-6} s^{-1} to 10^{-1} s^{-1} at multiple temperatures using various techniques have been reported [34, 178-184]. Compression testing my pose problems due to confinement issues affecting the uniaxial testing results [185].

This research performs compression testings in order to plot the stress-strain curve. The solders in this study were first cast into samples having a cylindrical geometry with dimensions of 4.8 mm diameter and 50 mm length. The stress-strain tests in this study were performed at the strain

rate of 0.001/s. This slow strain-rate is more closely resembled the strain-rate regime characteristic of thermal mechanical fatigue deformation [186].

4.2.5 Grain size measurement techniques

There are different methods to observe grains of a solder. One of the methods is using optical microscope under bright-field and cross-polarized light imaging in order to identify different Sn grains.

Sn as a birefringent material makes this possible. So, Sn crystals make a small rotation in the reflected polarized light angle. By viewing the reflected light through an analysing polarizer, the contrast which depends on the grain orientation can be seen [10, 187, 188]. Fig. 4-2 shows a cross-polarized light micrographs of SAC solder:

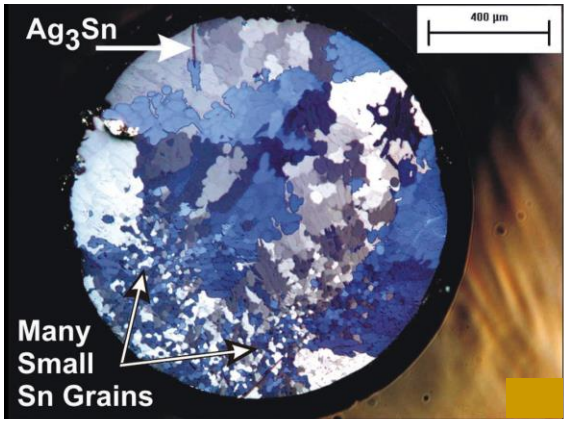

Figure 4-2 - Cross-polarized light micrograph of SAC solder [10]

Another common method to observe the solder grain is using electron back-scattered diffraction (EBSD). EBSD is a materials analysis technique which obtains crystallographic data from the specimen. EBSD has its unique capabilities of diffraction and imaging with a spatial resolution of 0.2-0.3 µm, which are all combined with regular capabilities of an SEM. When an electron beam enters the specimen, it is Bragg diffracted in three dimensions. A phosphor screen near the

sample inside the SEM chamber captures the back-scatter diffracted electrons to form an image on the screen. The generated image is a pattern of intersecting bands. The formed diffracted patterns consist of pairs of parallel lines which intersect at various places (Fig. 4.3). The geometrical arrangement of these bands is a function of the orientation of the crystal lattice. EBSD technique allows a spatial arrangement of lattice orientation on the surface of a sample to be mapped [189, 190].

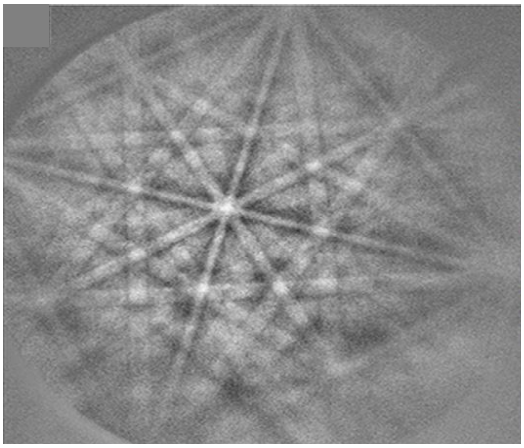

Figure 4-3 - EBSD pattern [7]

Colours are also used to define grains, in which clusters of the same colour are part of the same grain and share a common orientation. Fix 4.4 shows a colour map of a SAC solder which is generated by EBSD [7].

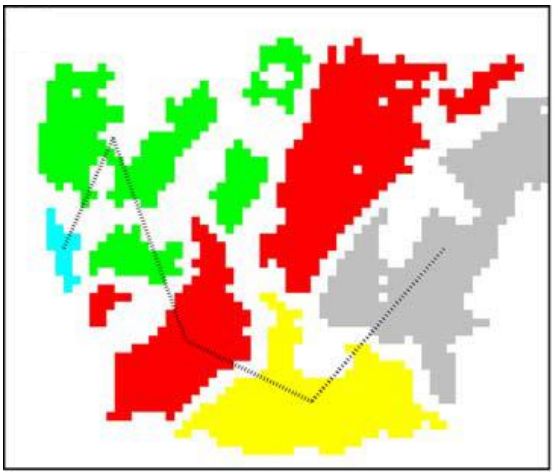

Figure 4-4 - Colour map: each colour presents a unique grain domain [7]

Etching the sample in order to make grain boundaries visible is another method for observation of grains. In most cases the polished sample is immersed in a diluted acid. Strong acid may etch some grains as well as grain boundaries which makes the sample over etched [97]. Another method of etching uses a CSP to etch the surface by bombardment with Ar ions and this is explained in detail in chapter 3. According to the facilities at the Division of Engineering at King's College London, this method was chosen as the method for grain observation. Fig. 4.5 shows a cross-section of SAC solder with clear grains and grain boundaries which is etched by CSP. In this image, grain boundaries are dark lines which separate grains.

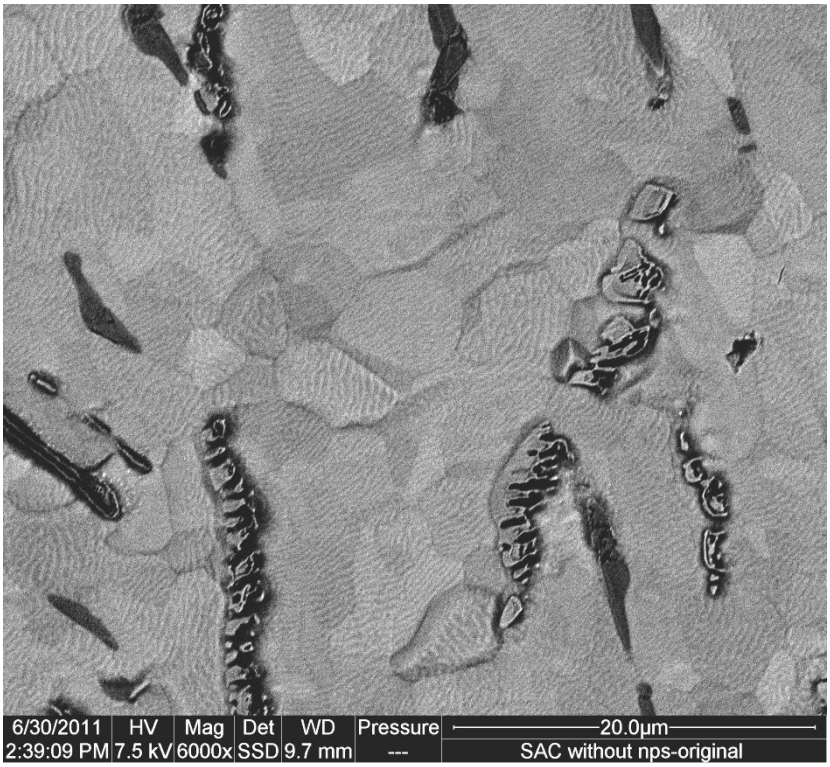

Figure 4-5 - A cross-section of SAC solder with clear grains and grain boundaries after etching by CSP

Fig. 4.5 is taken using a SEM which is one of the most practical instruments used to analyse the microstructure. SEM provides an image by acquisition of signals which are produced from the interactions between an electron beam and the specimen. In this thesis the field emission gun scanning electron microscopy (FEGSEM) is used which is facilitated with EDX which is an analytical technique for chemical characterization and elemental analysis of the sample [191].

Another method is to use an optical microscope under bright-field and cross-polarized light imaging in order to locate and identify the different phases [10]. Another study performed orientation imaging microscopy (OIM) using electron backscatter diffraction which was followed by developing orientation maps, pole figures and misorientation plots using TexSEM analysis software [192].

As was explained, there are various techniques for grain size measurements, such as EBSD, colour-polarized light imaging, and image analysis. As the EBSD facilities were not available on the campus, this method was not used. The colour-polarized light imaging and image processing method poses difficulties for the case of Sn-Ag-Cu solder. The reason was that Sn-Ag IMC plates introduce high noise levels for the image processing. Thus, the grain sizes were measured manually from the SEM images for the samples. In order to do the manual measurement samples were mechanically polished and etched by CSP. Five different areas of each sample were evaluated for the grain size measurement to gain the most accurate average results.

In the manual method in the current study, six different diameters of a grain were measured by choosing each diameter horizontally after rotating the image through 30 degrees. This method has given an average diameter for each measured grain. A schematic illustration of the manual grain measurement is shown in Fig. 4.6.

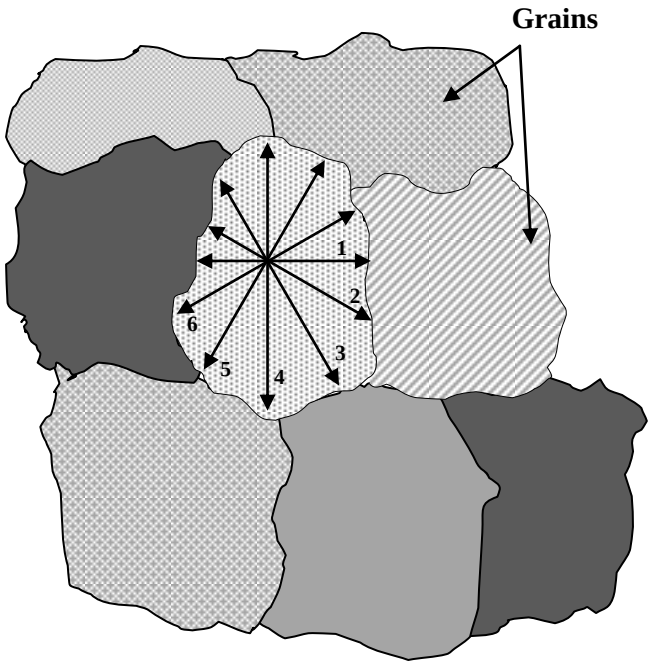

Figure 4-6 - A schematic illustration of the manual grain measurement

4.3 Experimental procedure

4.3.1 Nanoparticle observation

Nanoparticles are suspended in a solvent compatible with the flux, and then mixed with the flux, which is finally mixed with the Sn3.8Ag0.7Cu solder powder to form a solder paste. The preparation processes of nanoparticles are described elsewhere [167, 193]. The solder paste is reflowed in a bench top oven and cross sectioned using the CSP for 24 hours at 5.5kV ion accelerating voltage.

The advantage of this ion beam milling technique is that no hard polishing particles (e.g. diamond or Silicon Carbide) are embedded in the solder during preparation. By using the mechanical polishing method polishing particles would embed inside the solder resulting in

confusion in detecting nanoparticles. For Fig. 4.7, slightly larger (250 nm diameter) silica particles have been used to ease particle identification; 100nm silica particles are less easy to spot. These images were taken by a FEI QUANTA 200F Field Emission SEM which was equipped with EDAX, that allowed the SEM to detect and identify the silica nanoparticles. The EDAX system is supplied by AMETEK EDAX and the EDAX system software is Genesis Spectrum SEM Quant ZAF Version 3.60. One of the main advantages of CSP in sample preparation was clear in this case. If samples were polished by the mechanical polishing technique, embedded silicon carbide polishing particles would look like silica nanoparticles, resulting in confusion regarding silica nanoparticles detection.

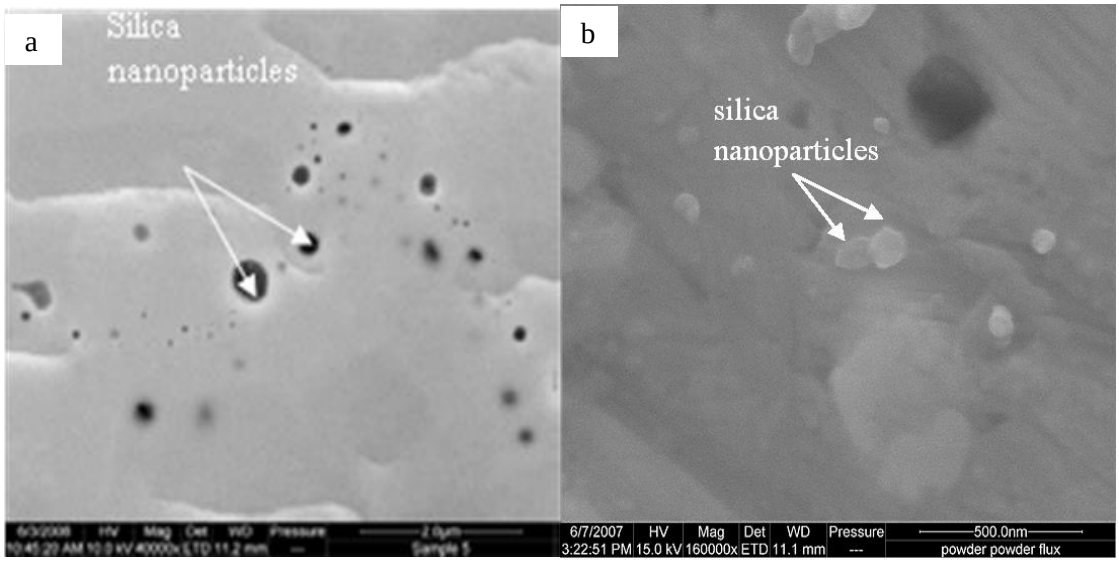

Figure 4-7 - Cross section of reflowed solder showing silica nanoparticles embedded within solder a) 250nm diameter particles b) 100nm diameter particles

4.3.2 Mechanical testing

To prepare solder paste without nanoparticles, 88.5% solder powder (SAC387; average particle diameter 30 μm) and 11.5% flux (LF318) were mixed mechanically for 10 minutes to produce a homogenous solder paste. A small amount of solder paste was placed on a glass microscope slide which was then placed inside a benchtop oven (MRO 160). The paste was preheated for 150 s at 140°C and ('reflowed') for 60 s at 260°C. This produces a small solder lump of approximately 0.2 g. Initially, solder paste was used directly to fill up the test tube. But solder paste was not melted properly at the desired time and temperature. Hence the experimental procedure was changed to make solder lumps first and then filling up the test tube with these solder lumps. This method allowed the solder to be melted properly inside the test tube resulting in a cylinder-shaped solder sample inside the test tube. The solder lumps were dropped to the bottom of a test tube with 4.8 mm diameter and 50 mm length. Some flux was placed at the bottom of the test tube to aid reflow. The test tube was placed in a brick and brick was placed inside the furnace (Lenton Thermal Design), heated for 30 minutes at 300°C and then cooled down to room temperature. Once the solder cooled down, the test tube was broken to produce solder rods.

These dimensions conform to the "short" length-to-diameter ratio of 1.5 per the ASTM E9-89A specification in order to minimize the likelihood of buckling under the compressive load and ensure homogeneous deformation. To prepare solder paste with nanoparticles, the nanoparticles are suspended in a solvent compatible with the flux, mixed with the flux, and then the steps to form the solder rods are identical to those for the solder paste without nanoparticles. Fig. 4.8 shows an image of solder powders mixed directly with the nanoparticles (without flux).

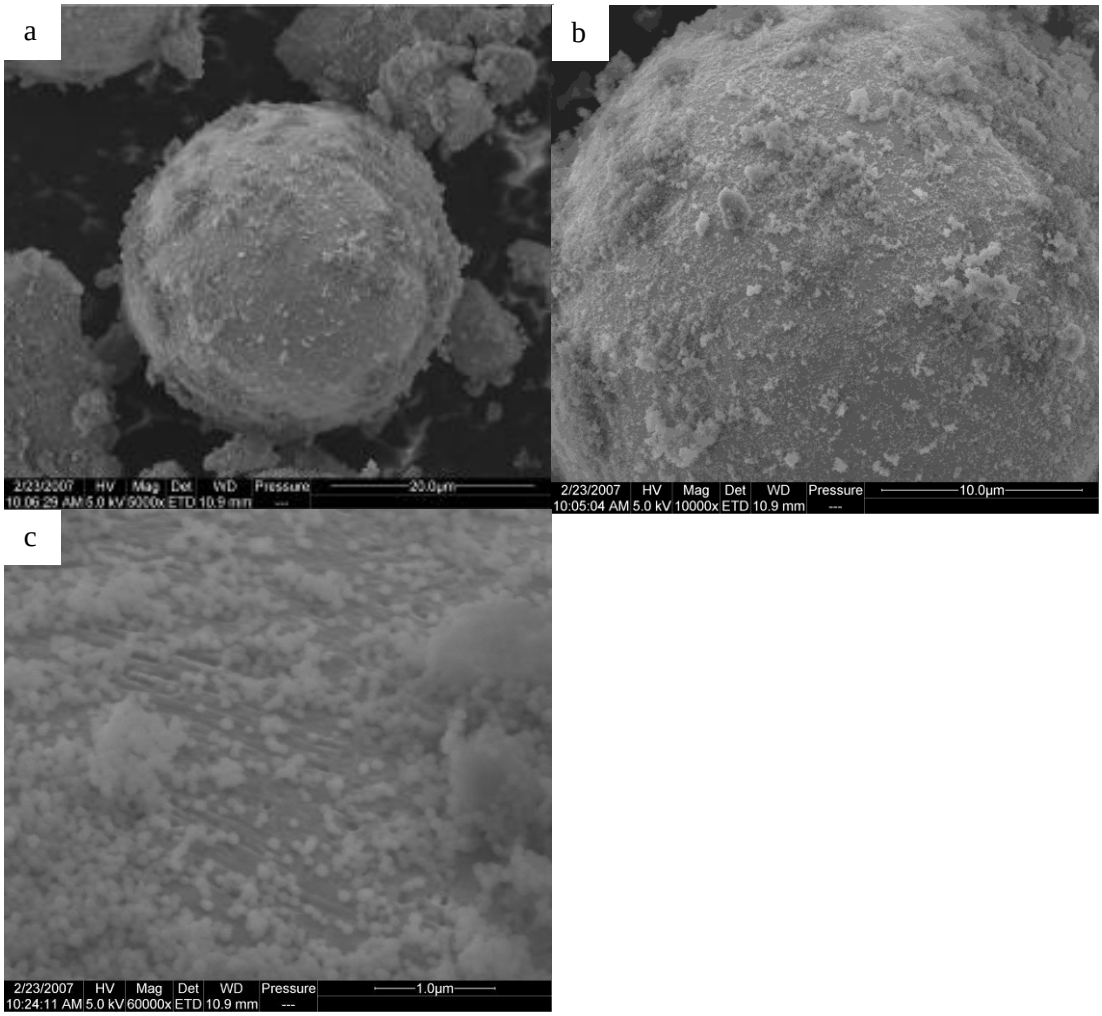

Figure 4-8 - (a) and (b) Images show nanoparticles which are deposited on solder particles, (c) image shows the solder particle with nanoparticles deposited on it

While the nominal volume composition of nanoparticles in the final solder is f=0.02, the actual composition is significantly lower as some nanoparticles will never come into contact with the solder particles and will be expelled along with the flux during reflow. By calculating the nanoparticle area fraction of images such as Fig. 4.7, the true value of f is estimated to be 0.001 (i.e. 0.1vol %). In order to calculate the volume fraction of nanoparticles, the area of

nanoparticles was divided by the total area of the SEM image. In order to calculate the volume fraction manually, a few SEM images were considered.

The mechanical hot compression tests were carried out by Dr. Ali Roshanghias at the Department of Materials Science and Engineering, Sharif University of Technology in Iran at temperatures of 25°C, 50°C, 100°C, and 150°C with the strain rate of 0.001/s. The specimens were compressed by using an Instron- 4208 universal testing machine, equipped with an electrical resistance furnace, which could maintain temperature variation within ±2C. Each specimen was kept for 10 min at the desired temperature to be homogenized. Mica sheet lubricant is used to minimize the interference of friction in the results. Stress-strain data was recorded.

After testing, the compressed cylinder-shaped samples were returned to King's College London where I carried out the microstructural analysis. The first step was to section the samples vertically. One of the halves was polished by mechanical polishing (graded silicon carbide cloths followed by 2 μm and 0.25 μm suspended diamond solutions) to prepare a smooth surface for microstructure examination. An argon ion beam Cross-Section Polisher (Jeol SM-09010) was used to etch the surface for ideal contrast between the grains. Each sample was bombarded at normal incidence by an Ar ion beam for 150s at an accelerating voltage of 3kV. Fig. 4.9 shows the schematic illustration of sample preparation for SEM observation after the compression test. And the details of etching by CSP have been given in the section 3.2. An FEI Quanta FEG SEM was used for the examination of the microstructure, using EDAX to identify and distinguish the silica nanoparticles from the solder matrix. In order to measure the grain sizes, images were taken by SEM and grains were measured by ruler manually (see section 4.2.5 Grain size measurement techniques). In addition to these mechanical compression tests at room

temperature were carried out in the Division of Engineering, King's College London with an Instron, bench-top tensile testing machine using a compression cage.

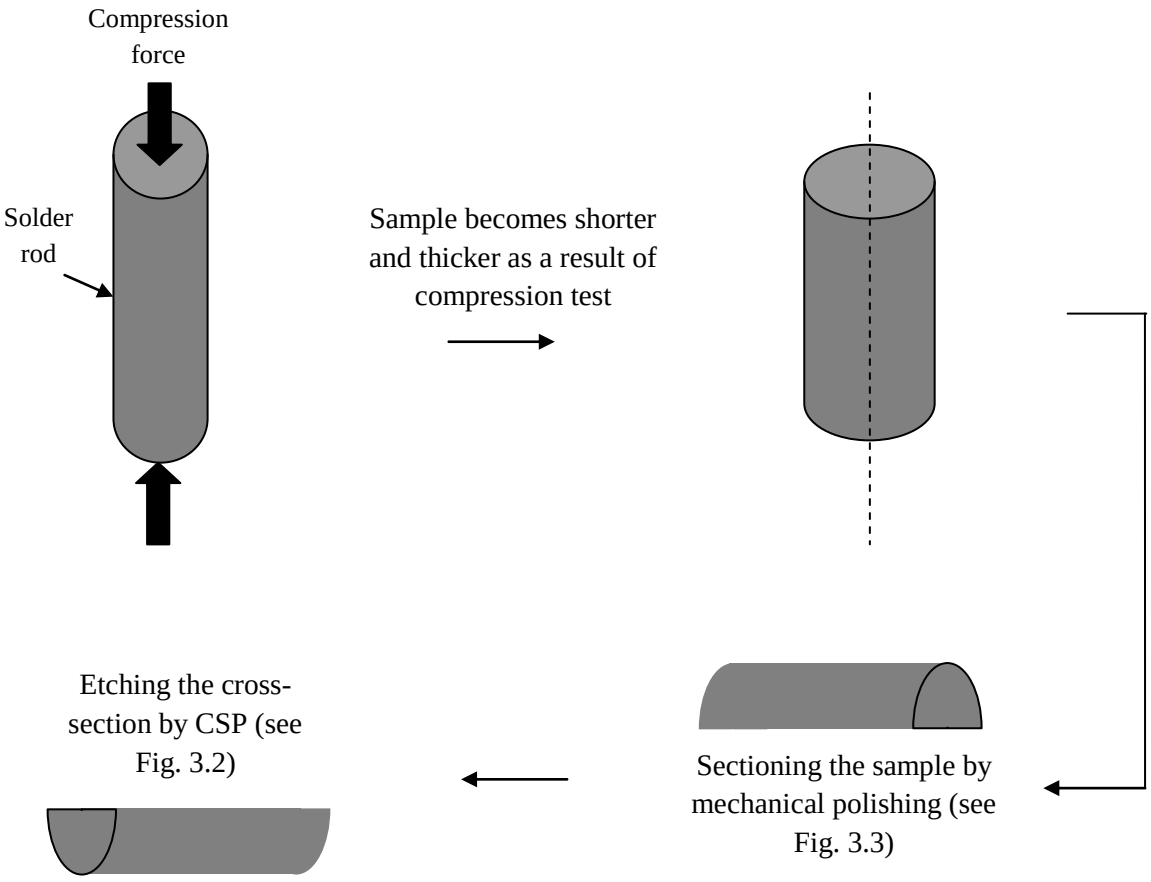

Figure 4-9 - The schematic illustration of the SEM sample preparation after the compression test

4.4 Results and discussion

Figure 4.10 and Table 4.3 show typical compression test data for the two alloys, SAC and SAC with nanoparticles, from the experiments carried out at King's College London at room temperature. The results are the average value for five samples for each case. Due to

unavailability of the data in table form at time of writing this thesis, the error bars could not be used on the curves. The samples containing the nanoparticles display a higher flow stress due to the dynamic recovery mechanisms requiring greater thermal activation for the dislocation motion to overcome the barriers provided by the dispersion of nanoparticles.

Table 4-3 - The compression threshold stress values for SAC and nano-enhanced SAC at room temperature

Solder / Strain	SAC at room temperature, MPa	SAC + nano at room temperature, MPa
0.1	42.0	43.5
0.2	45.5	47.0
0.3	47.0	49.0
0.4	48.0	51.0
0.5	49.5	52.5

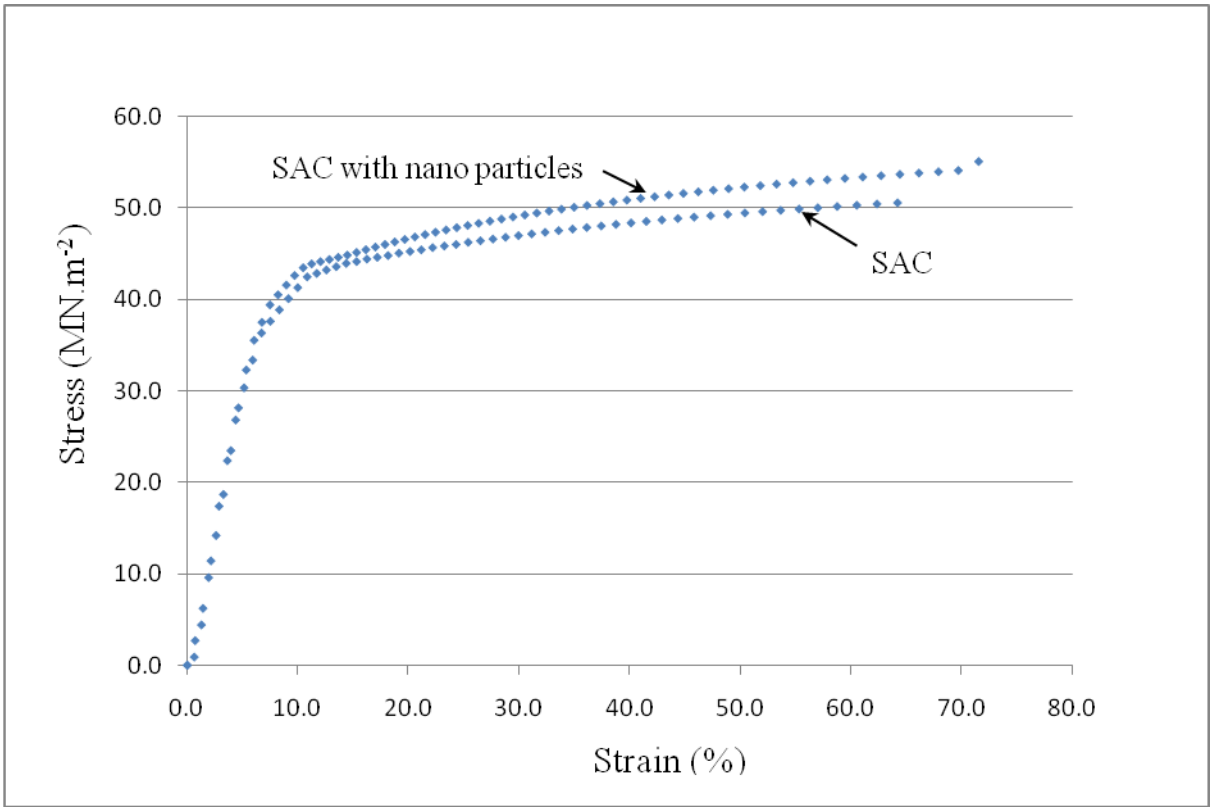

Figure 4-10 - Stress-strain curves showing the effect of the added nanoparticles

Fig. 4.11 and Table 4.4 show the results of the hot compression tests at 25, 50, 100 and 150 ºC. There is a clear difference between the SAC and the nano-enhanced SAC solder at 25 ºC (homologous temperature 0.6). However, the SAC and nano-enhanced SAC at 150 ºC show minimal differences in mechanical behaviour. Thus, as the homologous temperature approaches 0.86, the efficiency of the nanoparticles in restricting dislocation movement and grain boundary sliding decreases.

Table 4-4 - The compression threshold stress values for SAC and nano-enhanced SAC at 25-150 °C, MPa

Solder	SAC at 25 °C	SAC + nano at	SAC at 50 °C	SAC + nano at	SAC at 100 °C	SAC + nano at	SAC at 150 °C	SAC + nano at

Strain		25 °C		50 °C		100 °C		150 °C
0.2	33.86	40.33	25.97	29.19	18.74	20.27	13.01	13.40
0.3	35.18	42.12	26.54	29.74	18.91	20.79	12.86	13.41
0.4	36.33	43.32	26.86	30.06	18.45	21.07	12.55	13.21

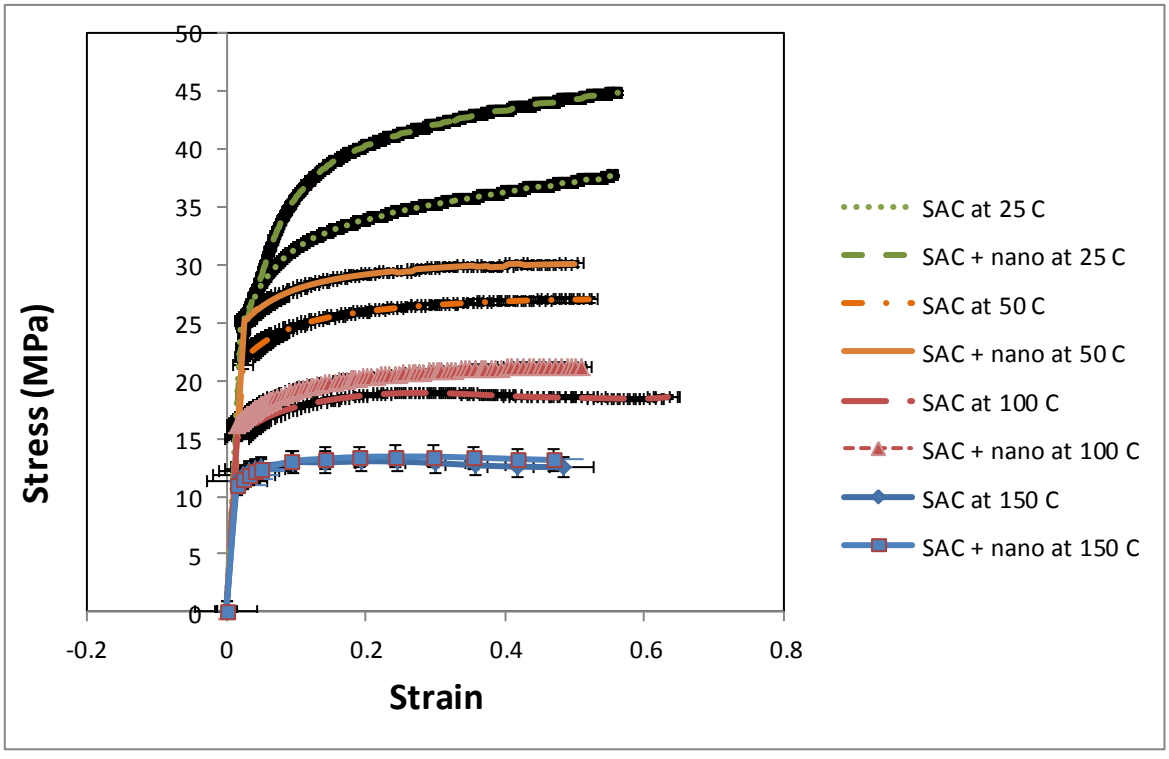

Figure 4-11 - The stress-strain curves in hot compression test at 25 °C, 50 °C, 100 °C, and 150 °C with the strain rate of 0.001/s.

Fig. 4.12 shows microstructure of eight samples, SAC and nano-enhanced SAC samples compressed at 25ºC, 50°C, 100°C and 150ºC. It can be seen that nanoparticles inhibit grain growth at 25ºC, effectively. However, at 150ºC, there is no considerable difference between the microstructure of SAC and nano-enhanced SAC which observation matches with the stress-strain curve at Fig. 4.11. The Table 4.5 and bar chart in Fig. 4.13 shows clearly the value of the difference between the grain diameters at different temperatures. Standard deviation of number of measurements from different grains is also shown in Table 4.5. It can be seen that at 150ºC, the average grain diameter for nano-enhanced SAC exceeds the value of SAC, slightly. The value of the difference is negligible. The reason could be because of the variation of the average of the grain diameter from one location to another even at the centre of the sample. It can be concluded that in hot compression tests, by increasing the temperature, the mechanical effect of the nanoparticles decreases. According to Fig. 4.13, nanoparticles are effective at temperatures up to 100°C. By increasing the temperature after 100°C, nanoparticles lose their efficiency in limiting the grain boundary sliding i.e. the pinning effect decreases with increasing temperature.

In addition to these SEM images of cross-sectioned samples, ZEISS Axio Lab. A1 optical microscopy was used for further examination of grain sizes for SAC and nano-enhanced SAC samples which compressed at 25 °C and 150 °C. These samples were etched with CSP for five more minutes to make grains more distinguishable. Fig. 4.14 shows the images which were taken by optical microscopy. As can be seen, Fig. 4.14 (c) and (d) represent some effects of nanoparticles after hot compression test at 150 °C, however, the mean value for grain size as represented in Table 4.5 show the inefficiency of nanoparticles after hot compression test at 150 °C.

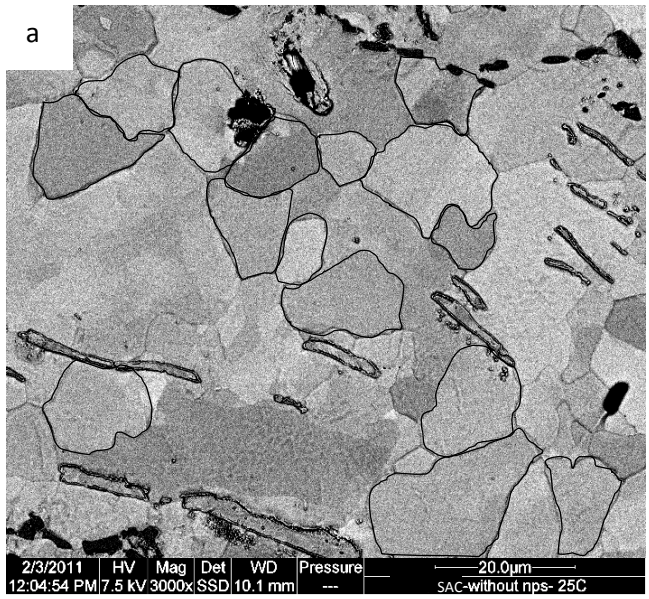
a
2/3/2011 HV Mag Det WD Pressure
12:04:54 PM 7.5 kV 3000x SSD 10.1 mm ---
20.0µm
SAC-without nps- 25C

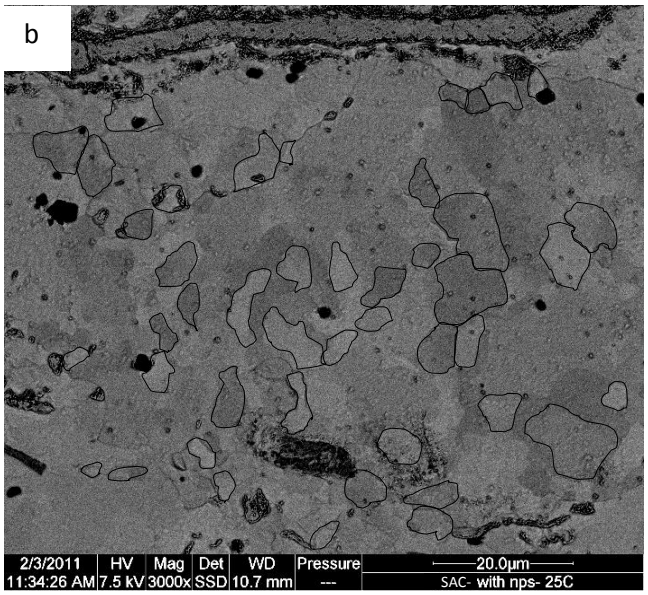
b
2/3/2011 HV Mag Det WD Pressure
11:34:26 AM 7.5 kV 3000x SSD 10.7 mm ---
20.0µm
SAC- with nps- 25C

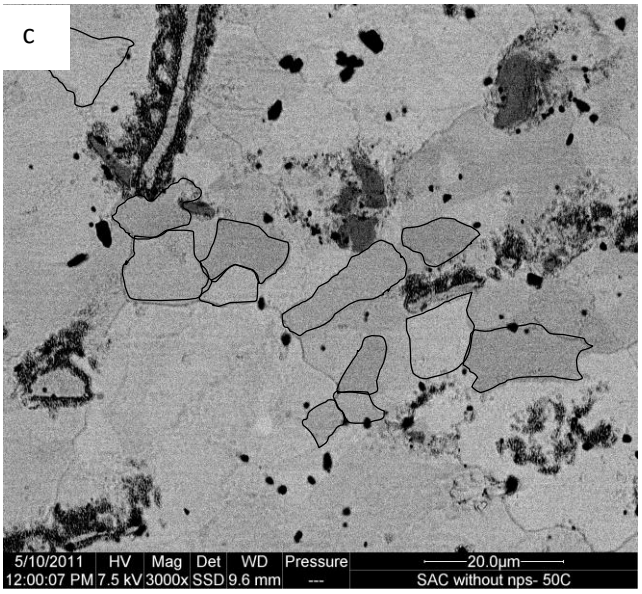
c
5/10/2011 HV Mag Det WD Pressure
12:00:07 PM 7.5 kV 3000x SSD 9.6 mm ---
20.0µm
SAC without nps- 50C

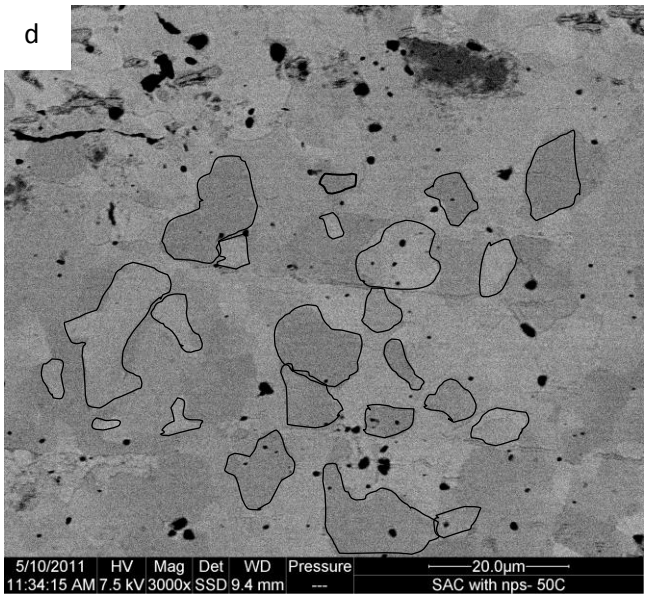
d
5/10/2011 HV Mag Det WD Pressure
11:34:15 AM 7.5 kV 3000x SSD 9.4 mm ---
20.0µm
SAC with nps- 50C

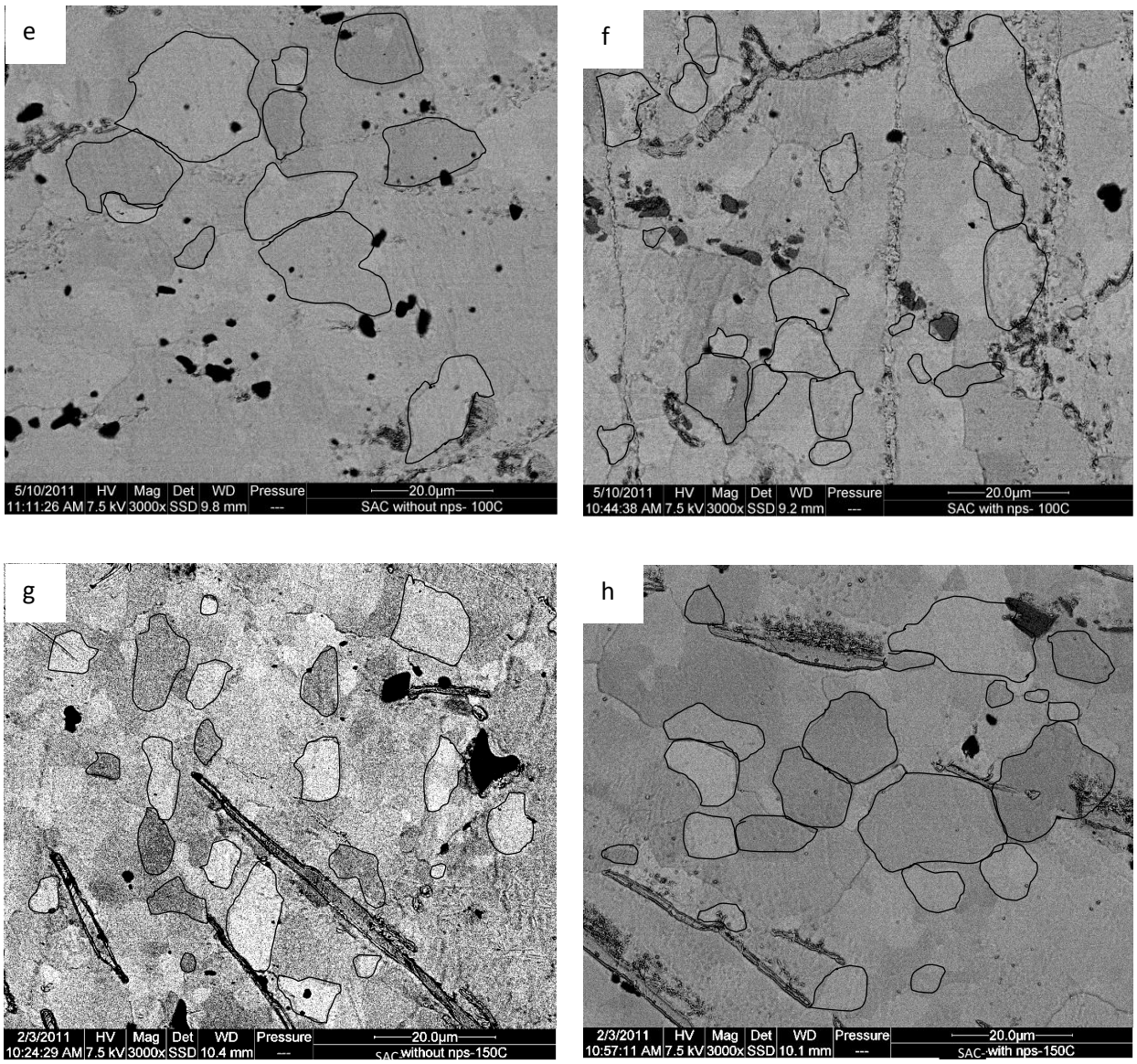

Figure 4-12 - Microstructure of samples after hot compression which were taken by SEM; a) SAC compressed at 25ºC, b) Nano-enhanced SAC compressed at 25ºC, c) SAC compressed at 50ºC, d) Nano-enhanced SAC compressed at 50ºC, e) SAC compressed at 100ºC, f) Nano-enhanced SAC compressed at 100ºC, g) SAC compressed at 150ºC and h) Nano-enhanced SAC compressed at 150ºC

Table 4-5 - The average grain diameters of SAC and nano-enhanced SAC compressed at 25, 50, 100 and 150 °C

	25 °C		50 °C		100 °C		150 °C	
	Mean (µm)	SD (µm)	Mean (µm)	SD (µm)	Mean (µm)	SD (µm)	Mean (µm)	SD (µm)
SAC	**9.7**	**1.46**	**10.8**	**1.51**	**14.5**	**2.1**	**13.3**	**1.81**
Nano-enhanced SAC	**4.2**	**1.86**	**7.0**	**1.67**	**9.9**	**1.75**	**14.3**	**3.33**

SD, Standard deviation

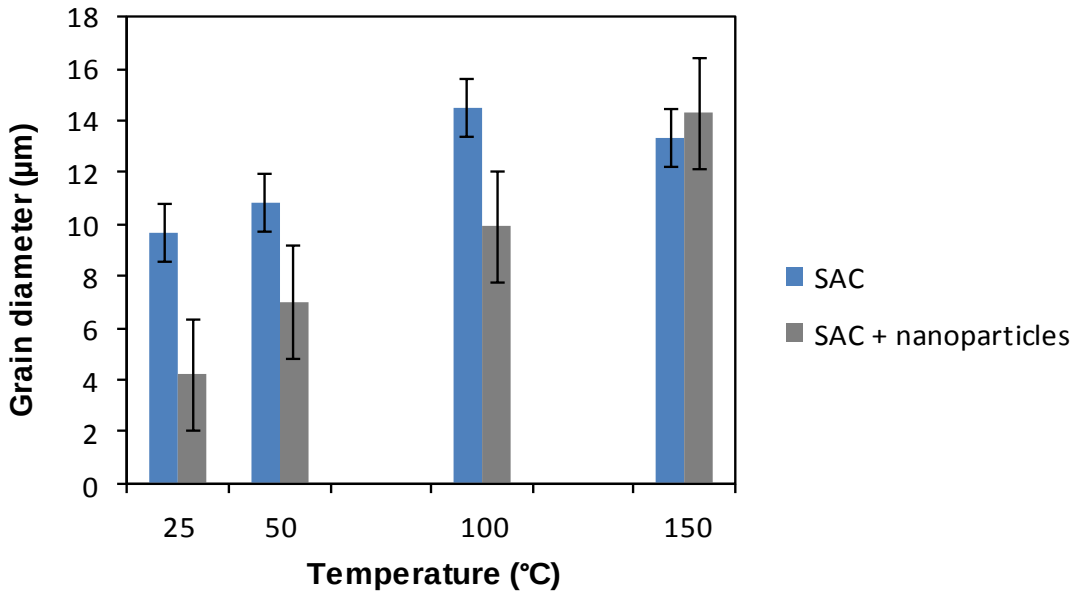

Figure 4-13 - The average grain diameters of SAC and nano-enhanced SAC compressed at 25, 50, 100 and 150 ºC.

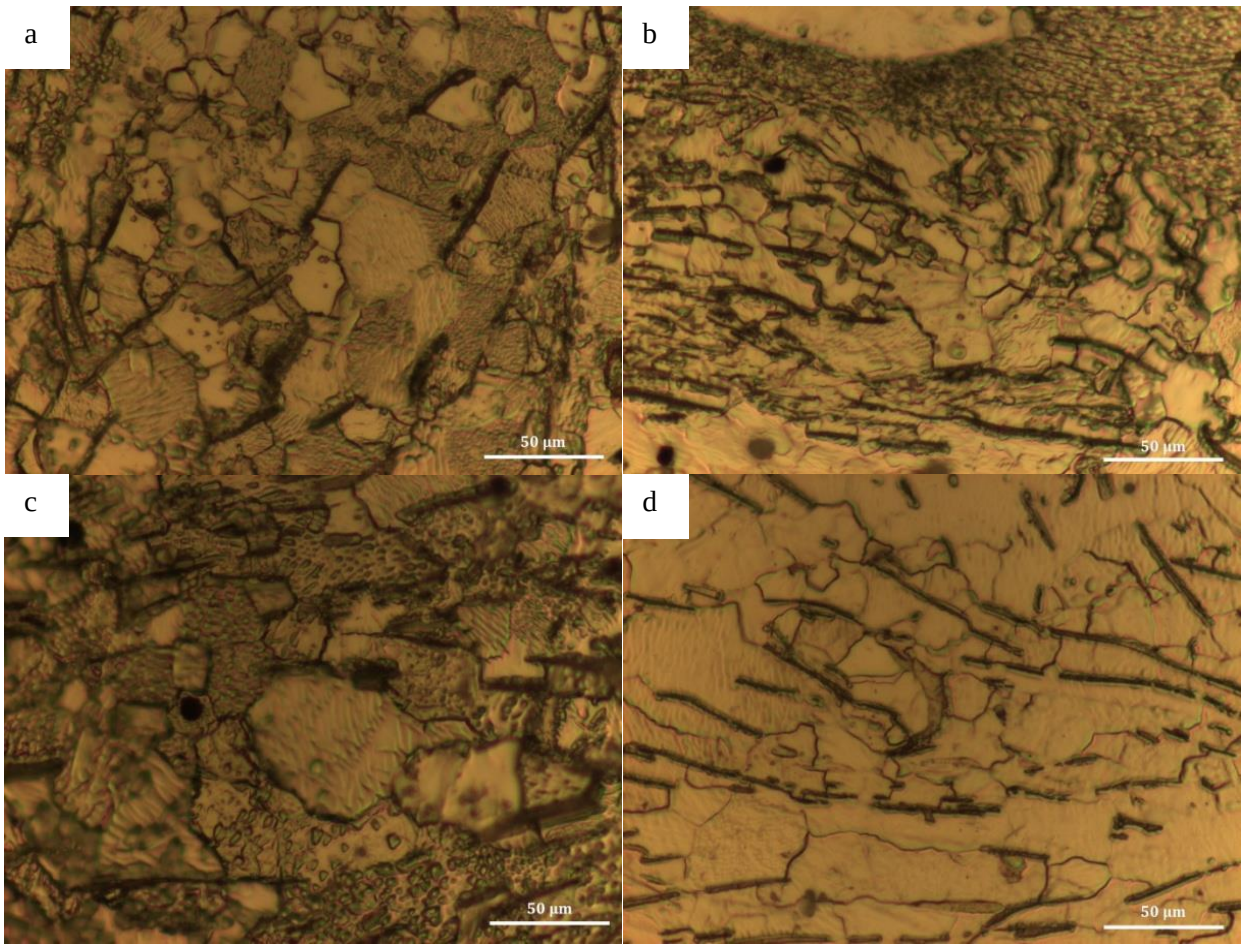

Figure 4-14 - Microstructure of samples after hot compression which were taken by optical microscopy; a) SAC compressed at 25ºC, b) Nano-enhanced SAC compressed at 25ºC, c) SAC compressed at 150ºC, d) Nano-enhanced SAC compressed at 150ºC.

Bate [194] has performed 2-D numerical simulations of dynamical grain boundary movement during compression of a Zener pinned structure, and notes that the resulting microstructure is weakly dependent on strain rate while the grain growth significantly reduces the aspect ratio increase that would otherwise be expected as the grains are deformed in the uniaxial flow field. While providing the mechanism for grain growth, this model has not been extended to 3-D and provides no accounting for the temperature dependent effects seen in our results.

On general grounds, it is expected that the grain boundary velocity, v_{gb}, will be given by an expression of the form [195]:

$$v_{gb} = \mu(\sigma_d - \sigma_z) \tag{4.1}$$

where μ is the grain boundary mobility, σ_d is the driving stress and σ_z is the pinning stress, given by [196]:

$$\sigma_z = \frac{3f\gamma}{4r} \tag{4.2}$$

where γ is the grain boundary energy per unit area. In the nanoparticle enhanced SAC case, the pinning stress is larger than in the SAC case, resulting in slower boundary movement. Fig. 4.15 shows a comparison between grain sizes in solders that have undergone compression testing and those that have not, at room temperature. Movement of grain boundaries has led to significant grain growth in the case of the SAC solder but in the case of the nanoparticle reinforced system grain growth is negligible.

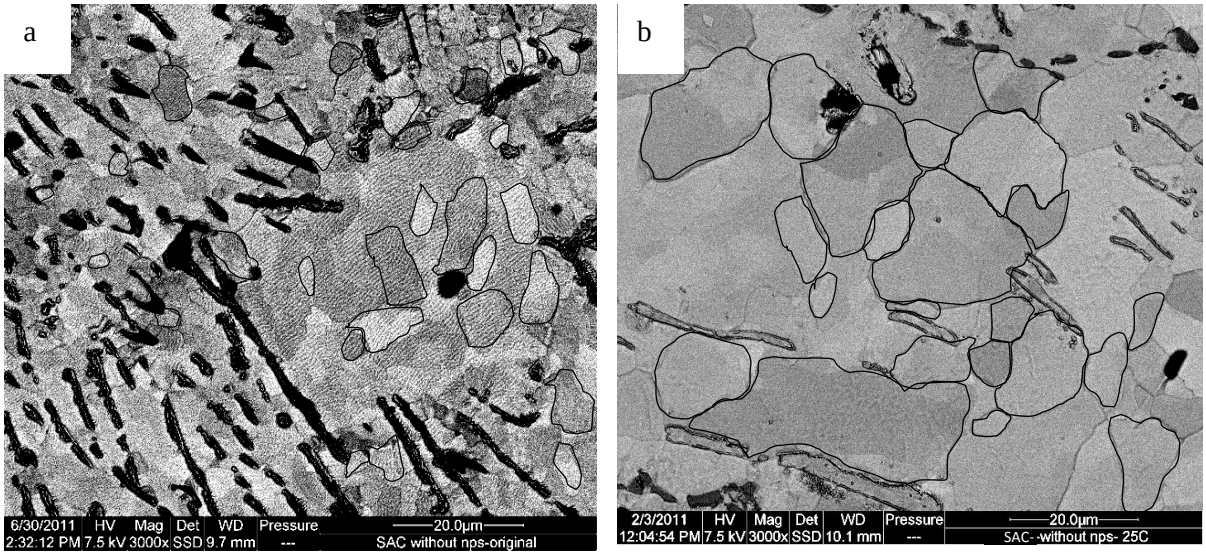

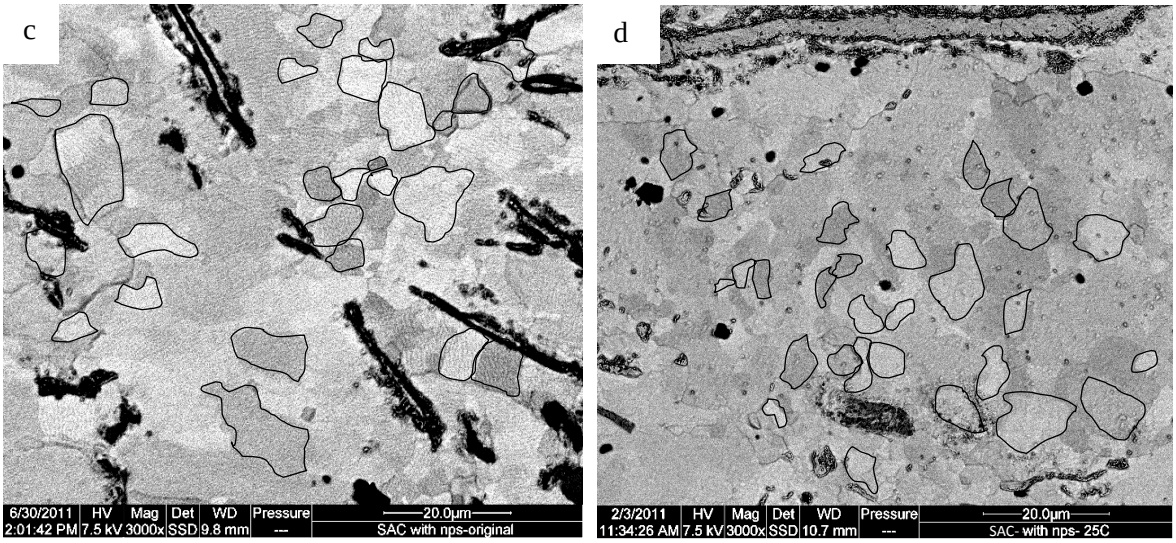

Figure 4-15 - SAC solder before (a) and after (b) compression test; nano-enhanced SAC before (c) and after (d) compression test.

As the temperature increases, μ is expected to increase, however it appears that the additional pinning stress due to the nanoparticles also decreases, resulting in convergence in microstructure in the two cases. This can be explained if it is assumed that due to the small size of the nanoparticles compared to the pinning structures in SAC, grain boundary movements governed by thermal fluctuations are sufficient to unpin the boundaries from the nanoparticles. Thus at any given point in time, the number of nanoparticles participating in pinning grain boundaries is reduced to f_{eff} :-

$$f_{eff} = f\left[1 - \exp\left(\frac{-Q}{RT}\right)\right] \tag{4.3}$$

where Q is an activation energy, R is the molar gas constant and T is the absolute temperature. The factor, [1-exp (-Q/RT)], represents the probability that a nanoparticle retains connection with its contacting grain boundary despite thermal fluctuations. This interpretation is supported by considering Fig. 4.15 (a and c) which show very little effect of the nanoparticles on microstructure prior to the compression tests. Because of the slow cooling rate due to the sample preparation method, grain boundary movement takes place at high homologous temperature and the initial microstructures are identical. Only when grain boundaries are forced to move due to the applied stress at low homologous temperatures do the effects of the nanoparticles become apparent. From a practical perspective, this limits the usefulness of spherical nanoparticles for strengthening materials at high homologous temperatures. Note however, that the same arguments would not apply to carbon nanotubes or other extended structures where small thermal fluctuations in the location of the grain boundary would not necessarily result in unpinning [197].

To analyze grain boundary fluctuations at the atomic level, providing the justification for equation (4.3), the vacancy mechanism of grain boundary movement needs to be considered. In the analysis, it is assumed that there is low correlation between successive atomic jumps as is appropriate for an fcc metal [1, 4, 5], resulting in a random walk. Atoms jump over the energy barrier, Q, with an attempt frequency, ν (approximated by the Debye frequency for Sn; see [122] for other estimates), and with the probability of a successful jump given by Boltzmann statistics. Hence the number of completed jumps, N, in time t_c is given by:-

$$N = \nu t_c \exp\left(\frac{-Q}{RT}\right) \tag{4.4}$$

and the displacement of the grain boundary, d, over this time period due to thermal fluctuations in a random walk is given by the lattice spacing $\times \sqrt{N}$:-

$$d = \lambda\sqrt{\nu t_c \exp(\frac{-Q}{RT})} \tag{4.5}$$

where λ is the lattice spacing. The relevant timescale, t_c can be estimated by the time taken for the grain boundary to move over a single particle diameter. Equation (4.3) can now be refined, by taking $d/2r$ as the measure of the fraction of particles which have become thermally unpinned, giving:-

$$f_{eff} = f\left[1 - \frac{\lambda}{2r}\sqrt{\nu t_c}\exp(\frac{-Q}{2RT})\right] \tag{4.6}$$

From Fig. 4.12 it can be seen that grain growth from the pinned room temperature microstructure is boundary movement of approximately 8 microns, that occurs over the lifetime of the compression tests (500 s). Hence the grain boundary velocity relative to the particles can be estimated as $V = 1.6 \times 10^{-8}$ m/s, giving:-

$$t_c = \frac{2r}{V} \approx 6\,\text{s} \tag{4.7}$$

using 298.15 K for T, 8.31 J/mol.K for R, 72 kJ/mol for Q (based on reported values of creep activation energy in solders [121]), 5.4×10^{12} Hz for ν, 50 nm for r and 5.82×10^{-10} m for λ [198], d is estimated as 2 nm and so even at room temperature some unpinning of grain boundaries is expected. At 100 °C, d increases to 30 nm which is still smaller than the particle size, indicating that the grain boundaries are not completely unpinned. At 150 °C d increases to 119 nm which is much larger than the particle diameter indicating complete unpinning of the grain boundaries. These results are shown in Fig. 4.16 below. From equation (4.6) and equation (4.7), it is seen that the movement of grain boundaries relative to particle size, d/r, will scale as $1/\sqrt{r}$. Furthermore, substituting equation (4.6) and (4.7) into equation (4.2) and maximizing the pinning stress as a function of r, we obtain:-

$$r_{opt} = \frac{9}{8}\frac{\nu\lambda^2}{V}\exp\left(\frac{-Q}{RT}\right) \tag{4.8}$$

where r_{opt} is the particle radius which maximizes the pinning stress. At a temperature of 150 °C, the optimum particle radius is seen to be 137 nm compared to the 50 nm particle radius used in the current experiments.

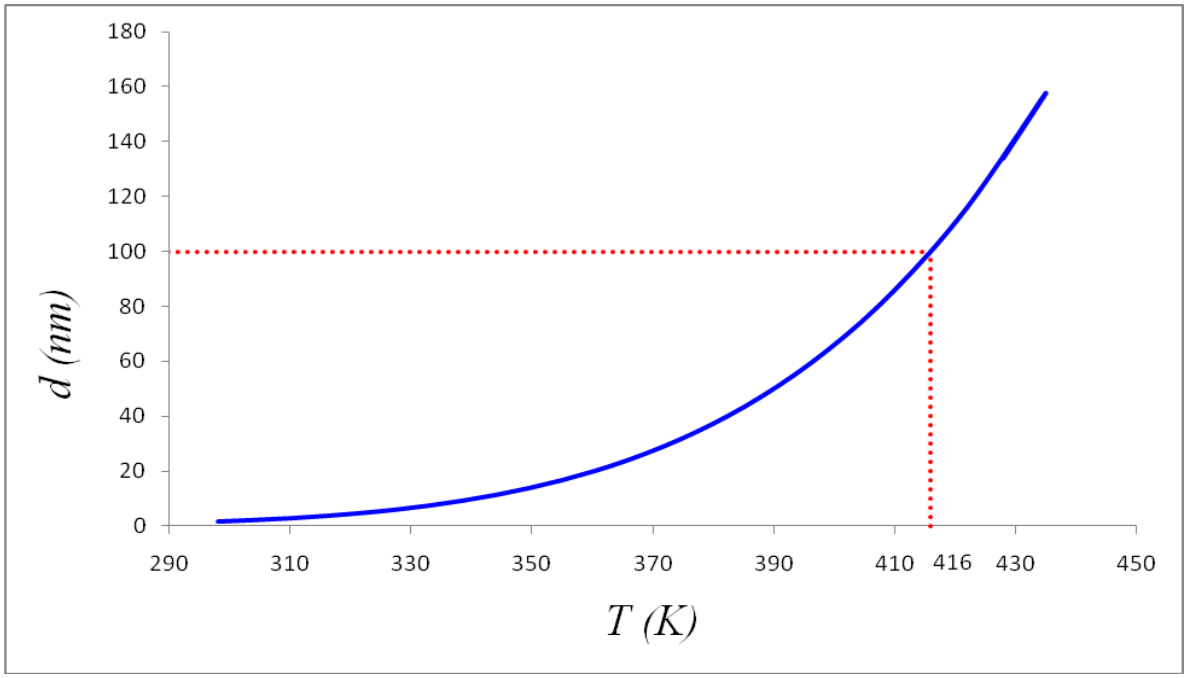

Figure 4-16 - The variation of thermal displacement of the grain boundary, *d*, versus temperature, *T*. The dotted line indicates the displacement corresponding to the particle diameter of 100 nm

4.4.1 Activation energy

The activation energy Q is the energy barrier due to the fact that for an atom to move from a higher energy location to a lower energy location, it must pass through a higher energy state [117]. The creep activation energy is one of the parameters which is used for measuring the creep resistance of a solder alloy. Solders with larger creep activation energy values have higher creep resistance [118].

As has been mentioned before (chapter 2), the interaction between fine particles and dislocation can change the threshold stress τ_0. This is because a threshold stress should be exceeded before

boundary dislocations can break away to produce sliding [119]. The relationship between τ_0 and Q_0 is expressed by equation (4.9):

$$\frac{\tau_0}{G} = B_0 \exp(Q_0 / RT) \tag{4.9}$$

Where τ_0 is the threshold stress, G is shear modulus, B_0 is a constant, Q_0 is creep activation energy, R is Boltzmann's constant and T is the absolute temperature. The value of τ_0 can be taken from Fig. 4.11 as $\frac{\tau_0}{G}$ and $\frac{\sigma_0}{E}$ are proportionate:

$$\frac{\tau_0}{G} \propto \frac{\sigma_0}{E} \tag{4.10}$$

where σ_0 is threshold stress and E is Young's modulus, the equation (4.9) can be rewritten as:

$$\frac{\sigma_0}{E} = B_0 \exp(Q_0 / RT) \tag{4.11}$$

The relationship between the logarithm of the normalized value of σ_0 and the reciprocal of temperature can be represented by a straight line. The value of Q_0 can be determined by taking the slope of the straight line in Fig. 4.17 [119].

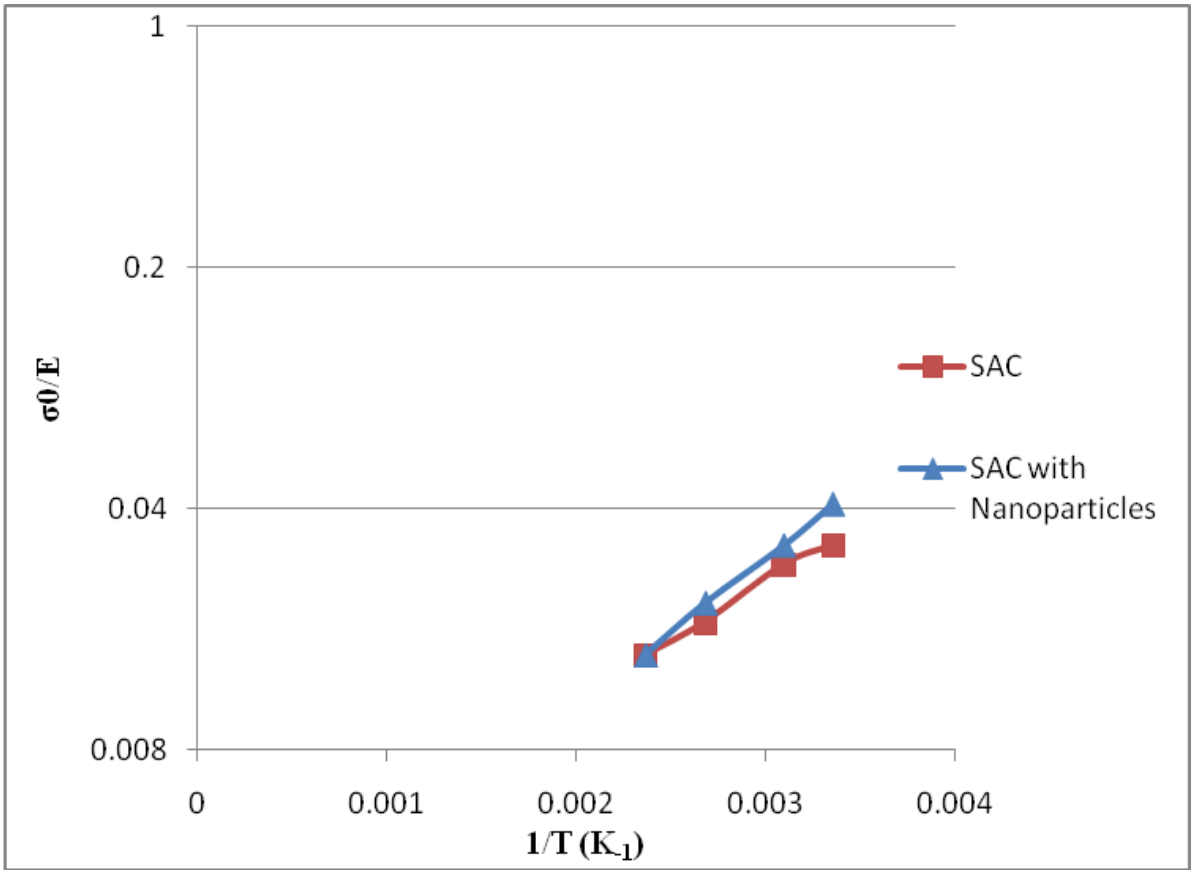

Figure 4-17 - A plot of logarithm of $\frac{\sigma_0}{E}$ as a function of 1/T for SAC and SAC with nanoparticles

Table 4-6 - The values of creep activation energy, Q_0, for SAC and SAC with nanoparticles, *kJ/mol*

	Q_0, kJ/mol
SAC	16.40
SAC with nanoparticles	26.49

The value of Q_0 can be extracted from Fig. 4.17 for both SAC and SAC with nanoparticles. The values of Q_0 for SAC and SAC with nanoparticles as shown in Table 4.6 are 16.40 and 26.49 kJ/mol, respectively. So, it can be seen from this data that nano-enhanced SAC has higher activation energy than SAC. However, according to the literature [118] the creep activation energy of Sn-3.8Ag-0.7Cu is about 54 kJ/mol which is significantly higher than 16.40 kJ/mol. There are some reasons for this difference. First of all, the value of threshold stress, σ_0, was taken from hot compression tests results which is from Fig. 4.11. In this figure the threshold stress is not clearly identifiable. The reason is at the time of hot compression test, determining the threshold stress was not the goal of the test. So the precise values for threshold stress were ignored. It was assumed that the difference in the correct threshold stress is the same in all graphs. This resulted in disagreement between these values and the published results in literature. However, the threshold stress is identifiable in the results of compression test at room temperature which was performed at King's College London and is with agreement with the results which are published in literature [178, 184].

4.5 Conclusion

The results show that the gold coating has allowed a fraction of the added nanoparticles to be captured within the solder during the solder reflow process. The nanoparticles have negligible effect on microstructures formed at high homologous temperature, such as during slow cooling. However, these nanoparticles do have a significant effect in restricting grain boundary movement and dynamic grain growth during compression at low homologous temperatures and hence provide a hardening effect to the solders. At higher homologous temperatures, the pinning effects of the nanoparticles decrease rapidly due to thermal fluctuations in the position of the grain boundary, which result in a decrease in the effective numbers of particles pinning the grain boundaries. The analysis of thermally activated grain boundary movement indicates that the

fluctuations of the grain boundary at temperatures under 100 °C are less than the particle diameter, resulting in effective pinning. However, at 150 °C, the displacement of grain boundaries becomes larger than the particle diameter resulting in unpinning of the grain boundaries. Larger particles should result in reduced thermal unpinning and the optimum particle diameter for 150 °C is predicted to be 274 nm.

The activation energy of the SAC and nano-enhanced SAC has been calculated and the results indicate that the nano-enhanced SAC has larger activation energy value than SAC. This higher activation energy provides the nano-enhanced SAC with a higher energy barrier to limit atomic movements inside the microstructure of the solder. However, the data used to calculate the activation energies is incomplete, and the experiments would have to be repeated for the errors to be reduced.

The outcome of this chapter was to show the capability of the grain growth limitation by the SiO_2 addition to the SAC solder matrix in high temperature environment. This research successfully illustrated an equation which provides the optimum effective diameter of the added SiO_2 particle for the desired working temperature. For future work, other passive particles such as TiO_2 can be tried. However, since passive articles cannot react with the solder and expel from the solder during the reflow (similar to the SiO_2) a coating process will also be needed.

5 Dissolution of Al in Sn

5.1 Introduction

This chapter is about the dissolution rate of Al in molten Sn. Dissolution kinetics is of considerable importance in the processes of soldering, brazing and welding. At King's College London, a programme of work investigating the use of nanoparticles of Al in solders is underway. The aim is to design nanoparticles to release Al into the solder at the optimum time in the solder reflow process so as to maximize Al reactions with the substrate while minimizing interference with solder wetting reactions. In order to achieve this, the dissolution rate of Al in liquid solder is an important parameter and hence fits into the overall aim of this thesis in developing nanoparticle enhanced solders.

The dissolution of solid material in a molten metal can be developed in two stages, the first involving migration of atoms or molecules of the solid material into the molten metal, and the second, mass transport of the dissolved material into the volume of the melt [147]. The dissolution of solid Al in molten Sn is the consequence of atomic diffusion through the Al/Sn interfaces. Fig. 5.1 shows the diffusion path of Al atoms into molten Sn.

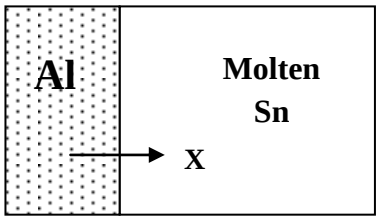

Figure 5-1 - Diffusion path of the Al atoms into molten Sn

As Al is very reactive with Oxygen, it was decided to coat the Al layer with different elements to find which structure best avoids oxidation. The experiments were hence designed to provide a clean unoxidized surface between Al and a coating layer, the latter dissolving into the liquid tin allowing Al dissolution rates to be measured. To explain the order of the coatings utilized, the names of coating layers have come after the name of the substrate (e.g. Cu-Sn-Al implies that Sn has been coated on top of Cu substrate and then Al has been coated on top of the Sn). Table 5-1 represents an overview for the experiments developed in this chapter.

Table 5-1 - Overview of experiments in this chapter

Top Layer	Order of Coating	Method of Heating	Results
Al	Cu/Sn/Al	Oven	1. Results show that as top surface of top layer is rough due to the nature of coating, Al layer cannot be the top layer since it became impossible to deduce how much Al has dissolved by Al thickness measurement. 2. As Cu and Ni(P) substrates dissolve in Sn, they interfere with the dissolution of Al in Sn. Also Si seemed to be cut easier than glass resulting in the choice of Si for the ideal substrate for later experiments.
	Ni(P)/Sn/Al	Oven	
	Glass/Sn/Al	Oven	
	Si/Sn/Al	Oven	
Sn	Si/Al/Sn	Oven	Results prove that Sn is not a suitable coating element as it could not prevent the oxidation of Al layer (See sections 5.3.7 Si/Al/Sn and 5.3.8 Si/Al/Au).
		Dipping in molten Sn	
Au	Si/Al/Au	Dipping in molten Sn	Results show that Au is not a suitable coating layer as only made Al and Au layers interdiffusing rather than enabling Al dissolution into Sn (See section 5.3.8 Si/Al/Au).
	Si/Cr/Au/Al/Au	Dipping in molten Sn	

None of the structures which are listed in the Table 5-1 provided reliable and repeatable determination of the dissolution of Al in liquid Sn. The experiments and results are explained and discussed in the remainder of the chapter.

5.2Methodology

5.2.1 The thin film deposition of Sn and Al

In this study, the main objective is to find out the dissolution rate of Al in Sn. Since, Al is highly reactive to Oxygen and easily forms the Aluminium Oxide, Al_2O_3, the main challenge of this research is to find a method to avoid the reaction of Al with Oxygen. Thus, it was decided to deposit Al and Sn layers on top of each other in a highly vacuumed chamber. By doing this, the possibility of the penetration of Oxygen to the contact between Al and Sn decreases to a minimum. Therefore, two different methods of thermal evaporation and sputtering were used.

5.2.1.1 Thermal evaporation

In this research, to investigate the dissolution rate of metals in liquid metals, a thin film of metal was coated on top of a silicon wafer. The liquid metal was introduced to the coated metal to examine the dissolution behaviour. Thermal evaporation and sputter coating were both used as coating methods in this research. The evaporation deposition technology utilizes the evaporation of a specific material from a source by thermal activation which can be electrical heating, lamp heater, etc. in a vacuum process. The thermally activated gas particles move with no interactions and deposit on the walls and substrates placed in the chamber, because of the low gas density. Particles which reach the substrate in evaporation method have equivalent energy to the thermal energy of the source. By increasing the vacuum, particles would have energy nearer to the source temperature. The following equation shows this relation:

$$kT = mv^2 \tag{5.1}$$

where v is particle speed, T is temperature (in K) and m is mass. The energy of evaporated particles reduces by the impact between them and cooler gas particles and walls of the chamber. By providing low enough pressure, particles would be able to carry their energy to the surface of the substrate which is due to free path length of gas. Typical particle energy for an evaporation process is about 100 meV. The low kinetic energy of particles provides low surface mobility which could result in strong structured surfaces with fine grains [199].

Vacuum conditions for thermal evaporation

After 45 minutes of pumping the sufficient vacuum was achieved to begin the coating process which was at the pressure of around 7×10^{-5} Torr.

5.2.1.2 Sputtering

Sputtering uses mechanical activation to detach particles from a source. One of the advantages of this method is that the materials which are difficult to evaporate can be used in this method. This method utilizes inert ions which are created in plasma and accelerated in an electric field for mechanical activation. The kinetic energy of ions needs to be higher than the binding energy of particles to be able to detach them. Usually, 2 to 3 orders of magnitude is needed to provide a sufficient deposition rate. The kinetic energy of particles in sputtering is higher than a similar particle in evaporation by several orders of magnitudes. So, the impact of sputtered particles is heavier than those thermalized [199].

Vacuum conditions for sputter coating

After 30 minutes of pumping the sufficient vacuum was achieved to begin the coating process which was at the pressure of around 7×10^{-5} Torr. From this point, a closely controlled flow of

argon, an inert process gas, was introduced while the pump was still running. This raised the pressure in the system to the levels which was needed to operate the magnetrons. The combination of pumping down to the high vacuum region and the continual throughput of process gas ensured that coating conditions are clean and reproducible.

5.2.2 Si wafer as the deposition substrate

Since the objective of this study is to investigate the dissolution rate of Al in Sn, the dissolution of any other element in Sn or Al could interfere with the accuracy of the result. Thus, Si wafer was chosen in most of the experiments as the deposition substrate, since Si does not react with Sn and Al.

5.3 Experimental procedures and results

5.3.1 Cu/Sn/Al

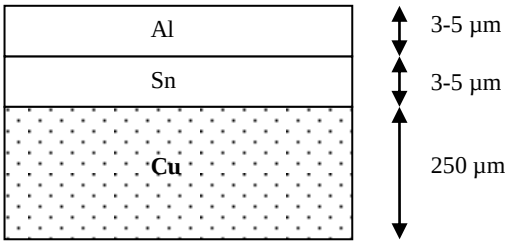

Figure 5-2 – A schematic image of the order of coating

In the first structure, Sn was sandwiched between Cu and Al layers as the interaction of Cu with the dissolved Al was deemed to be of interest. One Cu strip (150mm x 5mm x 0.25mm) has been sputter coating by Teer Coatings Ltd, first with 3-5 µm Sn and then 3-5 µm Al. It has been

assumed that as vacuum has not been broken during the coating there is no oxidation layer between Sn and Al.

As the surface condition of a material may play a vital role in the melting temperature of the material in a thin film, an initial experiment using Differential Scanning Calorimetry (DSC) was used to determine the melting temperature of a thin film of Sn. The range of temperatures for this experiment was set for 150-270 °C and the heating rate was 10 °C/min. The result show that the melting temperature of a thin film of Sn which has a thickness of about 3-5 µm is 227.93 °C. Fig. 5.3 shows the result of DSC. The DSC result indicates that the thin films may have picked up impurities that account for the width and range of the peak.

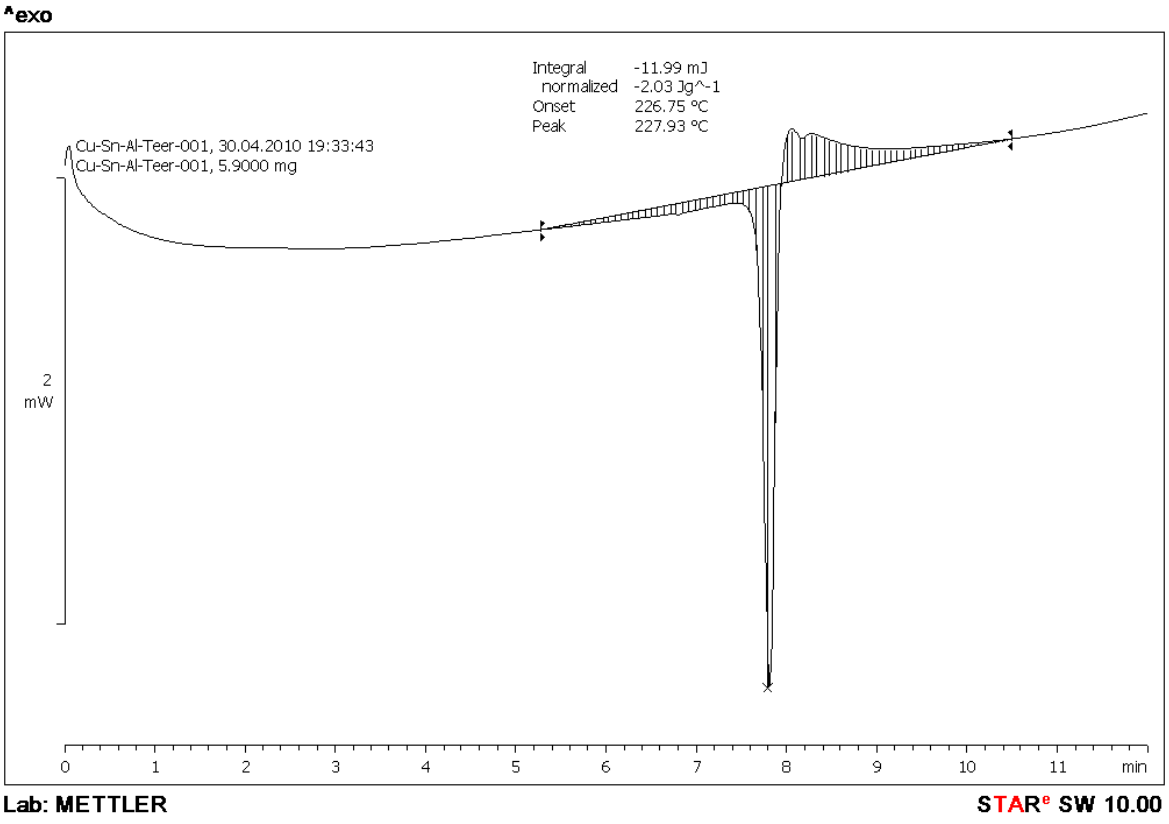

Figure 5-3 - The DSC result for melting point of thin film of Sn

As a result of the melting point determination, the oven was set for a temperature higher than 227.93 °C to reach the melting point of Sn. Coated Cu strip was placed inside a benchtop oven, preheated up to 230ºC for 60s and then reflowed at 265ºC for 60s. The reflowed sample has been cut by a diamond saw.

Another Cu strip with the same coating conditions was heated up to 265ºC for 1 hour in a tube furnace under vacuum. A third coated Cu strip was heated inside a tube furnace under vacuum for 5 hours. All three samples plus one original non-reflowed coated Cu sample have been polished by CSP for 20 hours at 5kV and have been examined by SEM.

The purpose of this experiment was to understand the interaction between Al and Sn and to see how much Al dissolves in a Sn film in contact with Cu, as well as subsequent reactions between the Cu-Sn IMCs and Al. Fig. 5.4 shows a Cu substrate which has been coated with Sn and Al before reflow. Al layer appears to be peeled off at the edge of the sample which resulted in not being polished by CSP.

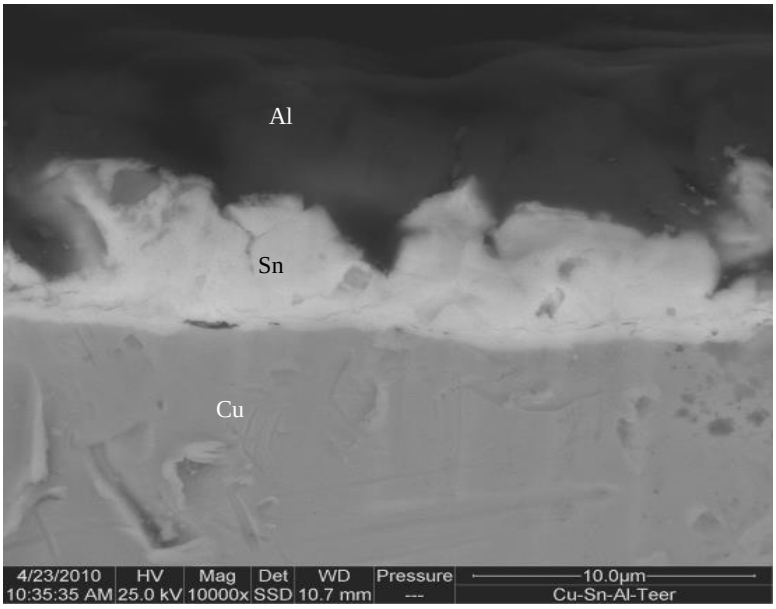

Figure 5-4 - Cu substrate coated with Sn and Al before reflow

The Sn layer seems to have a rough and bumpy surface at the interface with Al. Teer Coatings Ltd believes this is inherent in sputtered coatings of Sn. Fig. 5.5 shows a coated Cu substrate after a normal reflow. A thick layer of Sn-Cu Intermetallic can be seen between the Sn layer and Cu substrate. It seems that diffused Cu atoms interfere with the dissolution of Al in Sn and that interpretation of the experiment is problematic due to the large number of potential processes involved. Also as the Al top surface was originally rough because of the nature of coating, this method will be unable to measure the Al thickness after reflow and hence determine the extent of Al dissolution.

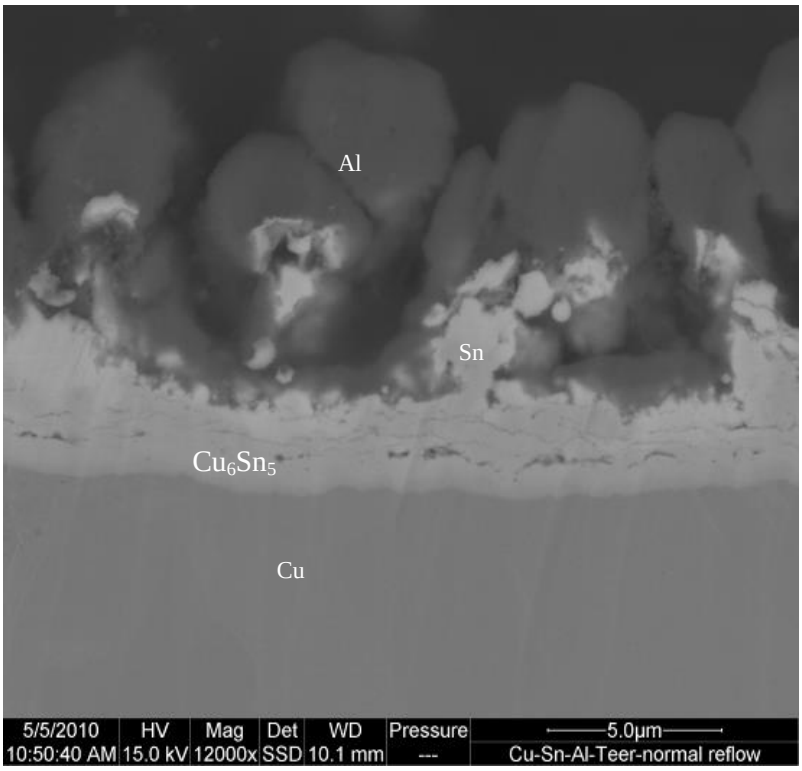

Figure 5-5 – Coated Cu substrate after normal reflow

Fig. 5.6 illustrates the coated Cu after 1 hour heating at 265ºC inside a tube furnace under vacuum. As Aluminium is very reactive with Oxygen, this experiment was performed under vacuum (10^{-5} Torr) to avoid the oxidation effect. A layer of Sn-Cu IMC can be seen in this image as well. Al layer appears to be peeled off at the edge of the sample which resulted in not being polished by CSP.

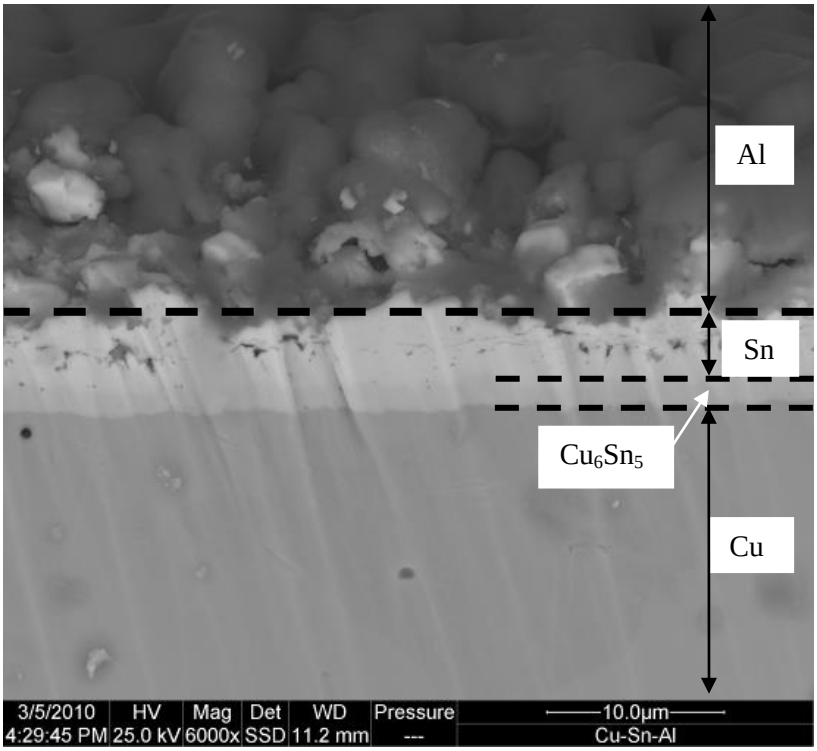

Figure 5-6 – Coated Cu substrate after heating up to 265ºC under vacuum for 1 hour

Line analysis (elemental analysis) has been used to evaluate the distribution of the elements after 1 hour of reflow. Fig. 5.7 shows the result of the line analysis. It can be seen clearly that Sn and Cu is present in the Al, but the likeliest explanation is that molten Sn has penetrated into cracks in the Al layer.

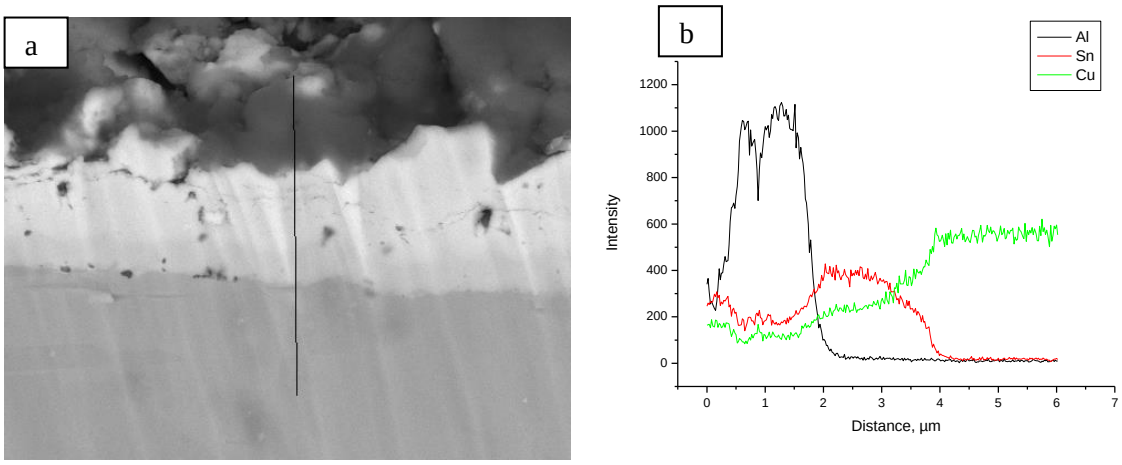

Figure 5-7 – (a) Elemental analysis of Sn and Al on Cu substrate after reflow, (b) Result of the elemental analysis

The sample which was heated up for 5 hours under vacuum has been shown in Fig. 5.8. It can be seen that Sn-Cu IMC is thicker in this experiment than in the 1 hour one. Also Sn reached some parts of Cu substrate far from the interface. As we can see from Fig. 5.5 and 5.6, the presence of Cu complicates interpretation and is a source of error in this experiment.

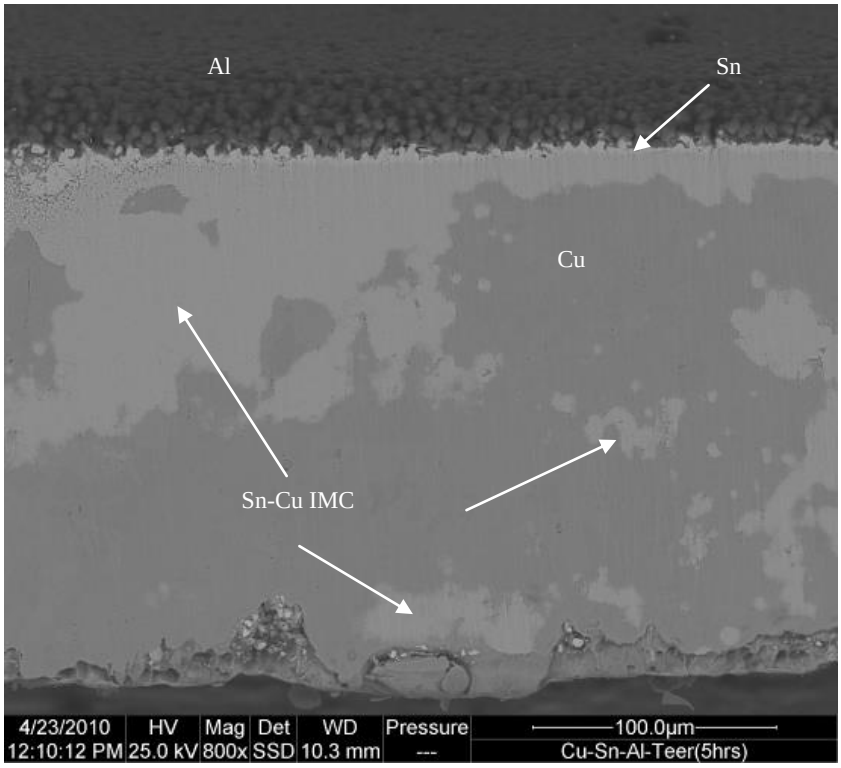

Figure 5-8 - Coated Cu substrate after heating up to 265ºC under vacuum for 5 hours

5.3.2 Ni(P)/Sn/Al

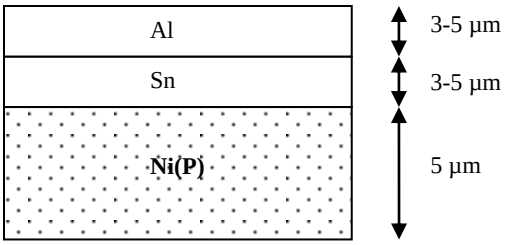

Figure 5-9 – A schematic image of the order of coating

One Ni(P) substrate has been sputter coated with Sn and Al by Teer Coatings Ltd. A Ni(P) substrate which is called ENIG, is an electroless nickel layer capped with a thin layer of immersion gold. The gold layer protects the nickel layer from oxidation and is rapidly dissolved in solder [200, 201].

The thicknesses of both coatings are 3-5 μm. The prepared sample has been reflowed for 1 hour under vacuum at 265ºC. Also, another coated Ni(P) substrate has been placed inside a benchtop oven, preheated up to 230ºC for 60s and then reflowed at 265ºC for 60s. The reflowed samples and the original coated Ni(P) substrate have been cross-sectioned by CSP. The polished samples have then been observed by SEM.

In this experiment the dissolution of Al in a thin layer of Sn has again been studied, while the modifications due to the presence of Ni(P)-Au are also of interest. Fig. 5.10 shows the coated Ni(P) sample. Al and Sn coating layers can be seen on top of a Phosphorus layer. The Sn layer in Fig. 5.11 seems to be a flat layer which could be a result of a thermal effect. But IMCs do not seem clearly visible.

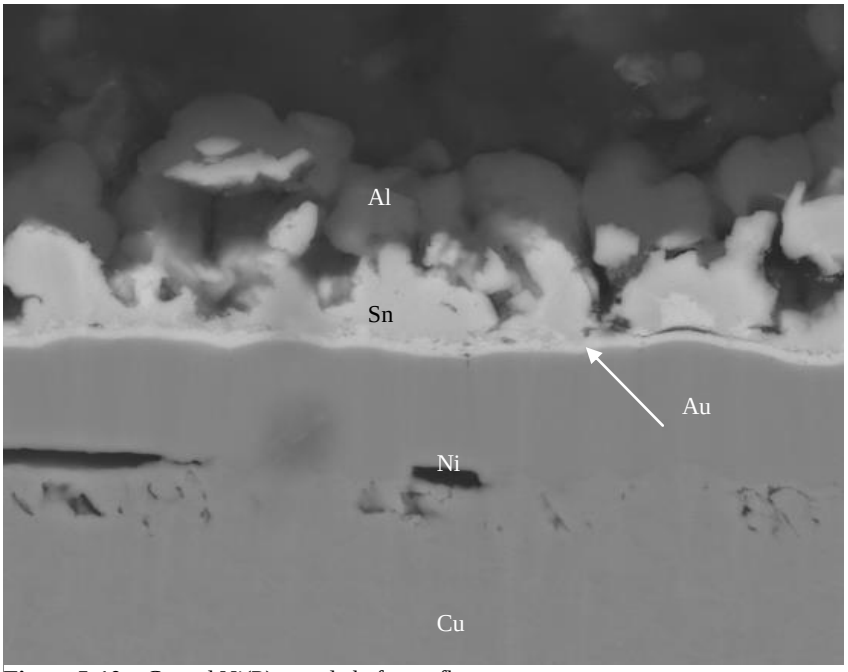

Figure 5-10 – Coated Ni(P) sample before reflow

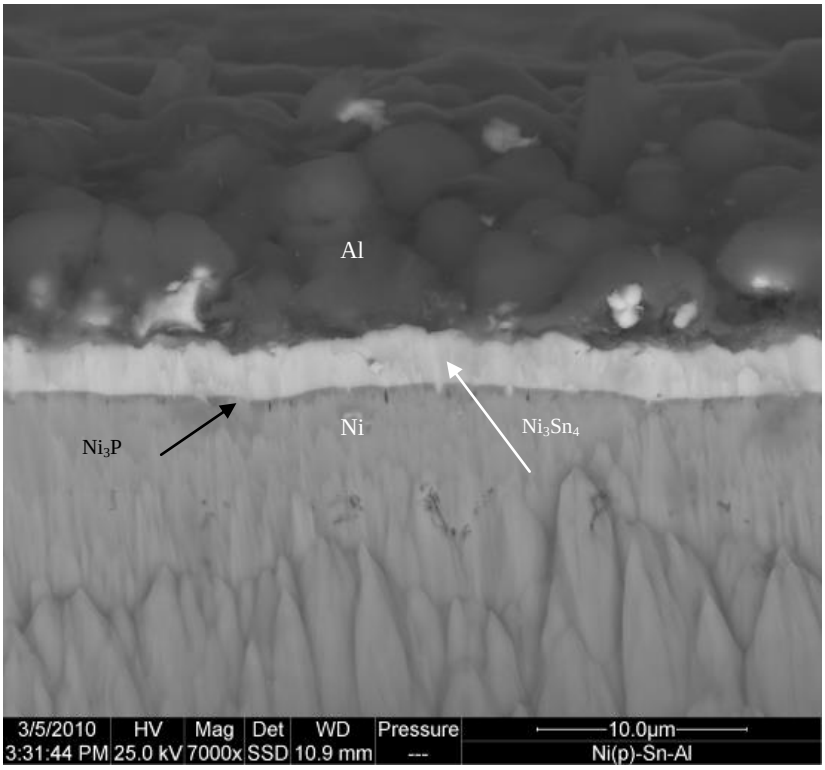

Figure 5-11 – Coated Ni(P) sample after 1 hour reflow under vacuum

However, IMCs are clearly visible at the interaction between Ni(P) and Sn in Fig. 5.12, which demonstrates the coated Ni(P) sample after a benchtop oven reflow. Also Fig. 5.13 shows a line analysis of Sn and Al on Ni(P) substrate after a benchtop oven reflow.

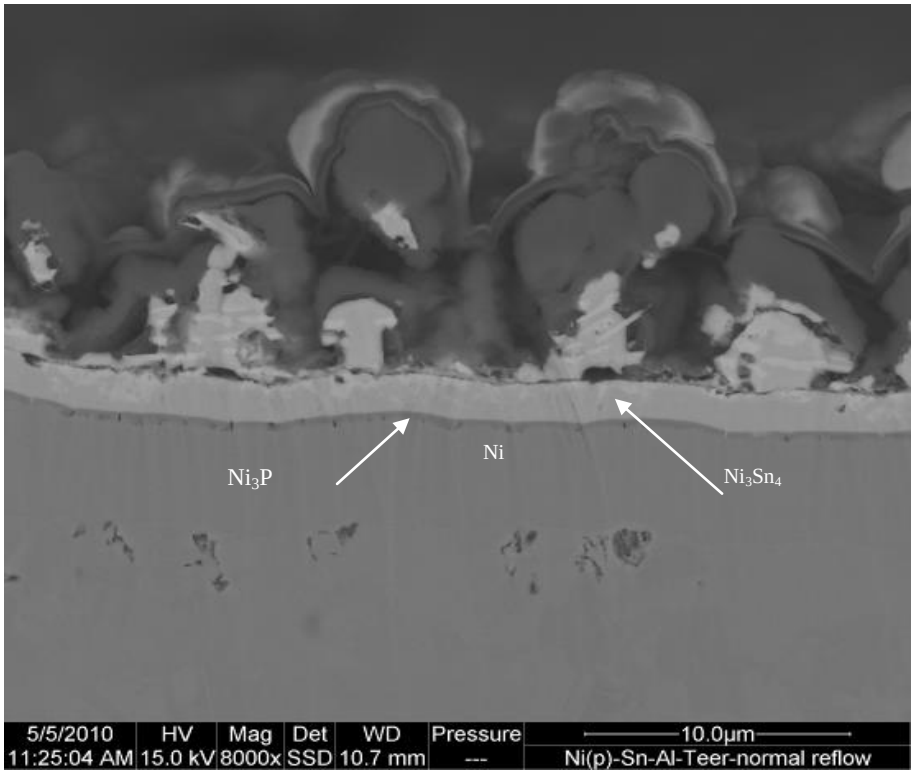

Figure 5-12 – Coated Ni(P) sample after a benchtop oven reflow

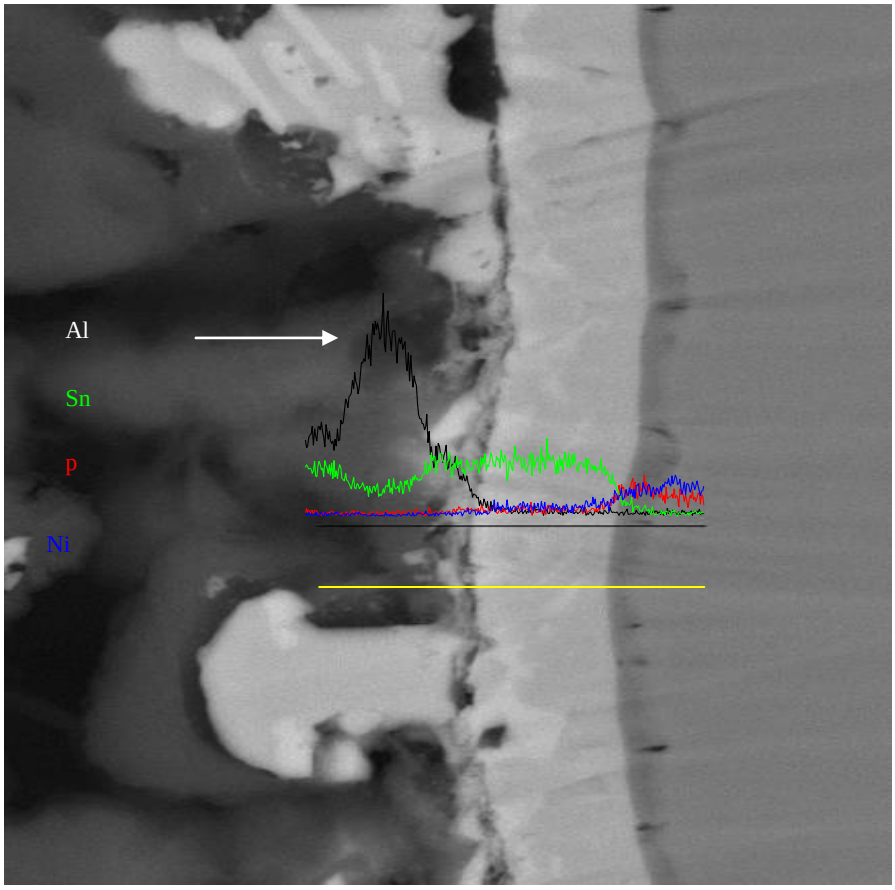

Figure 5-13 - Elemental analysis of Sn and Al on Ni(P) substrate after a normal reflow

It appears that the Sn has again penetrated into the Al layer, rendering interpretation of the experiments difficult. No trace of Al is found in the Sn based IMCs with either Ni or Cu substrates which is one relevant finding, but the remainder of this chapter deals with simplified Sn – Al systems where the presence of all other elements is avoided as much as possible.

5.3.3 Glass/Sn/Al

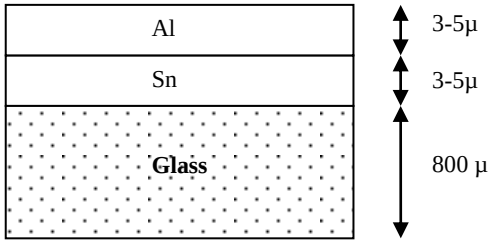

Figure 5-14 – A schematic image of the order of coating

One microscope slide was sputter coated by Teer Coatings Ltd, with first 3-5 µm Sn and then 3-5 µm Al. This experiment has been done to evaluate the dissolution of Al in Sn. The purpose of using Glass is to avoid any bonding between Sn and the substrate and also to avoid any interference in the dissolution process of Al into the liquid Sn from the substrate. Before any dissolution experiment, a coated glass slide has been cross-sectioned by CSP in preparation for SEM to investigate the original coating layers.

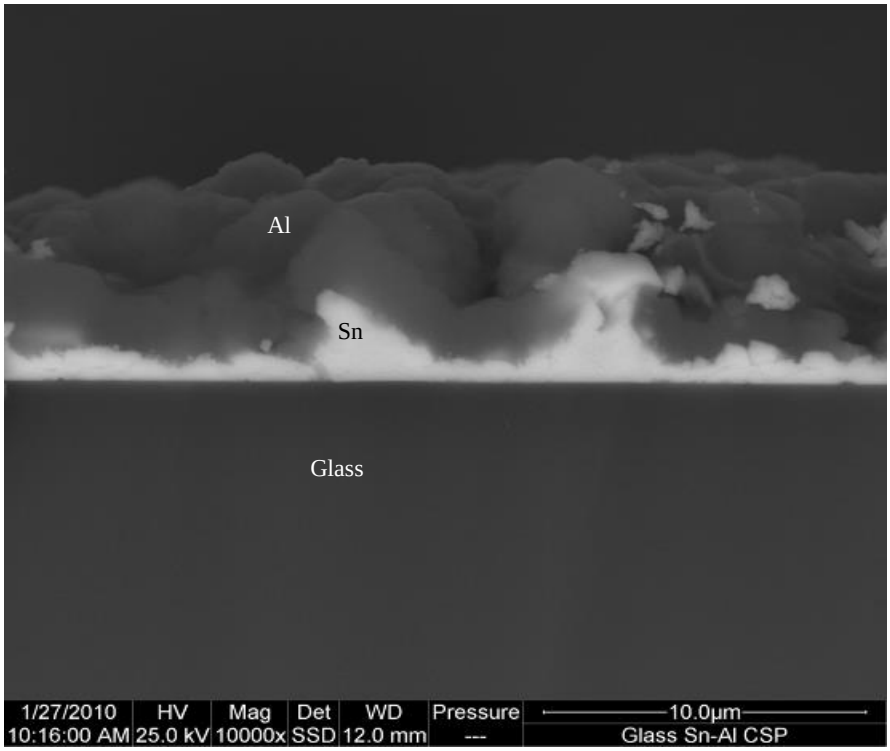

Figure 5-15 – The glass coated with Sn and Al before reflow

As can be seen in Fig. 5.15, Sn again has a rough surface at the interface with Al which will be a source of error in studying the dissolution of Al in Sn. Also, it was found that cutting the Si wafer is easier than glass. So, experiments shifted to using Si instead of glass without any dissolution experiment.

5.3.4 Si/Sn/Al

One Si substrate has been sputter coated by Teer Coatings Ltd with 3-5 µm Sn and 3-5 µm Al. The purpose of this experiment was to measure the dissolution of Al in Sn without interference of the substrate in dissolution. Thus, Si has been used, as Si does not make any compounds with Sn at the low temperatures of these experiments. Also, cutting Si using a glass cutter turned out to be easier than cutting glass. Before any dissolution experiment, coated Si substrate were cross-sectioned by CSP for preparation for SEM to investigate the original coating layers.

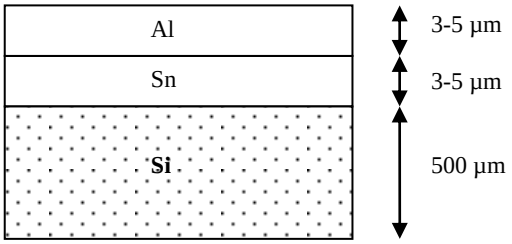

Figure 5-16 – A schematic image of the order of coating

Fig. 5.17 shows a Si substrate which has been coated with Sn and Al. We can see that both Sn and Al have a rough surface which could be source of error in our experiment. Also we see a flat interface between Si and Sn. No experiment was performed with this sample. The reason is the irregularity of the interfaces and top surfaces would render any attempt to quantify dissolution impossible. Thus, the results of these four samples led to the conclusion that in order to obtain a flat Sn-Al interface, Si should be used as the substrate and Al should not be on top as the rough top surface of Al does not allow a precise thickness measurement. New geometries were therefore trialled.

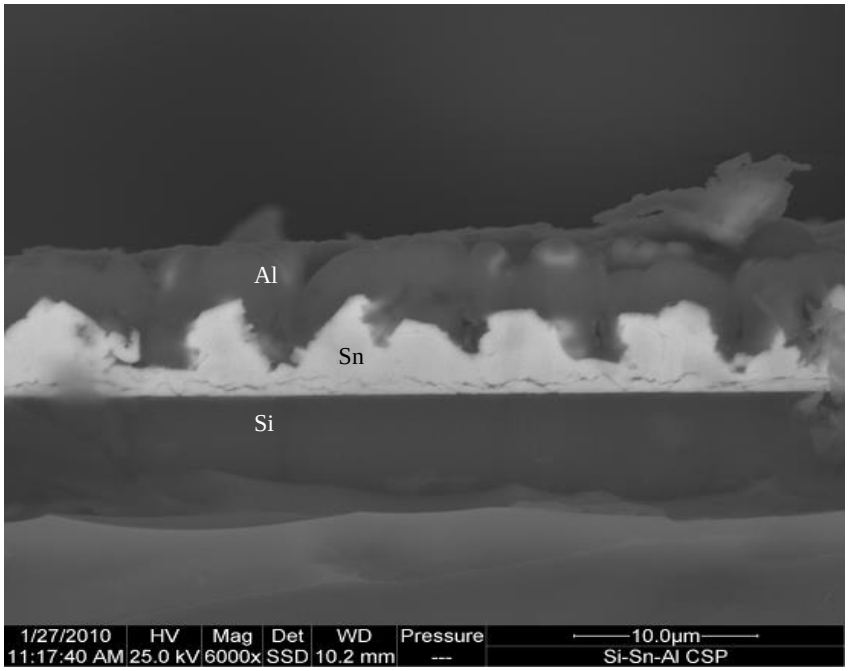

Figure 5-17 – Si sample coated with Sn and Al before reflow

5.3.5 Cu/Sn/Al/Sn

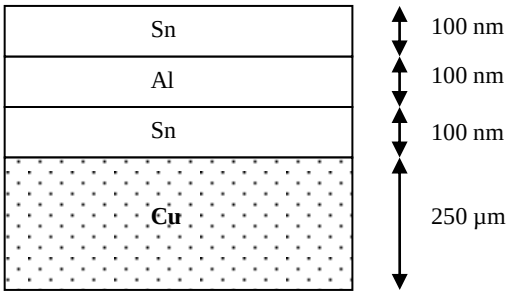

Figure 5-18 – A schematic image of the order of coating

As King's College London has its own coating facilities, it was decided for the next set of experiments to be performed at King's College London.. The purpose of this experiment was to study the multilayer of Sn and Al. This experiment was not helpful to measure the dissolution of

Al in Sn. But it was helpful to examine the structure of Sn and Al multilayers which will be used in later experiments. Fig. 5.18 shows a schematic view of sample geometries. As King's coating facilities cannot reach as thick a coating as Teer Coatings Ltd can, the thickness of coating layers was decided to be about 100 nm.

Two pure Cu strips 150mm x 5mm were coated with tin, aluminium and tin. A Leybold Vacuum Coater U300, which is a thermal evaporator, was used for this coating. As the coater was located at King's College London, the cost associated with preparing samples was minimal. This coater is facilitated with two sources allowing Al and Sn coatings without intermediate exposure to air, with vacuum of 10^{-6} mbar. One boat made of Molybdenum or Tungsten was used to hold the Sn source and a filament made of Tungsten was used to hold Aluminium. The thermal evaporator was facilitated with a Bio-Rad E5550 Film Thickness Monitor (FTM). The FTM was used to monitor and control the thickness of the coating layers by monitoring the frequency shift of an oscillating quartz crystal. The error of the FTM is about ±10% of the final value. One of the sources of errors in FTM was the heat inside the thermal evaporator chamber. The heat affects the accuracy of the FTM by heating up the head of the monitor which contains the quartz crystal.

For the first strip, the first 100 nm of tin has been coated on top of a Cu strip. 100 nm of Al was coated on top of the tin and again 100 nm of Sn was coated on top of the Al. A second Cu strip has been coated with 500 nm of each. The coated samples have been mounted using the CSP and found to provide smooth and flat surfaces. The CSP was set up at 5kV for 20 hours. The polished sample was evaluated by SEM.

Fig. 5.19 shows two images of multilayers of Sn and Al on top of Cu substrate. In addition, the thermal evaporation route was found to be superior to sputtering in providing measurable and uniform thicknesses of Al and Sn.

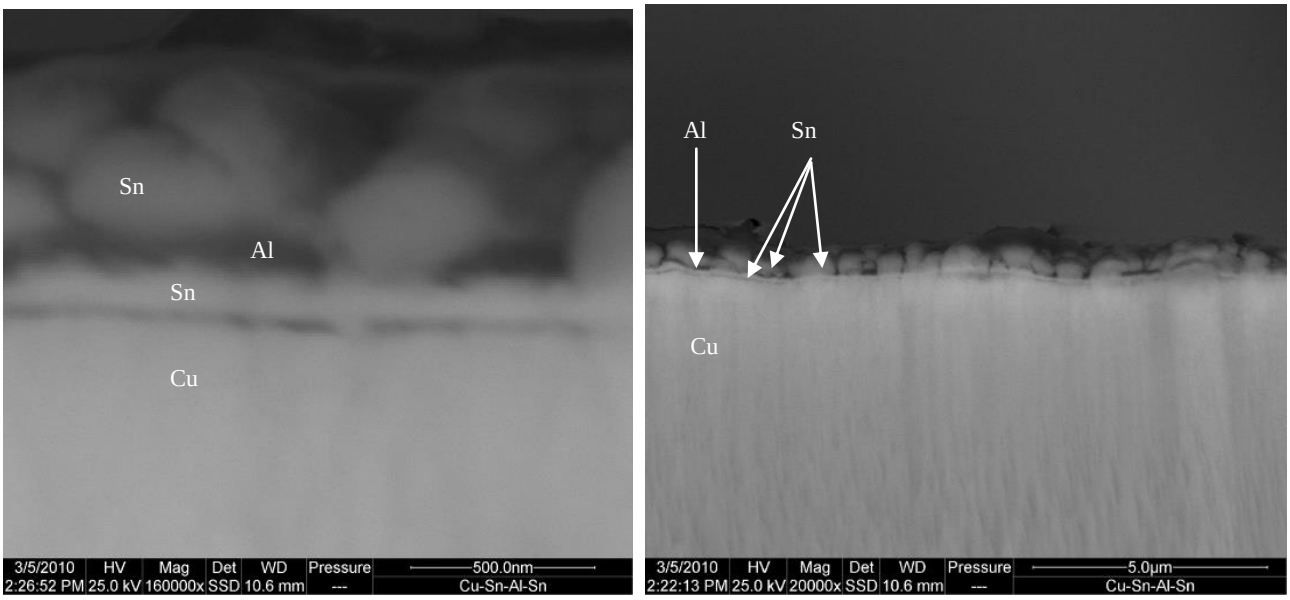

Figure 5-19 – Cu sample coated with multilayer of Sn, Al and Sn before reflow

5.3.6 Si/Al/Sn (by thermal evaporator)

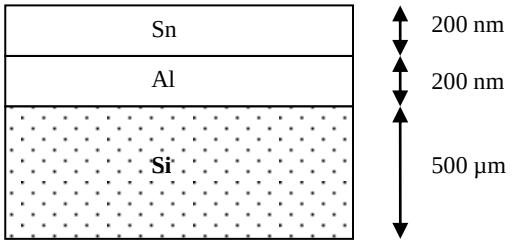

Figure 5-20 – A schematic image of the order of coating

As the thermal evaporator at King's struggles to coat thicknesses over 200 nm, two sets of experiments were prepared. In the first, which was prepared at King's, 200 nm thicknesses were

used for each layer. Secondly, Teer Coatings Ltd was asked to provide layers with about 3µm thickness for easier SEM examination.

For the first experiment, one Si wafer disk has been cut by a glass cutter into small strips about 50mm x 5mm x 500µm. Si strips have been coated by a thermal evaporator with 200 nm Al and then 200 nm Sn on top of Al. The Si sample which has been coated by thermal evaporator can be seen in Fig. 5.21. The purpose of this experiment was to study the quality of the thermal evaporator coating and then to investigate the dissolution of Al in Sn. The order of coating Al and Sn has been switched to make a flat surface on both sides of Al so as to make it possible to measure the thickness of Al before and after reflow. As can be seen in Fig. 5.21, the thermal evaporator provided Sn and Al with smooth and flat layers.

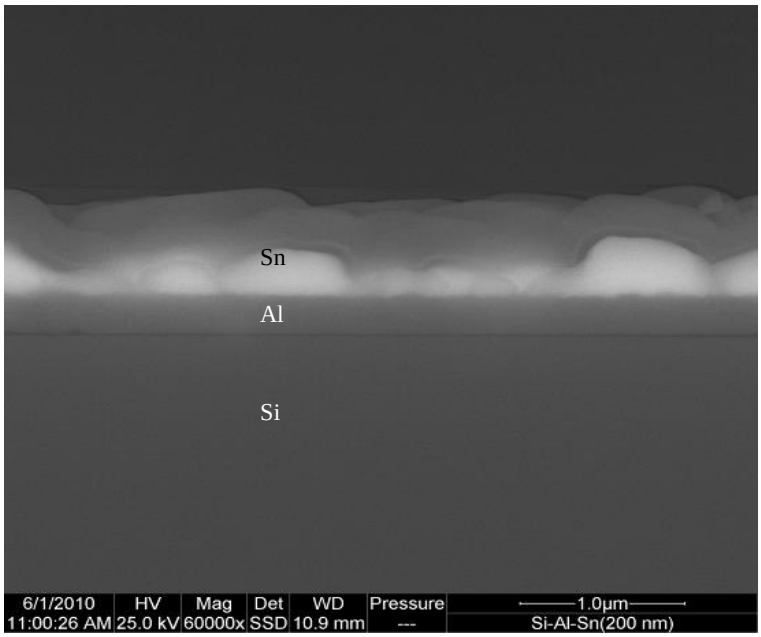

Figure 5-21 – Si substrate coated with Sn and Al by thermal evaporator before reflow

5.3.7 Si/Al/Sn (sputter coating by Teer Coatings Ltd)

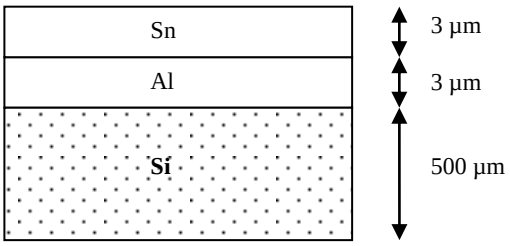

Figure 5-22 - A schematic image of the order of coating

For this set of experiments, coating of Al and Sn were performed by Teer Coatings Ltd, on Si wafer strips. The plan of this set of experiment is based on two methods of introducing Sn to Al. First one is dipping coated samples into molten Sn and the second one placing solder paste on top of coated layers. In both methods, the main aim is to provide an unlimited amount of Sn for Al to dissolve into.

For the first method, a clay graphite crucible (height 70 mm and diameter 50 mm) which contained 150 g Sn was placed inside an oven and left there for about one hour at 260ºC (with about ±10 ºC error) until the Sn became molten. Coated samples were dipped into molten 260ºC Sn and held there for 10, 30 and 120s. Fig. 5.23 shows the coated Si which is dipped in molten Sn.

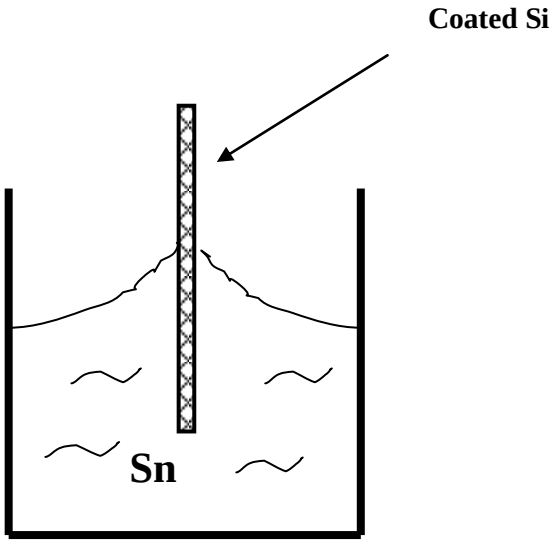

Figure 5-23 - Coated Si which is dipped in molten Sn

Three more samples which were coated by Teer Coatings Ltd were dipped in 260ºC molten Sn but this time with flux for 10 s, 30 s and 120 s. All samples were cross-sectioned by CSP for 20 hours at 5kV and evaluated by SEM.

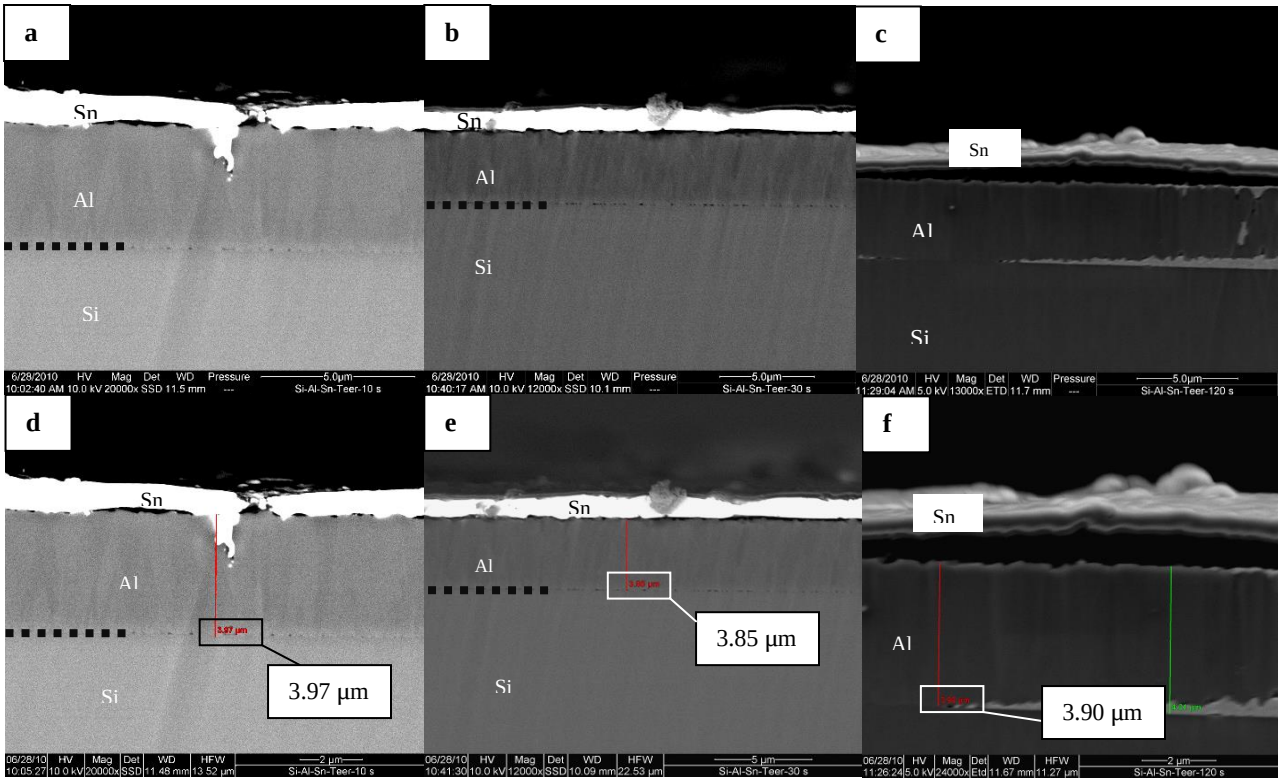

Figure 5-24 – Coated Si sample after dipping in 260 ºC molten Sn for (a) 10 s, (b) 30 s and (c) 120 s and their thickness measurements in (d-f)

Fig. 5.24 shows images of Si coated samples by Teer Coatings Ltd, after dipping in 260 ºC molten Sn for 10s, 30 s and 120 s. It can be seen clearly that Al does not dissolve in these experiments. One reason could be an oxidation layer on top of the Al coating layer which works as a barrier for Sn to dissolve and subsequently confines dissolution of Al to just the original coating thickness. To avoid this oxidation, flux has been used in latter experiments. Fig. 5.25 proves that using flux did not help Al to dissolve in molten Sn.

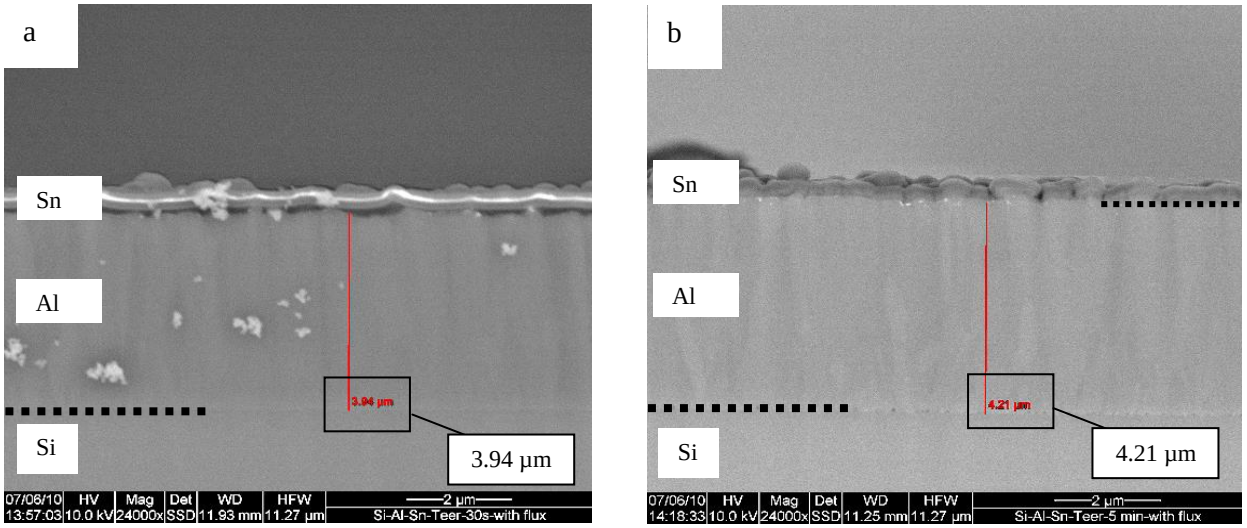

Figure 5-25 – Coated Si substrate after dipping in 260ºC molten Sn with using flux for (a) 30s and (b) 5 min

As can be seen in Fig. 5.25 Al has not dissolved to any significant extent in the molten solder. There is a possibility that oxygen has diffused through the Sn layer, reached the Al and has made an oxidation layer on top of the Al layer, which does not let Al dissolve. Fig. 5.26 shows similar result for 1 hour dipping.

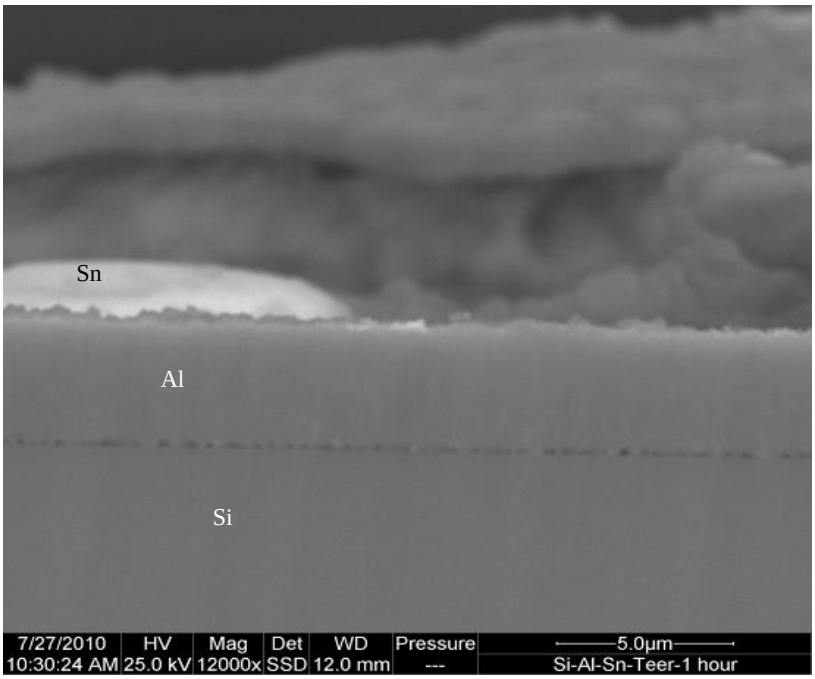

Figure 5-26 - Coated Si substrate after dipping in 260ºC molten Sn with using flux for 1 hour

To avoid the oxygen reaching Al when molten Sn touches the coated sample, the last sample was examined using solder paste. In this case, it is believed that as solder paste is covering an area of the coated Sn on top of the sample, there would not be any chance for oxygen to reach Al and hence Al could dissolve in Sn. Thus, solder paste was placed on top of a coated sample and then placed inside the benchtop oven. First, the sample was preheated up to 230ºC for 60s and then reflowed at 265ºC for 60s.

Fig. 5.27 shows a coated Si substrate after a reflow inside a benchtop oven. The thickness of the Al is about 3.40 µm which is thinner than the original 3.96 µm. There could be a sign of dissolution here. However, when this experiment repeated under vacuum the results were not consistent (Fig. 5.28).

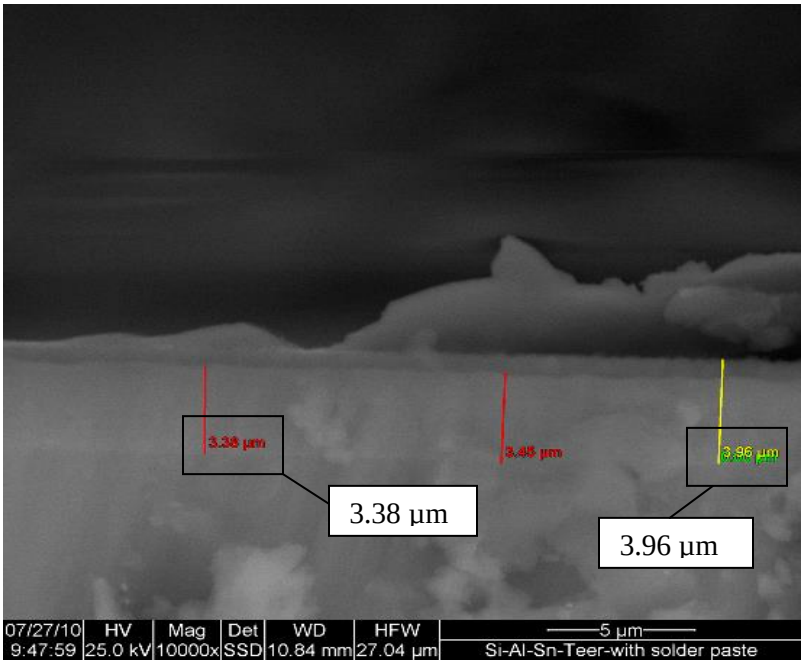

Figure 5-27 - Coated Si substrate with solder paste on top after reflow in a benchtop oven

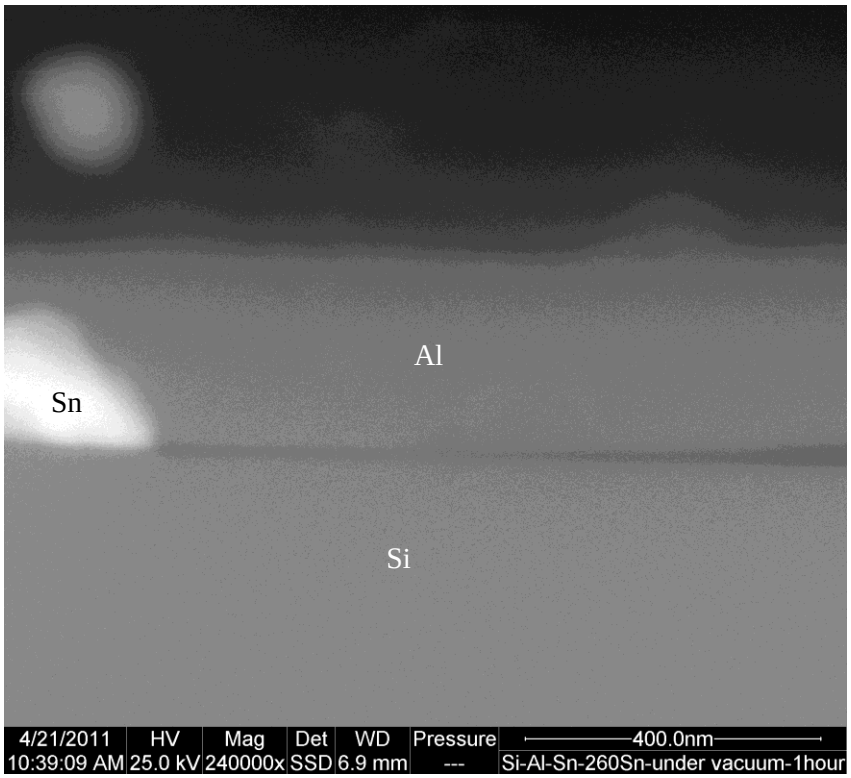

Figure 5-28 - Coated Si substrate with solder paste on top after reflow under vacuum for 1 hour

5.3.8 Si/Al/Au

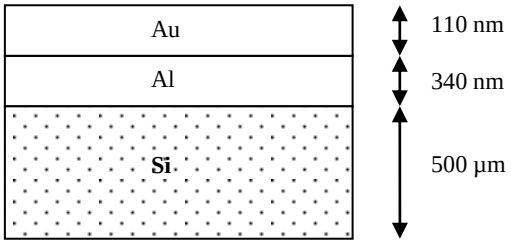

Figure 5-29 – A schematic image of the order of coating

One Si wafer which has been cut into thin strips by a glass cutter has been coated by thermal evaporator with first 340 nm of Al and then 110 nm of Au on top of it. The coated strips have been dipped in 260ºC Sn for 1 min and 3, 6, 12 and 24 hours. Two other coated strips have been dipped at 500ºC for 1 min and for 1 hour. All samples have been cross-sectioned by CSP at 5kV for 20 hours. Cross-sectioned samples have been evaluated by SEM.

It was concluded in the previous experiments that Sn is not a good oxidation resistant coating for Al and another element is needed with better coating characteristics. Although Sn has been used as a practical coating for preventing Cu oxidation, the amount of diffused oxygen which forms a problematic Al oxide layer barrier is much lower than the amount of diffused oxygen which creates problems for Cu [202].

Au has been chosen because of its proven use as an oxidation barrier on e.g. Ni(P) coatings, and because it can dissolve easily in molten Sn [203]. Fig 5.30 shows an original coated Si substrate before dipping in molten solder. It can be seen in Fig. 5.31 that Al has not dissolved after dipping in molten Sn for 1 minute. There is a bright layer attached to the Al layer in Fig. 5.32 (a). This is identified as Sn which has been attached to Al after dissolution of the protective Au layer. There is no sign of dissolution of Al in Fig. 5.32. Also it can be seen that the Al layer has detached along certain portions from the Si substrate in Fig. 5.32 (a).

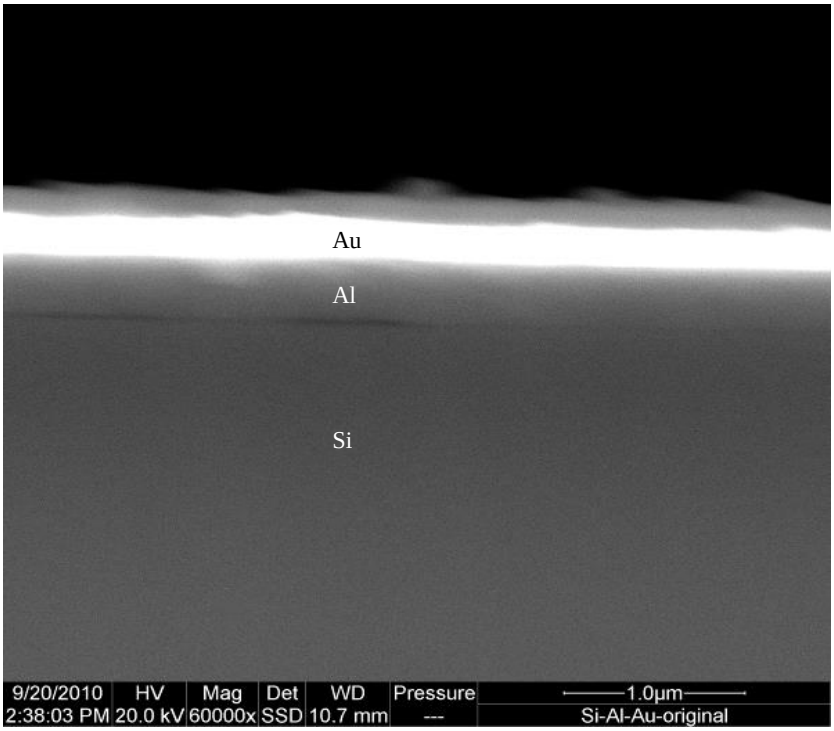

Figure 5-30 – Si substrate coated with Al and Au before reflow

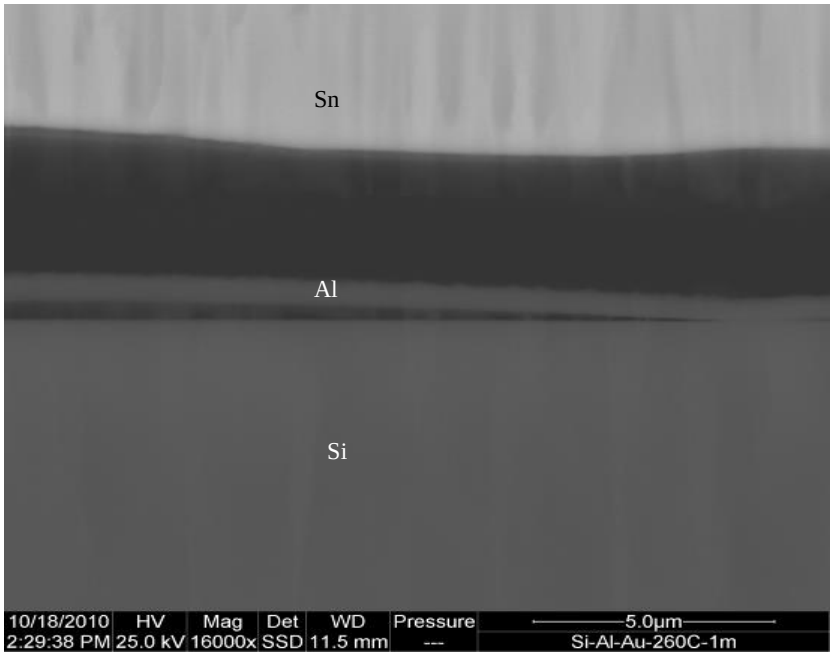

Figure 5-31 - Coated Si sample after dipping in 260 ºC molten Sn for 1 minute

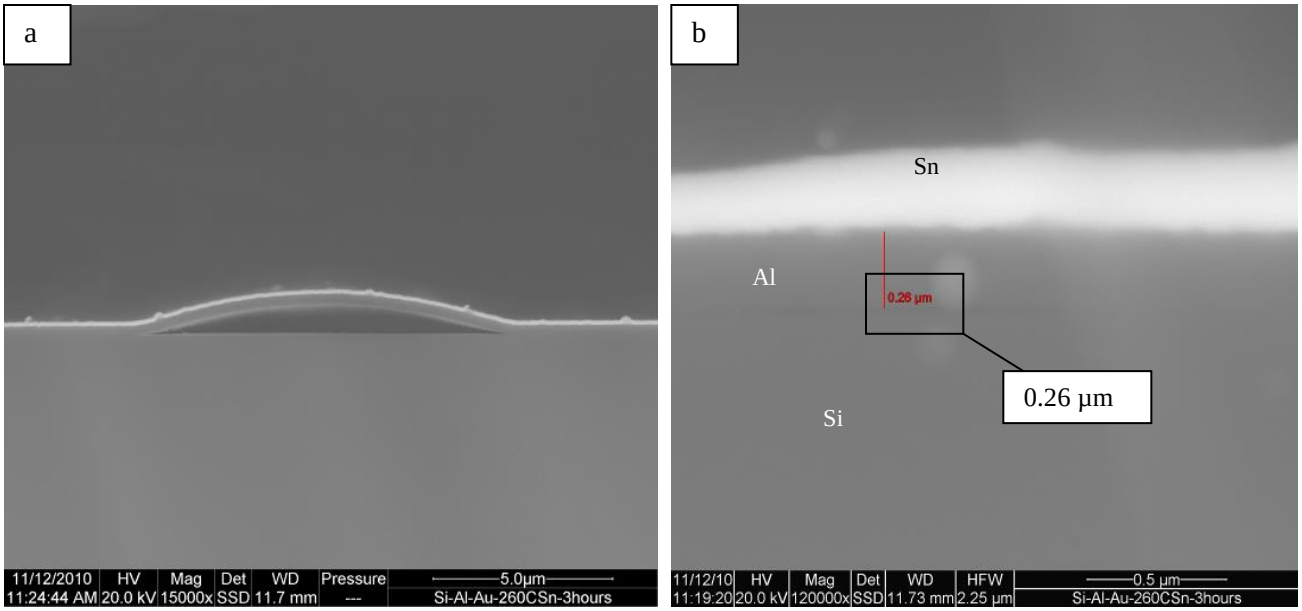

Figure 5-32 – Coated Si substrate after dipping in 260 ºC molten Sn for 3 hours

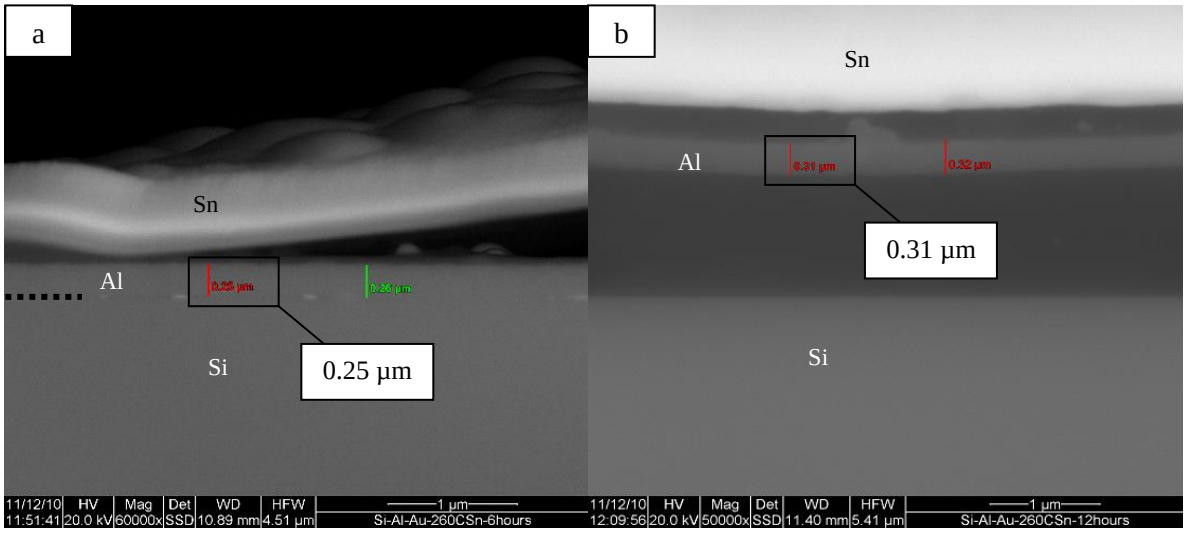

Figure 5-33 – Coated Si substrate after dipping in 260 ºC molten Sn for (a) 6 hrs and (b) 12 hrs

Fig. 5.33 illustrates coating layers after dipping in molten Sn for 6 and 12 hours. There is no sign of dissolution of Al in these cases. In Fig. 5.33 (b), the Al layer can be seen detached from the substrate. Also the bright layer on top of Al layer is solidified Sn.

There is something new happening in Fig. 5.34 which shows the result of dipping the Al for 24 hours. It seems that some part of the layer on top of the Si substrate has similar colour to Al and some part has a brighter colour. One reason could be that after 24 hours of dipping the sample in molten Sn, Al and Au bond with each other and there is no pure Al layer to dissolve in Sn anymore. In this case, any dissolution of the layer in Sn cannot be counted as dissolution of Al as the layer is a mixture of Al and Au.

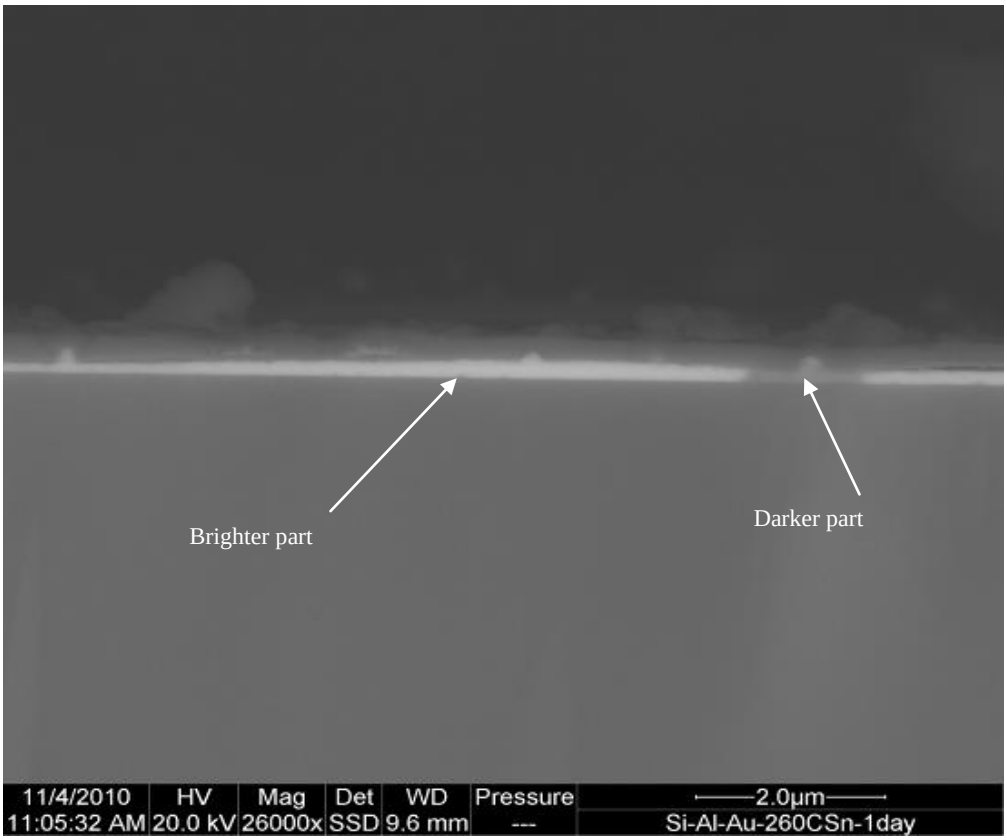

Figure 5-34 – Coated Si substrate after dipping in 260 ºC molten Sn for 24 hrs

Another experiment which has been done with these coated samples was dipping them in 500ºC molten Sn for 1 minute and for 1 hour. Fig. 5.35 shows an image from the sample after 1 minute of dipping. It seems that coated layers have been detached from the Si substrate because of the high temperature. One piece of Al with Au layer attached to it but up-side-down has been deposited on the Si substrate. They might have been detached from Si substrate, floating in molten Sn and then deposited on Si substrate. Fig. 5.36 shows two different images from samples after dipping in 500 ºC molten Sn for 1 hour.

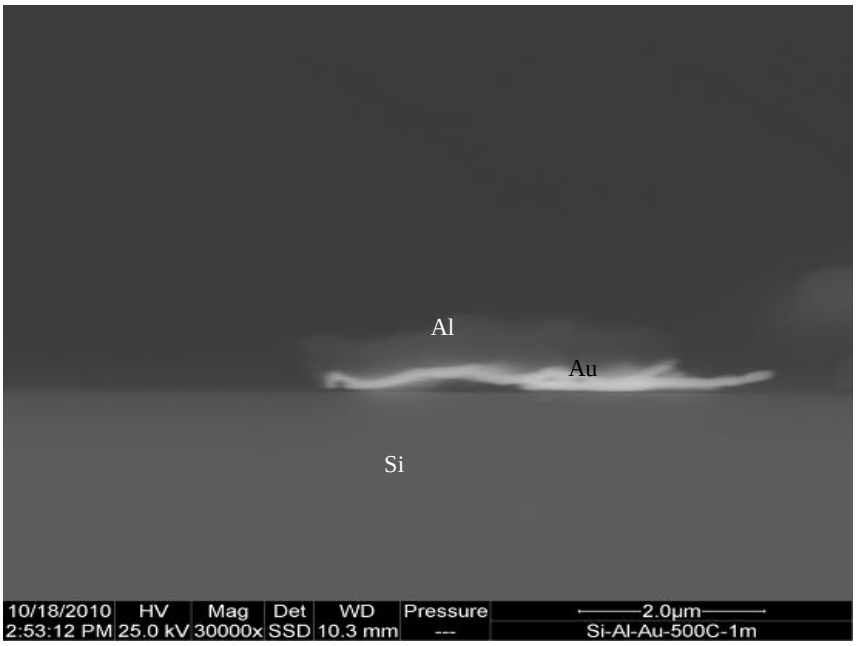

Figure 5-35 - Coated Si substrate after dipping in 500 ºC molten Sn for 1 minute

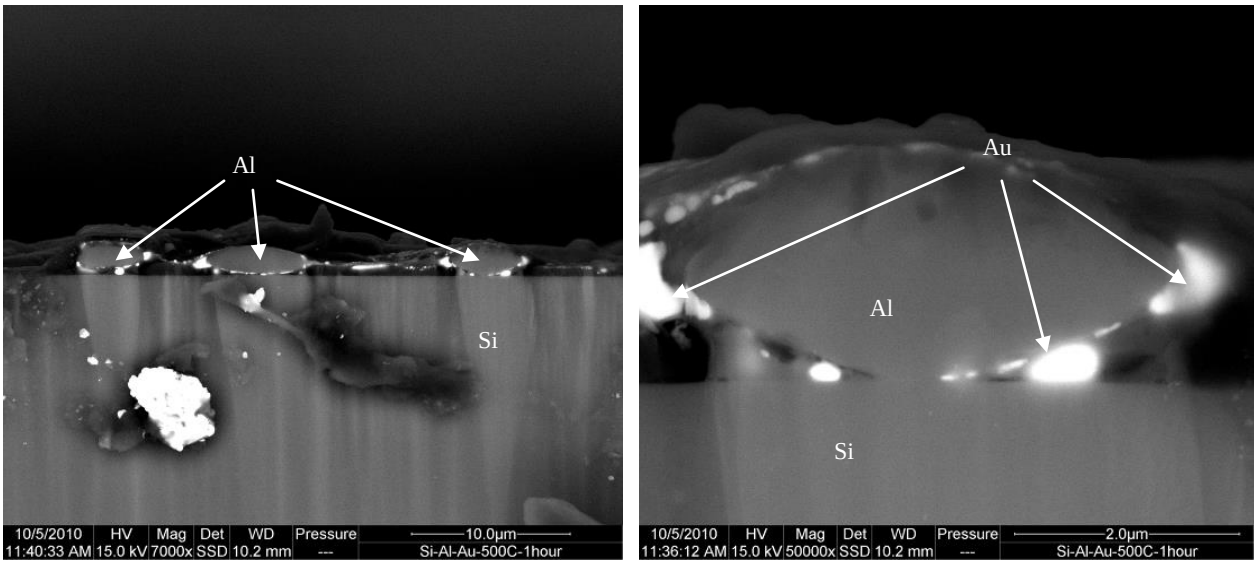

Figure 5-36 – Two images from samples after dipping in 500 ºC molten Sn for 1 hour

It seems that the Al has coalesced into grains rather than dissolving into the Sn. The bright particles are Au which appears to have recombined with the Al from the molten solder due to affinity between the two elements and there is a possibility of forming Al-Au IMCs.

5.3.9 Si/Cr/Au/Al/Au

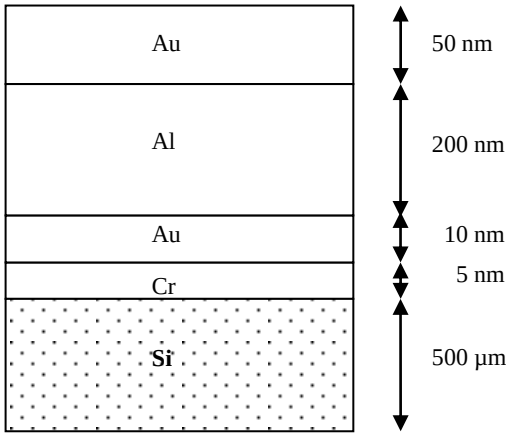

Figure 5-37 – A schematic image of the order of coating

One Si wafer has been cut to strips. Strips have been coated by a thermal evaporator with first 5 nm of Cr and then 10 nm of Au on top of that. The vacuum of the thermal evaporator chamber has been broken to change the Cr source with Al source, as this coater can have only two sources. After setting up the Al source, the chamber has been vacuumed again to coat 200 nm of Al followed by 50 nm of Au. The purpose of the Cr layer is to provide better adhesion between the Al and the Si

The coated Si wafers have been dipped in 260ºC Sn for 1, 3, 6 and 12 hours. All samples have been cross-sectioned by CSP for 20 hours at 5kV. Cross-sectioned samples have been evaluated by SEM.

Fig. 5.38 shows an image of an original coated Si sample which has been coated with Cr, Au, Al and Au. As the thickness of Cr is only 5 nm that is very hard to distinguish between thin layer of Au and Cr at the bottom of Al.

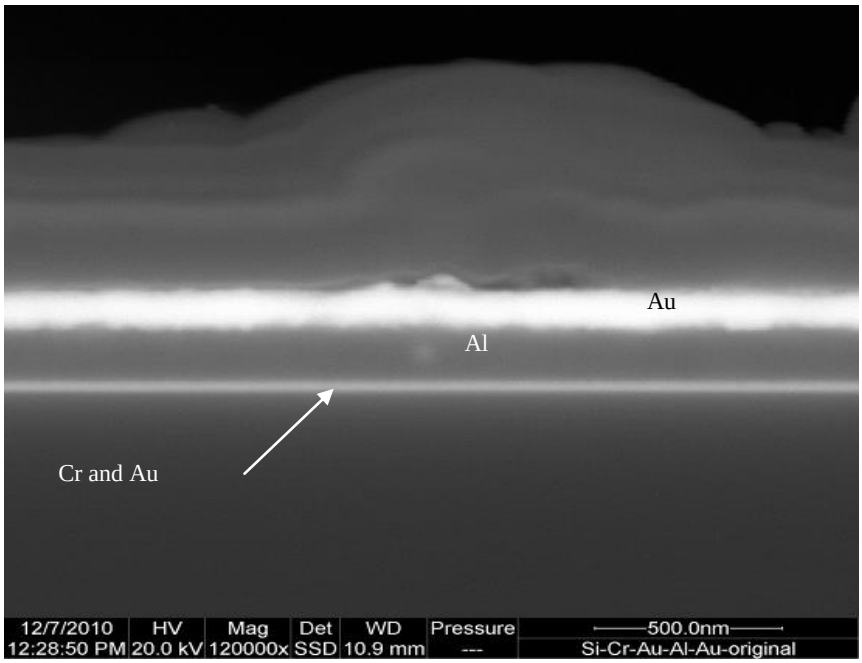

Figure 5-38 – Si substrate coated with Cr, Au, Al and Au before reflow

Fig. 5.39 demonstrates the sample after 1 hour of dipping in 260 ºC Sn. The thin layer on top of Si substrate is Al-Au layer. It seems that Al and Au layers interdiffusing as the Al strip became brighter than its original colour. Also the thick layer on top on the thin layer is another mixture layer of Al-Au. The gap between two Al-Au layers can be a result of breaking vacuum during the experiment for replacing Cr source with Al source. It can also be seen that the thick Al/Au strip is broken off the substrate at one point.

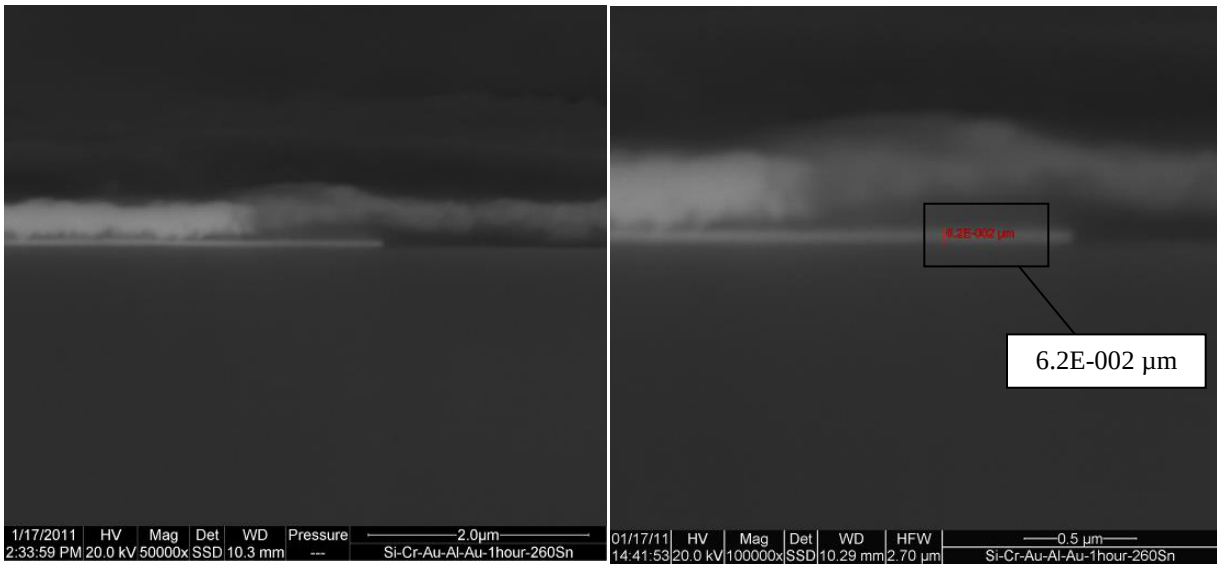

Figure 5-39 - Coated Si substrate after dipping in 260ºC molten Sn for 1 hour

Fig. 5.40 shows the sample after 3 hours of dipping in 260 ºC Sn. The thin and dark layer at the bottom of the bright layer seems to be Al-Au layer.

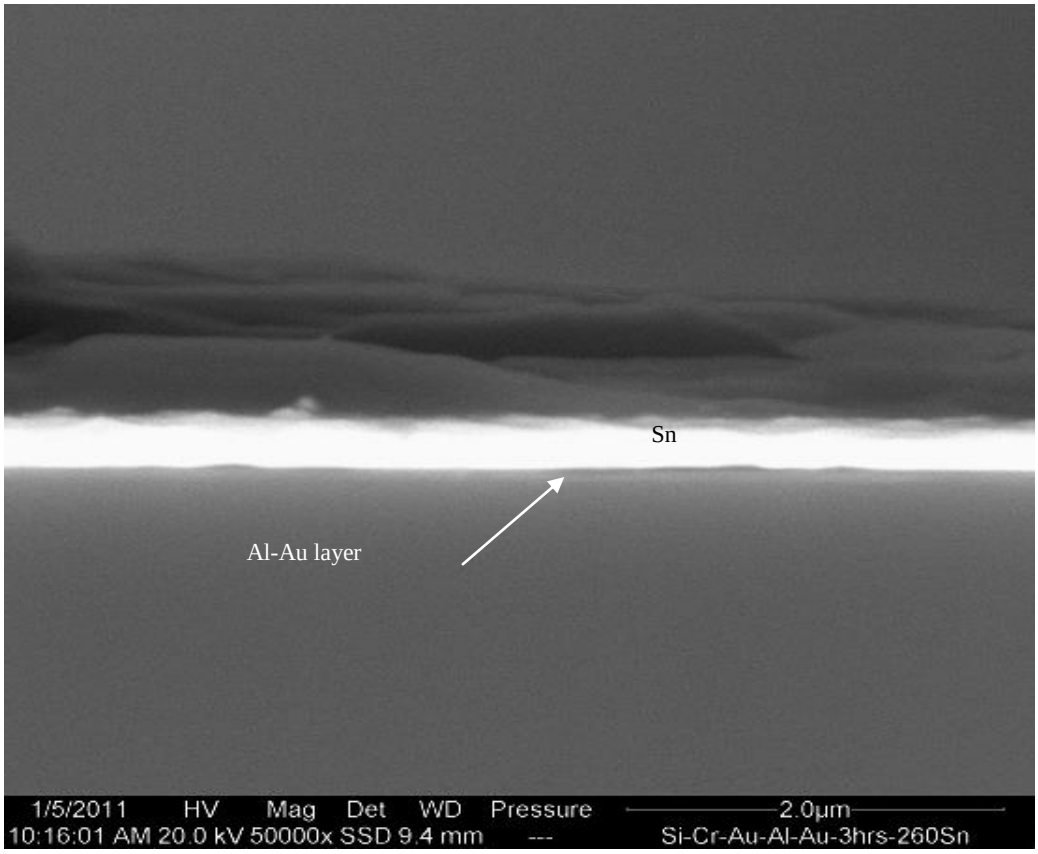

Figure 5-40 - Coated Si substrate after dipping in 260 ºC molten Sn for 3 hours

Fig. 5.41 shows the sample after 6 hours of dipping in 260 ºC Sn. A very thin layer of Al can be seen in this image. It seems the layer has been detached from the substrate and the thickness is about 34 nm. As it has been experienced before it might be a mixture of Al and Au.

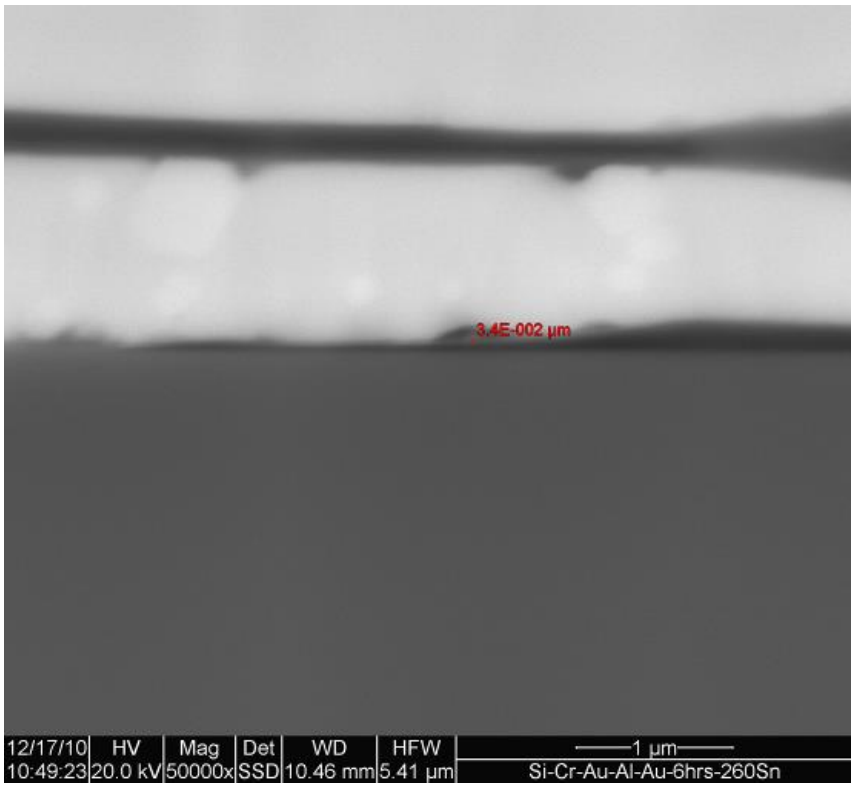

Figure 5-41 - Coated Si substrate after dipping in 260 ºC molten Sn for 6 hours

Fig. 5.42 shows the sample after 12 hours of dipping in 260 ºC Sn. The thin layer after 12 hours seems brighter than the one after 6 hours of dipping. The reason could be that Au has been dissolved in the Al thin layer and made that brighter. The thickness of the layer after this experiment is about 30 µm.

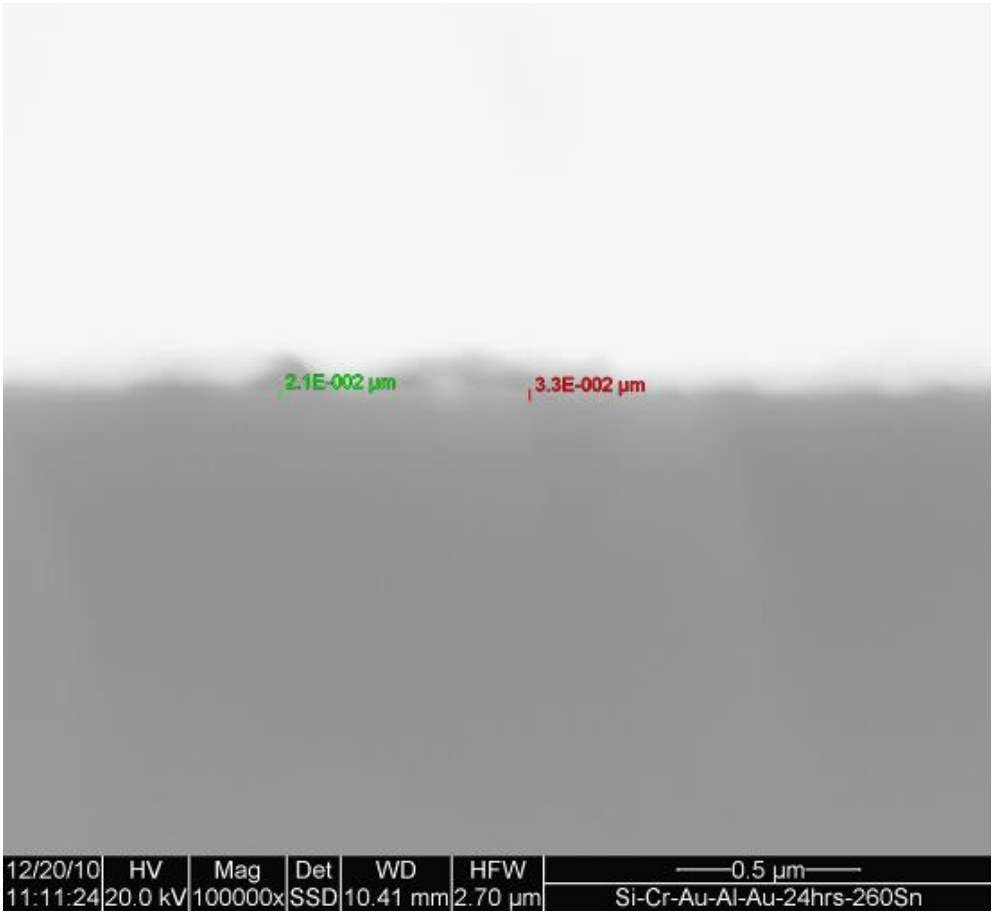

Figure 5-42 - Coated Si substrate after dipping in 260 ºC molten Sn for 12 hours

5.4 Discussion

Experiments can be divided into three subgroups; Al coated on top, Sn coated on top and Au coated on top. In the first one, the thermal evaporation method shows a more uniform layer structure in comparison to sputter coating of Sn. Sn coated by sputter coating appeared to have a rough surface. To measure the dissolution rate of Al in Sn, data on the precise thicknesses of the original Al and Sn layer is necessary. Because of this, the thermal evaporation method was chosen as the coating method of choice, especially for Sn. Glass and Si substrates worked better

than Cu and Ni(P) substrates as Si and glass do not dissolve in Sn, hence not influencing the Al dissolution in Sn. The Cu and Ni(P) substrates were used to see whether the Ni and Cu would react with the Al after reacting with the intermediate Sn but no definitive conclusions can be drawn on this, though Al and Ni traces were observed in the Al, these could be from the close proximity of the Sn-Cu and Sn-Ni IMCs. Working with Si cutting is easier than glass as it is easier to cut. Hence Si was chosen to be the most promising substrate in comparison with glass. Coating of Al on top of Sn is found not to be an effective method as the top layer of Al was rough and it was impossible to deduce how much Al has dissolved by Al thickness measurements. In summary, the first set of experiments led to the use of Si as the preferred substrate and prevention of coating Al on top of Sn.

The second method has a Sn layer coated on top of the other layers. Results do not show any sign of the dissolution of Al in Sn. The most likely cause preventing dissolution of Al in Sn is that oxygen has diffused through the Sn layer, reached the Al and has made an oxidation layer at the Al-Sn interface which prevents Al dissolving. It seems that Sn is not the best coating element for this experiment. Even using solder paste (Figs. 5.27 and 5.28), with its inherent fluxing action did not result in repeatable Al dissolution although one result alone did suggest that some Al had dissolved at a rate of 500nm/minute. One possible reason can be that flux acids have partially eroded Al layer and Al did not dissolve into Sn. However, analysis of flux residues can clarify this. Therefore, further investigation is needed. In all other results Al appeared to keep its original thickness after experiments indicating that there is no dissolution of Al in Sn.

The third method had Au coated on top of other layers. As was mentioned earlier (see section 5.3.8 Si/Al/Au) Au was chosen because of its proven use as an oxidation barrier on e.g. Ni(P) coatings and can rapidly dissolve into molten Sn. At high temperatures, the Al film was seen to

coalesce into beads but still these did not dissolve into the Sn. It was seen that Al detached from the substrate in some cases, especially, in the longer experiments. Cr coating was added in order to adhere the Al layer to the substrate until the end of the experiment. The adhesion seems to have improved but only made Al and Au layers interdiffusing rather than enabling Al dissolution into Sn. So, again the results represent no sign of the dissolution of Al in Sn. It should be noted from the binary phase diagram of Al-Sn that Sn should dissolve 0.5 wt% Al [144, 204] at 260 °C so that the sub-micron thicknesses of Al used should dissolve into the solder baths without saturating it (see section 2.4.1 Dissolution of Al in Sn).

5.5 Modelling of the dissolution of Al in Sn

Here, the mathematical theory of diffusion of Al in Sn which is based on Fick's second law (see section 2.4.2 The mathematics of diffusion) of diffusion was used to investigate the concentration of Al inside the molten Sn. The analytical solution to Fick's second law, which is given by Stephenson [205] is as follows:

$$C = C_s + (C_i - C_s)\sum_{n=0}^{\infty} a_n \exp\left(-\frac{n^2\pi^2\alpha t}{L^2}\right)\sin\left(\frac{n\pi x}{L}\right) \tag{5.2}$$

Where $a_n = \frac{4}{n\pi}$ for odd n, zero for even n, C_s= C(0, t) = 1 is the boundary condition and L is 2 x the thickness of the finite layer. This analytical solution is solved numerically by MATLAB and the result is plotted in Fig. 5.43. This figure shows the concentration of Al versus the

distance from the Al substance. The initial condition was assumed that to be C(x, 0) = 0 and boundary condition assumed that to be C (0, t) = 1 and $\frac{\partial C}{\partial X}(1,t) = 0$.

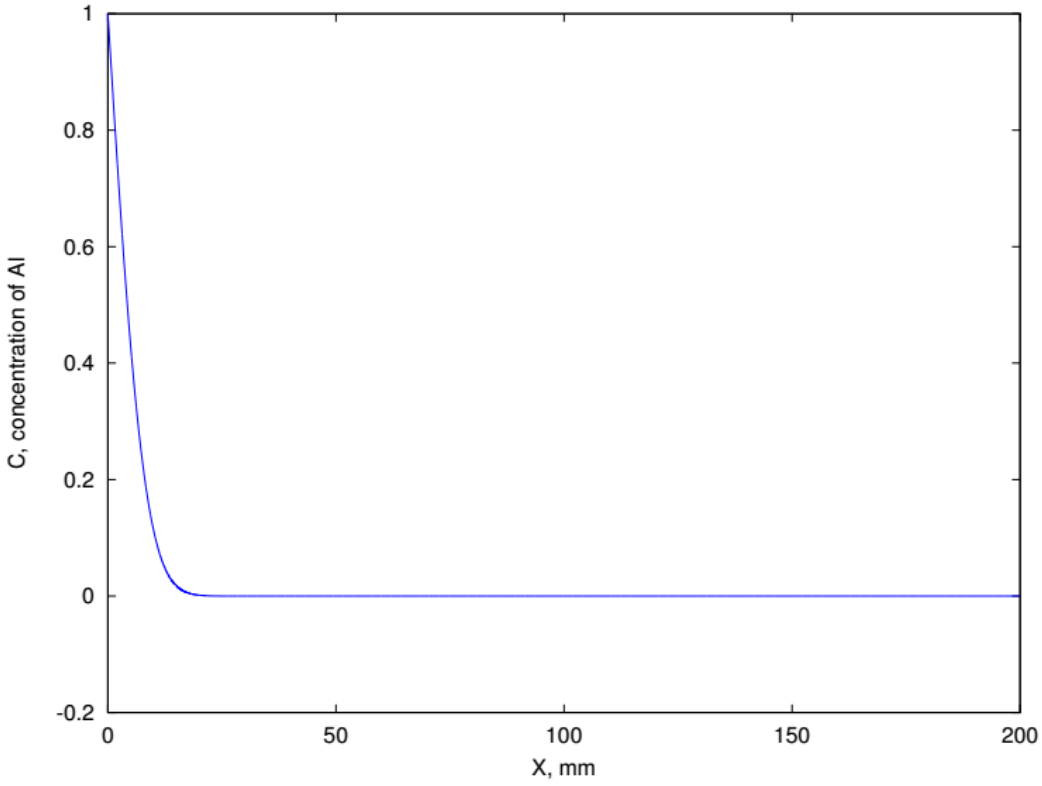

Figure 5-43 - Concentration of Al in molten Sn versus the distance from the Al substance

As can be seen in this figure, the concentration of Al decreases sharply with increasing distance from the Al substance.

5.6 Conclusion

This study was performed to investigate the dissolution rate of Al in Sn. Since Al is very reactive to Oxygen, any contact between Al and Oxygen should have been avoided. Thus, in this study, the coating layers of Sn and Al on top of each other inside the highly vacuumed chamber was attempted.

The results show no consistent and repeatable signs of dissolution of Al in molten Sn. Three sets of experiments were developed to investigate the dissolution of Al in molten Sn. Experiments were designed to provide a clean surface between Al and Sn or Al and Au. First Al was coated on top of other layers. The top layer of Al was rough and since the measurement of Al layer thickness was the main theme of this research, Al should not be the top layer and this methos was doomed to be in effective

The second method of coating was coating Sn on top of Al resulting in flat and smooth layer of Al in contact with coated Sn. This method also did not provide repeatable evidence of dissolution of Al in Sn but indicated dissolution in just one case (see Fig. 5.27), using solder paste. Since the result was not consistent, one possibility could be that flux acids have partially eroded the Al layer and Al did not dissolve into Sn. Should any investigator repeat this experiment in future, investigation of the flux residues can clarify this. The most likely reason for inefficiency of coating Sn on top of Al is that oxygen diffused through Sn and reached Al, forming an oxide layer on top of the aluminium layer. This oxide layer did not allow Al to be wetted by molten Sn. It was concluded that Sn is not a promising coating layer for this experiment.

Au was chosen as a replacement coating layer for Sn. This method did not show dissolution of Al in Sn. Au dissolved in molten Sn and Al layer. The brightness of the Al layer imaged in the

SEM increased after the experiment indicating the existence of Au in the Al layer and the Al layer may have become a mixture of Al and Au which could not be considered as a dissolving Al layer anymore. Therefore, Au also proved to be an unsuitable coating layer for Al layer.

The original aim of the work described in this chapter was to investigate the possibility of reaction between Al and Sn and also to determine the dissolution rate of Al in Sn in the temperature range applicable to soldering, so that the behaviour of Al nanoparticles during soldering could be predicted. Although we were not able to determine dissolution rates, we have demonstrated that both Sn and Au are not suitable candidates for preventing the Al from oxidizing at the interface with Sn, even when the deposition took place in high vacuum. In order to make further progress, the use of an ultrahigh vacuum chamber during the coating of Sn onto the Al is recommended, with the heating and dissolution steps also carried out in vacuum or inert atmosphere.

As was explained in the introduction (see section 5.1), the main purpose of the investigation of the dissolution rate of Al in Sn is to design nanoparticles to release Al into the solder at the optimum time during the reflow. This would maximize Al reactions with the substrate while minimizing the interference with solder during wetting reactions. In addition to Al, other elements such as Zn can also be investigated. Since Zn is not as reactive as Al with Oxygen, it has proven easier to introduce Zn nanoparticles and Zn micron-size particles into the solder and produce the required barrier layers [11, 141, 206].

6. Conclusions

6.1 CSP method

After the introductory chapters, in the third chapter, the interaction between solder and Cu substrate, ENIG, and inert (glass) substrates was investigated with both methods of mechanical polishing and CSP. In this chapter, the emphasis was on studying IMC structures and grain boundaries, and on the use of the argon ion beam as an alternative to mechanical polishing. The cross-section polishing method has proved to provide a high quality cross-section and results suggested that for delicate and brittle samples CSP is potential to provide more efficient than the mechanical method while final assertion needs further work.

For example, for the sample which was investigating the interaction between the solder and the Cu substrate, the CSP method was able to simultaneously show the crystalline structure of the Cu substrate and both the Sn and Ag_3Sn phases in the solder while in the sample which was mechanically polished, the details of Cu substrate or the bulk solder are not clear. In another example, a large Ag_3Sn plate IMC with detailed internal platelet like structures was clearly shown which was polished by CSP. Thus, over all, the CSP method has shown several advantages over mechanical polishing method. For example, CSP does not need an expert to run it and a practitioner with a basic level of expertise of that machine can polish the sample, however, mechanical polishing needs experience.

This chapter sets up the best polishing method for this body of work for analysing nanoparticle enhanced solders and other soft solders as used in the rest of thesis and potentially for other users. For example, this method was highly effective in SEM evaluation of nano-enhanced solder in chapter 4. This method was also vital for cross-sectioning the nano-layers of chapter 5 in which SEM was used to examine the thickness of layers. Therefore, the main outcome of this chapter was to represent the capability of the CSP in providing excellent polished surfaces of

materials for the investigation by SEM. According to the miniaturization trends of the microelectronic materials, the need for CSP in studying new materials used in semiconductor industry will be increased.

6.1.1 Further work suggested from the CSP chapter results

Using same condition sample for comparison

- As was mentioned earlier (see section 3.3) one of the disadvantages of CSP is the limitation in mounting a sample inside the CSP chamber for polishing. Polishing further than 75 µm from the edge of the sample is impossible as 75 µm is the maximum length which can be jutted out from the shield plate to be polished.

  In order to compare the quality of polishing between mechanical polishing and CSP two samples were compared. A large difference in size of interfacial IMCs between the two samples was observed even though they were prepared under identical conditions, and made it harder to compare the two methods. The discrepancy may be caused by the fact that the cross section of the sample which was polished by CSP was taken 75 µm from the edge of the substrate while the other sample which was cross sectioned by mechanical polishing resulted in a section further in towards the center. This was caused by the "edge effect" which is the result of diffusion and IMC formation kinetics at the solder bump edge (see section 2.2.4 Geometry of solder and the "edge effect"). This problem can be avoided by additional steps:

  1. Samples which are being cross-sectioned by CSP can be milled away by several 75 slices, in order to reach the middle of the solder bump. However, this would be time consuming.

2. Prior to apply CSP, a low speed diamond saw can be applied in order to reach the middle of the solder bump. This would then be followed by CSP cross-sectioning.

3. Prior to apply CSP, FIB can be used to take out a small size slice of solder out from the middle of the solder bump. This would then be followed by CSP cross-sectioning.

6.2 Nano-composite solders

The fourth chapter was about adding passive Silica (SiO_2) nanoparticles to lead-free solder to improve solder reliability, especially, for high temperature applications. Nanoparticles proved effective in restricting grain boundary movement at room temperature.

In this chapter passive Silica (SiO_2) nanoparticles were added to Sn3.8Ag0.7C solder paste to fabricate nano-composite solder. Nano-composite solder was cross-sectioned by CSP and evaluated by SEM to detect nanoparticles. After detection of nanoparticles inside nano-composite solder, solder rods were prepared for mechanical testing. Compression tests were performed at room and elevated temperatures (25 °C, 50 °C, 100 °C and 150 °C). Compressed solder rods were cross-sectioned and evaluated by SEM to examine the effectiveness of nanoparticles in limiting grain growth.

Results show that at higher homologous temperatures, the pinning effects of the nanoparticles decrease due to thermal fluctuations in the position of the grain boundary. This results in a decrease in the effective number of particles pinning the grain boundaries. The analysis of thermally activated grain boundary movement indicates that the fluctuations of the grain boundaries at temperatures under 100 °C are less than the particle diameter, resulting in effective pinning. However, at 150 °C, the displacement of grain boundaries becomes larger than the particle diameter resulting in unpinning of the grain boundaries. Larger particles should

result in reduced thermal unpinning and the optimum particle diameter for 150 °C is predicted to be 274 nm. Lastly, the activation energy of the SAC and nano-enhanced SAC has been examined. Higher activation energy provides higher energy barriers to limit atomic movements inside the microstructure of materials. The results showed that the nano-enhanced SAC has larger activation energy values than SAC. Thus, results in this chapter provide the optimum radius size of passive nanoparticles to be added to solder for a wide range of temperatures for high temperature electronics. Therefore, the main outcome of chapter four was to describe the capability of grain growth limitation by SiO_2 addition to the SAC solder matrix as a function of temperature. This work has led to an equation which predicts the optimum effective diameter of the added SiO_2 particle for the desired working temperature.

6.2.1 Further work investigating creep reduction in solders arising from chapter 4

6.2.1.1 Experimental modification

Grain measurements - The grain measurement in this chapter were performed manually by measuring six different diameters of a grain which were measured by choosing each diameter horizontally after rotating the image through 30 degrees. This method has given an average diameter for each measured grain. The grain measurement method can be improved in order to reduce the error. As was mentioned earlier, EBSD can be used in order to improve the accuracy of the grain size measurement but was not originally used as it was not available at KCL. Future work should utilize EBSD capabilities which include imaging grains via grain orientation with a spatial resolution of 0.2-0.3 μm, combined with regular capabilities of an SEM.

6.2.1.2 Investigation on grain growth limitation at high temperature without mechanical loading

Chapter four investigated the effectiveness of nanoparticle addition in reducing creep. As was explained in the literature review (chapter two), both heat and applied stress contribute to creep. In chapter four solders with and without added nanoparticles were compared under conditions of combined heat and stress. This suggests a further study on the efficiency of nanoparticles at high temperature and the optimum size of nanoparticles for preventing grain growth in the absence of mechanical loading (applied stress).

6.2.1.3 Investigation on alternatives to nanoparticles

- Other passive particles such as TiO_2 can also be tried. However, since passive particles cannot react with the solder and are expelled from the solder during the reflow (similar to the SiO_2) a coating process will be also needed.

- It was shown that the effectiveness of nanoparticles in reducing creep at high homologous temperature decreases as the thermal fluctuations of grain boundaries became larger than the particle diameter, resulting in unpinning of the grain boundaries. One of the advantages of using nanoparticles is the large pinning stress developed by having a small radius of curvature. The work of chapter four suggests that an extended structure can overcome the problem of unpinning due to thermal grain boundary fluctuations. Thus a nanotube which exhibits a small radius of curvature in one dimension (and hence high pinning strength) but a micron sized longitudinal dimension to make thermal unpinning harder may be of greater effectiveness. Carbon nanotubes or other extended structures where small thermal fluctuations in the location of the grain

boundary would not necessarily result in unpinning may therefore be of greater use in order to limit the grain boundary movements at high homologous temperatures.

6.3 Dissolution of Al in Sn

The fifth chapter concerns the dissolution of sub-micron Al thin films in Sn – an important topic for the introduction of reactive elements into solders via nanoparticles. As Al is very reactive with oxygen, preventing direct contact between Al and oxygen has been attempted by coating different elements onto Al to provide a clean surface between Al and a coating layer prior to the contact of Al and molten Sn. Sn and Au were the main coating elements which were used in this research. Al was contacted to molten Sn by two methods of heating. One was dipping coated Al in 260 °C molten Sn and the other one was placing the coated Al in a bench top oven with solder paste. After the heating process the thickness of Al was examined by SEM to investigate the change in Al thickness. The results show no consistent signs of dissolution of Al in molten Sn. Three set of experiments were developed to examine the dissolution of Al in molten Sn. In the first experiment, Al was coated on top of Sn and Sn was coated on top of four different substrates which were, Si, glass, Ni(P) and Cu. This experiment was not successful as the top layer of Al was rough due to the coating process which did not allow the thickness to be measured. In the second experiment, Sn was coated on top of Al. This method did not provide any dissolution of Al in Sn. The reason could be that oxygen diffused through Sn and reached Al which resulted in an oxide layer forming on top of the Al. This layer did not allow Al to be wetted by molten Sn. In one case where solder paste covered an area of coated Sn on top of the sample and in which the Al thickness changed slightly dissolution of Al into Sn may have been observed. However, when the experiment was repeated the results were not consistent. One possible reason could be that flux acids have partially eroded the Al layer and Al did not

dissolve into Sn. Investigation of the flux residues can clarify this. The last method used Au as a coating element. This method did not show dissolution of Al in Sn. This experiment only resulted in Al and Au layers interdiffusing rather than enabling Al dissolution into Sn. Therefore, while the original aim of this chapter which was to determine the reactions between Al and Sn and also to quantify the dissolution of Al in Sn, were not successfully achieved, however, several different methods of applying a protective coating onto Al which would dissolve at the start of soldering have been trialled and found ineffective so that future researchers can improve on the methods used.

6.3.1 Further work investigating Al dissolution in Sn arising from chapter 5

6.3.1.1 Experimental modification

- Future work which may lead to successful measurements should utilise an ultra-high vacuum chamber during the coating of Sn layer on top of the Al layer to minimize the possibility of the oxidation of Al, and soldering should also be carried out in an inert atmosphere to minimize oxidation.

- Coating of Al on Sn (Si/Sn/Al) was not successful (see section 5.3.4 Si/Sn/Al) since the Al coating showed a rough surface which was a source of error for the measurement of Al thickness. One alternative method can be used to prevent the error caused. In this method instead of Al coating, Al foil can be dipped or sputter coated in/by Sn. This would ensure the Al was a comparatively smooth surface.

6.3.1.2 Investigation on alternatives to Al

- The purpose of this research was to investigate the possibility of using Al addition to the solder in order to suppress the intermetallic growth at the solder/IMC interface.

Therefore, the dissolution rate value of Al in Sn would help in the design of nanoparticles to release Al into the solder at the optimum time in order to maximize Al reaction with the substrate while minimizing the interference with the solder during wetting reactions. The method of Chapter 5 however could be applied to other elements with similar properties. For example, Zn can also have a similar effect on suppressing the intermetallic layers at the solder/IMC interface as proven in work that was carried out in parallel with the Al investigations [11, 141, 206]. Zn is also reactive with Oxygen but the rate of reaction is much less than one between Al and Oxygen. Therefore, studying the dissolution rate of Zn in Sn, with the same method and same set of experiments might be successfully done without trying ultra-high vacuum conditions.

- In addition to Zn, the effect of addition of other elements (a fourth metallic element) into a SAC + X system can also be studied. Anderson et al. [207] have discussed including the electronegativity of the elements as an essential criterion, in addition to choosing elements with a similar atomic radius to Cu in which shows a 'Darken-Gurry ellipse'. This ellipse provides a combined analysis of electronegativity and atomic radius, allowing one to predict which elements would dissolve in solid solution to around 5 at.% in a solvent. In the ellipse, the solvating element is Cu, and is therefore placed at the centre of the ellipse, and it is seen that all of the elements used in the analysis lie within the ellipse (Si, Ti, Cr, Mn, Ni, Ge, and Zn) with the exception of Ti. However, it is known from other sources (specifically, the Cu-Ti phase diagram) that Ti will dissolve in Cu up to 8 at.%, so it can be included in the list of potential alloying elements. The resultant list of elements then includes ones with atomic radii both larger and smaller than that of Cu. The solubility of these alloying elements in Cu is significant because it is considered that by inhibiting the interdiffusion of Sn and Cu, void formation and coalescence at the Cu_3Sn/Cu interface in joints after high temperature

aging can be suppressed. By closely matching Cu with the alloying elements, one can promote substitution of X into the Cu_3Sn and Cu_6Sn_5 IMCs, a move which is intended to increase lattice strain and reduce vacancy diffusion, therefore slowing the layer growth and associated void formation. In order to test the assertions made here one would need to make detailed observations of the time-dependant concentration gradients of Cu and Sn at various isothermal aging temperatures. However, in practice this is a complicated measurement to make as there exists only a very narrow interface region [25, 207].

As was proved before [4], for the case of Zn addition, by addition of 0.5-1 wt.% Zn the interfacial IMC is $(Cu, Zn)_6Sn_5$, however, when the Zn concentration is 1.5 wt.%, a Cu_5Zn_8 IMC layer forms which is followed by massive spalling leaving the more thermodynamically stable Cu_6Sn_5 IMC to form at the Cu/solder interface. Similar investigation can be performed for the elements identified as being of interest (Si, Ti, Cr, Mn, Ni and Ge). In this case, the effect of concentration of the added element from low concentration (0.5-1 wt.%) to high concentration (1.5 wt.%) can be examined in order to investigate the possibility of formation of a new IMC layer on top of Cu_6Sn_5 IMC or replacing the Cu_6Sn_5 and Cu_3Sn layers entirely.

Appendix

List of Publications

1. List of publications which arose directly from the work at King's College London related to the PhD thesis:

Journal Papers:

- **Mokhtari O.**, Roshanghias A., Ashayer R., Kotadia H.R., Khomamizadeh F., Kokabi Amir H., Clode, M.P., Mannan, S.H. (2012) "Disabling of nanoparticle effects at increased temperature in nanocomposite solders", *Journal of Electronic Materials*, 41(7): 1907-1914.

- H.R. Kotadia, A. Panneerselvam, **O. Mokhtari**, M. P. Clode, M. A. Green, S. H. Mannan, (2012) "Massive spalling of Cu-Zn and Cu-Al intermetallic compounds at the interface between solders and Cu substrate during liquid state reaction", *Journal of Applied Physics*, 111(7): 074902-6.

- Hiren R. Kotadia, **O Mokhtari**, M P Clode, M A Green, S H Mannan. (2012) "Intermetallic Compound growth suppression at high temperature in SAC solders with Zn addition on Cu and Ni-P substrates" *Journal of Alloy Compounds*, 115(1): 176-188.

- Kotadia, H.R. **Mokhtari, O.** Bottrill, M. Clode, M.P. Green, M.A. and Mannan, S.H. (2010). "Reactions of Sn-3.5Ag-Based solders containing Zn and Al additions on Cu and Ni(P) Substrates". *Journal of Electronics Materials*, 32(12): 2720-2731.

- **Mokhtari Amirmajdi, O**. Ashyer-Soltani, R. Clode, M.P. Mannan, S.H. Yunqi Wang Cabruja, E. Pellegrini, G.(2009). "Cross-Section Preparation for Solder Joints and MEMS Device Using Argon Ion Beam Milling". *IEEE Transactions on Electronics Packaging Manufacturing, 32(4):* 265 – 271.

Conference Papers:

- R. Durairaj, R. Ashayer, H. R. Kotadia, N. Haria, C. Lorenz, **O. Mokhtari**, S. H. Mannan, "Pressure free sintering of silver nanoparticles to silver substrate using weakly binding ligands", IEEE NANO 2012: 12th International Conference on Nanotechnology 20 - 23 August, Birmingham, UK.

- **O. Mokhtari**, A. Roshanghias, R. Ashayer, H.R. Kotadia, F. Khomamizadeh, A.H. Kokabi, M.P. Clode, M. Miodownik, S.H. Mannan, "Nanoparticle enhanced solders for high temperature reliability", Proceedings of MRS Fall, SS15.18, November 2011, Boston USA.

- Kotadia, H.R.; **Mokhtari, O.**; Bottrill, M., et al. "Effect of Al and Zn alloying elements on Sn-3.8Ag-0.7Cu and Sn-3.6Ag solder reaction with Cu and Ni(P) substrate". 2010 International Symposium on Advanced Packaging Materials: Microtech (APM): 17-21.

- H.R. Kotadia, **O. Mokhtari**, M. Bottrill, M.P. Clode, M.A. Green, S.H. Mannan, "High temperature solders containing Aluminium", Proceedings of HITEC 2010, pp.122-128, Albuquerque, USA.

- Kotadia, HR; **Mokhtari, O**; Bottrill, M, et al. "Reactions of Sn-3.5Ag-Based Solders Containing Zn and Al Additions on Cu and Ni(P) Substrates". 2010. 139th TMS Annual

Meeting and Exhibition on Pb-Free Solders and Emerging Interconnect and Packaging Technologies, FEB 14-18, Seattle WA

- **Mokhtari, O.** Ashayer, R. Mannan, S.H. Clode, M.P. "Nanoparticle Enhanced Solders for High Temperature Reliability". IMAPS International Conference on High Temperature Electronics Network (HiTEN 2009).

- Ashayer, R. Cobley, A. **Mokhtari, O.** Mannan, S.H. Sajjadi, S. Mason, T. "Nanoparticle synthesis and formation of composite solder for harsh environments". 2008 2nd Electronics System integration Technology Conference, (vol.2) 929-34.

2. List of publications which arose from the work after PhD at Joining and Welding Research Institute, Osaka University, Japan:

Journal papers:

- **Mokhtari O.**, Kim M.-S., Nishikawa H., Kawashiro F., Itou S., Maeda T., Hirose T., and Eto T. "Investigation on formation and growth behavior of Cu/Al intermetallic compounds during isothermal aging", *Transactions of The Japan Institute of Electronics Packaging, (submitted in June 2014 - accepted in September 2014 to be published in Vol. 7 in December 2014).*

- **Mokhtari O.** and Nishikawa H. (2014) "Effects of In and Ni addition on the microstructure of Sn-58Bi solder joint", *Journal of Electronic Materials*, 43(11), 4158-4170.

Conference papers:

- **O. Mokhtari** and H. Nishikawa, "The effect of Cu particle additions on the microstructure and melting point of Sn-Bi for die attachment", 4th IEEE International Workshop on Low Temperature Bonding for 3D Integration (LTB-3D), 2014, July 15-16, Tokyo, Japan.
- **O. Mokhtari** and H. Nishikawa, "The Melting-point Increase of Sn-Bi Solder Joint by Cu Particles Addition", International Conference on High Temperature Electronics (HiTEC 2014), May 13-15, Albuquerque, New Mexico, USA.
- **O. Mokhtari,** M. Kim and *et al.,* "Effect of isothermal aging on the growth behavior of Cu/Al intermetallic compounds", International Conference on Electronics Packaging (ICEP) 2014, April, Toyama, Japan.

- **O. Mokhtari** and Hiroshi Nishikawa, "Effects of Cu particle additions on the melting point of Sn-Bi solder joint", 15th International Conference on Electronic Materials and Packaging (EMAP) 2013, SIT-0220, October, Seoul, South Korea.

- **O. Mokhtari** and H. Nishikawa, "Coarsening of Bi phase and intermetallic layer thickness in Sn-58Bi-X (X=In and Ni) solder joint", 14th International Conference on Electronic Packaging Technology (ICEPT), B42, p. 250-253, August 2013, Dalian, China.

- **O. Mokhtari** and H. Nishikawa, "Effects of Cu particle additions on the microstructure of Sn-Bi solder alloy", The International Symposium on Visualization in Joining and

Welding Science through Advanced Measurements and simulation, 186-187, November 2012, Osaka, Japan.

- J. Wang, H. Nishikawa and **O. Mokhtari**, "Effects of Cu pad on fracture behavior of BGA joints in impact test", The International Symposium on Visualization in Joining and Welding Science through Advanced Measurements and simulation, NMJ-3, November 2012, Osaka, Japan.

Bibliography

1. Tu, K.N., *Solder Joint Technology: Material, Properties, and Reliability*2007: Springer.
2. Tu, K.N., A.M. Gusak, and M. Li, *Physics and materials challenges for lead-free solders.* Journal of Applied Physics, 2003. **93**(3): p. 1335-1353.
3. Tu, K.N. and K. Zeng, *Tin-lead (SnPb) solder reaction in flip chip technology.* Materials Science & Engineering R-Reports, 2001. **34**(1): p. 1-58.
4. Kotadia, H.R., et al., *Intermetallic compound growth suppression at high temperature in SAC solders with Zn addition on Cu and Ni-P substrates.* Journal of Alloys and Compounds, 2012. **511**(1): p. 176-188.
5. Ashby, M.F., and Jones, D.R.H., *Engineering Materials 1: An Introduction to Properties, Applications and Design*, 2005, Butterworth Heinemann.
6. Keng, Z. and Tu, K.N., *Six cases of reliability study of Pb-free solder joints in electronic packaging technology*, Materials Sicence and Engineering 2002. R, **38**: 55-105.
7. Sylvestre, J. and Blander, A., *Large-scale correlations in the orientation of grains in lead-free solder joints.* Journal of Electronic Materials, 2008. **37**(10): p. 1618-1623.
8. Schaefer, M., Fournelle, R.A., and Liang, J., *Theory for intermetallic phase growth between Cu and liquid Sn-Pb solder based on grain boundary diffusion control.* Journal of Electronic Materials, 1998. **27**(11): p. 1167-1176.

9. Amirmajdi, O.M., et al., *Cross-Section Preparation for Solder Joints and MEMS Device Using Argon Ion Beam Milling.* Ieee Transactions on Electronics Packaging Manufacturing, 2009. **32**(4): p. 265-271.

10. Lehman, L.P., et al., *Growth of Sn and intermetallic compounds in Sn-Ag-Cu solder.* Journal of Electronic Materials, 2004. **33**(12): p. 1429-1439.

11. Manko, H.H., *Solders and Soldering*. fourth ed2001: McGraw-Hill.

12. So, A.C.K. and Chan, Y.C., *Reliability studies of surface mount solder joints – effect of Cu-Sn intermetallic compounds,* IEEE Transaction on Components, Packaging, and Manufacturing Technology, 2002, **19**(3): p. 661-668.

13. Li, J.F., et al., *Dissolution and interfacial reaction of Nb in contact with the molten 52In-48Sn solder.* Acta Materialia, 2007. **55**(15): p. 5057-5071.

14. Arenas, M.F., He, M., and Acoff, V.L., *Effect of flux on the wetting characteristics of SnAg, SnCu, SnAgBi, and SnAgCu lead-free solders on copper substrates.* Journal of Electronic Materials, 2006. **35**(7): p. 1530-1536.

15. Laurila, T., Vuorinen, V., and Kivilahti, J.K., *Interfacial reactions between lead-free solders and common base materials.* Materials Science & Engineering R-Reports, 2005. **49**(1-2): p. 1-60.

16. Abtew, M. and Selvaduray, G., *Lead-free solders in microelectronics.* Materials Science & Engineering R-Reports, 2000. **27**(5-6): p. 95-141.

17. Tummala, R., Rymaszewski, E.J., and Klopfenstein, A.G., *Microelectronics Packaging Handbook*. 2nd ed1997, Norwell: Kluwer Academic Publishers.

18. Evans J.W., Kwon, D., and Evans J.Y., *A Guide to Lead-Free solders: Physical Metallurgy and Reliability*. 2007, Springer.

19. Glazer, J., *Metallurgy of Low-Temperature Pb-Free Solders for Electronic Assembly.* International Materials Reviews, 1995. **40**(2): p. 65-93.

20. Gamalski, J., *A European perspective from a global OEM*, (May 2002) IPC/Jedec Conference on Lead Free Electronic Components and Assemblies, San Jose, CA.

21. Nimmo, K., *Review of European Legislation and Lead Free Technology Roadmap*, Proceedings of International conference on Lead-Free Electronic Components and Assemblies, 2002: San Jose, CA.

22. Suraski, D. and Seelig, K., *The current status of lead-free solder alloys.* Ieee Transactions on Electronics Packaging Manufacturing, 2001. **24**(4): p. 244-248.

23. Zeng, G., et al., *A review on the interfacial intermetallic compounds between Sn-Ag-Cu based solders and substrates.* Journal of Materials Science-Materials in Electronics, 2010. **21**(5): p. 421-440.

24. Laurila, T., Vuorinen, V. and Paulasto-Krockel, M., *Impurity and alloying effects on interfacial reaction layers in Pb-free soldering.* Materials Science & Engineering R-Reports, 2010. **68**(1-2): p. 1-38.

25. Kotadia, H.R., Howes, P.D. and Mannan, S.H., *A review: On the development of low melting temperature Pb-free solders.* Microelectronics Reliability, 2014. **54**(6-7): p. 1253-1273.

26. Shi, X.Q., et al., *Effect of temperature and strain rate on mechanical properties of 63Sn/37Pb solder alloy.* Journal of Electronic Packaging, 1999. **121**(3): p. 179-185.

27. Ding, Y., et al., *Aging effects on fracture behavior of 63Sn37Pb eutectic solder during tensile tests under the SEM.* Materials Science and Engineering a-Structural Materials Properties Microstructure and Processing, 2004. **384**(1-2): p. 314-323.

28. Hacke, P.L., Fahmy, Y., and Conrad, H., *Phase coarsening and crack growth rate during thermo-mechanical cycling of 63Sn37Pb solder joints.* Journal of Electronic Materials, 1998. **27**(8): p. 941-947.

29. Guo, Z.F. and Conrad, H., *Effect of microstructure size on deformation kinetics and thermo-mechanical fatigue of 63Sn37Pb solder joints.* Journal of Electronic Packaging, 1996. **118**(2): p. 49-54.

30. Jung, K. and Conrad, H., *Microstructure coarsening during static annealing of 60Sn4OPb solder joints: II eutectic coarsening kinetics.* Journal of Electronic Materials, 2001. **30**(10): p. 1303-1307.

31. Wei, Y., et al., *Characteristics of creep damage for 60 Sn-40Pb solder material.* Journal of Electronic Packaging, 2001. **123**(3): p. 278-283.

32. Jung, K. and Conrad, H., *Microstructure gradient in 60Sn40Pb solder joints annealed under an external electric field.* Journal of Materials Science, 2004. **39**(5): p. 1803-1804.

33. Lau, J.H., Pan, S.H., and Chang, C., *Creep analysis of wafer level chip scale package (WLCSP) with 96.5Sn-3.5Ag and 100In lead-free solder joints and microvia build-up printed circuit board.* Journal of Electronic Packaging, 2002. **124**(2): p. 69-76.

34. Amagai, M., et al., *Mechanical characterization of Sn-Ag-based lead-free solders.* Microelectronics Reliability, 2002. **42**(6): p. 951-966.

35. Zhao, J., et al., *Fatigue crack growth behavior in 63Sn-37Pb and 95Pb-5Sn solder materials.* Journal of Electronic Materials, 2001. **30**(4): p. 415-421.

36. Chen, C.J. and Lin, K.L., *Electroless Ni-Cu-P barrier between Si/Ti/Al pad and Sn-Pb flip-chip solder bumps.* Ieee Transactions on Components and Packaging Technologies, 2001. **24**(4): p. 691-697.

37. Strandjord, A.J.G., Popelar, S., and, Jauernig, C., *Interconnecting to aluminum- and copper-based semiconductors (electroless-nickel/gold for solder bumping and wire bonding).* Microelectronics Reliability, 2002. **42**(2): p. 265-283.

38. Schoeller, H., et al., *Microstructure Evolution and the Constitutive Relations of High-Temperature Solders.* Journal of Electronic Materials, 2009. **38**(6): p. 802-809.

39. Ding, Y., Wang, C.Q., and Li, M.Y., *Scanning electron microscope in-situ investigation of fracture behavior in 96.5Sn3.5Ag lead-free solder*. Journal of Electronic Materials, 2005. **34**(10): p. 1324-1335.

40. Ding, Y., et al., *Influence of aging treatment on deformation behavior of 96.5Sn3.5Ag lead-free solder alloy during in situ tensile tests.* Journal of Alloys and Compounds, 2007. **428**(1-2): p. 274-285.

41. Yan, C., Qin, Q.H., and Mai, Y.W., *Nonlinear analysis of plastic ball grid array solder joints.* Journal of Materials Science-Materials in Electronics, 2001. **12**(11): p. 667-673.

42. Jang, J.W., et al., *Morphology of interfacial reaction between lead-free solders and electroless Ni-P under bump metallization.* Journal of Applied Physics, 2000. **88**(11): p. 6359-6363.

43. Sundelin, J.J., et al., *Mechanical and microstructural properties of SnAgCu solder joints.* Materials Science and Engineering a-Structural Materials Properties Microstructure and Processing, 2006. **420**(1-2): p. 55-62.

44. Xiao, Q., Bailey, H.J., and Armstrong, W.D., *Aging effects on microstructure and tensile property of Sn3.9Ag0.6Cu solder alloy.* Journal of Electronic Packaging, 2004. **126**(2): p. 208-212.

45. Xiao, Q. and Armstrong, W.D., *Tensile creep and microstructural characterization of bulk Sn3.9Ag0.6Cu lead-free solder.* Journal of Electronic Materials, 2005. **34**(2): p. 196-211.

46. Zhang, Q., Dasgupta, A., and Haswell, P., *Isothermal mechanical durability of three selected Pb-free solders: Sn3.9Ag0.6Cu, Sn3.5Ag and Sn0.7Cu.* Journal of Electronic Packaging, 2005. **127**(4): p. 512-522.

47. Cho, M.G., et al., *Interfacial reaction between 42Sn-58Bi solder and electroless Ni-P/immersion Au under bump metallurgy during aging.* Journal of Electronic Materials, 2006. **35**(1): p. 35-40.

48. Young, B.L. and Duh, J.G., *Interfacial reaction and microstructural evolution for electroplated Ni and electroless Ni in the under bump metallurgy with 42Sn58Bi solder during annealing.* Journal of Electronic Materials, 2001. **30**(7): p. 878-884.

49. Miao, H.W., Duh, J.G., and Chiou, B.S., *Thermal cycling test in Sn-Bi and Sn-Bi-Cu solder joints.* Journal of Materials Science-Materials in Electronics, 2000. **11**(8): p. 609-618.

50. Darveaux, R., *Shear Deformation of Lead Free Solder Joints*, in *Electronic Components and Technology Conference*, 2005, Vol. 1, p. 882-893.

51. Sundelin, J.J., et al., *Microstructure, creep properties, and failure mechanism of SnAgCu solder joints.* Journal of Electronic Materials, 2006. **35**(7): p. 1600-1606.

52. Zeng, G., et al., *A review on the interfacial intermetallic compounds between Sn-Ag-Cu based solders and substrates.* Journal of Materials Science-Materials in Electronics. **21**(5): p. 421-440.

53. Dariavach, N., et al., *Intermetallic growth kinetics for Sn-Ag, Sn-Cu, and Sn-Ag-Cu lead-free solders on Cu, Ni, and Fe-42Ni substrates.* Journal of Electronic Materials, 2006. **35**(7): p. 1581-1592.

54. Manko, H.H., *Solders and Soldering*. 4th ed2001.

55. Chuang, C.M. and Lin, K.L., *Effect of microelements addition on the interfacial reaction between Sn-Ag-Cu solders and the Cu substrate.* Journal of Electronic Materials, 2003. **32**(12): p. 1426-1431.

56. Kao, S.T., Lin, Y.C., and Duh, J.G., *Controlling intermetallic compound growth in SnAgCu/Ni-P solder joints by nanosized Cu6Sn5 addition.* Journal of Electronic Materials, 2006. **35**(3): p. 486-493.

57. Kang, H.-B., et al., *Control of interfacial reaction layers formed in Sn-3.5Ag-0.7Cu/electroless Ni-P solder joints.* Scripta Materialia, 2009. **60**(4): p. 257-260.

58. Flanders, D.R., Jacobs, E.G., and Pinizzotto, R.F., *Activation energies of intermetallic growth of Sn-Ag eutectic solder on copper substrates.* Journal of Electronic Materials, 1997. **26**(7): p. 883-887.

59. Cheng, M.D., Wang, S.S., and Chuang, T.H., *Soldering reactions between In49Sn and Ag thick films.* Journal of Electronic Materials, 2002. **31**(3): p. 171-177.

60. Kim, H.K. and Tu, K.N., *Kinetic analysis of the soldering reaction between eutectic SnPb alloy and Cu accompanied by ripening.* Physical Review B, 1996. **53**(23): p. 16027-16034.

61. Jung, I., Cho, M.G., and Lee, H.M., *Wetting Properties and Interfacial Reactions of Mechanically Alloyed Cu(5)Zn(8)-Bearing Pb-Free Solders on a Copper Substrate.* Journal of Electronic Materials, 2009. **38**(11): p. 2301-2307.

62. Shen, J., et al., *Formation of bulk Ag3Sn intermetallic compounds in Sn-Ag lead-free solders in solidification.* Journal of Electronic Materials, 2005. **34**(12): p. 1591-1597.

63. Kim, K.S., Huh, S.H., and Suganuma, K., *Effects of cooling speed on microstructure and tensile properties of Sn-Ag-Cu alloys.* Materials Science and Engineering a-Structural Materials Properties Microstructure and Processing, 2002. **333**(1-2): p. 106-114.

64. Kim, K.S., Huh, S.H., and Suganuma, K., *Effects of intermetallic compounds on properties of Sn-Ag-Cu lead-free soldered joints.* Journal of Alloys and Compounds, 2003. **352**(1-2): p. 226-236.

65. Ochoa, F., Williams, J.J., and Chawla, N., *The effects of cooling rate on microstructure and mechanical behavior of Sn-3.5Ag solder.* Jom-Journal of the Minerals Metals & Materials Society, 2003. **55**(6): p. 56-60.

66. Kang, S.K., et al., *Controlling Ag3Sn plate formation, in near-ternary-eutectic Sn-Ag-Cu solder by minor Zn alloying.* Jom, 2004. **56**(6): p. 34-38.

67. Gong, J., et al., *Formation of Ag3Sn plates in SnAgCu solder bumps.* Materials Science and Engineering a-Structural Materials Properties Microstructure and Processing, 2010. **527**(10-11): p. 2588-2591.

68. Henderson, D.W., et al., *Ag3Sn plate formation in the solidification of near ternary eutectic Sn-Ag-Cu alloys.* Journal of Materials Research, 2002. **17**(11): p. 2775-2778.

69. Gong, J., et al., *Evolution of CuSn intermetallics between molten SnAgCu solder and Cu substrate.* Acta Materialia, 2008. **56**(16): p. 4291-4297.

70. Sigelko, J., et al., *Effect of cooling rate on microstructure and mechanical properties of eutectic Sn-Ag solder joints with and without intentionally incorporated Cu6Sn5 reinforcements.* Journal of Electronic Materials, 1999. **28**(11): p. 1184-1188.

71. Bader. W. in *Proceedings of the Conference on Physical Metallurgy, Metal Joining St. Louis, MO*. 1980. Warredale, USA.

72. Hung, K.C., et al., *Correlation between Ni,Sn, intermetallics and Ni3P due to solder reaction-assisted crystallization of electroless Ni-P metallization in advanced packages.* Journal of Materials Research, 2000. **15**(11): p. 2534-2539.

73. Alam, M.O. and Chan, Y.C., *Effect of 0.5 wt% Cu in Sn-3.5%Ag solder to retard interfacial reactions with the electroless Ni-P metallization for BGA solder joints application.* Ieee Transactions on Components and Packaging Technologies, 2008. **31**(2): p. 431-438.

74. Lee, C.Y. and Lin, K.L., *The interaction kinetics and compound formation between electrless Ni-P and solder.* Thin Solid Films, 1994. **249**(2): p. 201-206.

75. Choi, W.K., Kang, S.K., and Shih, D.Y., *A study of the effects of solder volume on the interfacial reactions in solder joints using the differential scanning calorimetry technique.* Journal of Electronic Materials, 2002. **31**(11): p. 1283-1291.

76. Choi, W.K. and Lee, H.M., *Effect of Ni layer thickness and soldering time on intermetallic compound formation at the interface between molten Sn-3.5Ag and Ni/Cu substrate.* Journal of Electronic Materials, 1999. **28**(11): p. 1251-1255.

77. Song, H.G., Morris, J.W. and McCormack, M.T., *The microstructure of ultrafine eutectic Au-Sn solder joints on Cu.* Journal of Electronic Materials, 2000. **29**(8): p. 1038-1046.

78. Islam, M.N., Sharif, A., and Chan, Y.C., *Effect of volume in interfacial reaction between eutectic Sn-3.5% Ag-0.5% Cu solder and Cu metallization in microelectronic packaging.* Journal of Electronic Materials, 2005. **34**(2): p. 143-149.

79. Schaefer, M., Laub, W., Fournelle, R.A., and Liang, J. *Design and reliability of solders and solder interconnects*. in *TMS*. 1997. Warrendale, PA.

80. Chada, S., et al., *Copper substrate dissolution in eutectic Sn-Ag solder and its effect on microstructure.* Journal of Electronic Materials, 2000. **29**(10): p. 1214-1221.

81. Huang, Z.H., et al., *Effect of solder bump geometry on the microstructure of Sn-3.5 wt% Ag on electroless nickel immersion gold during solder dipping.* Journal of Materials Research, 2005. **20**(3): p. 649-658.

82. Huang, Z., Conway, P.P., and Thomson, R.C., *Microstructural considerations for ultrafine lead free solder joints.* Microelectronics Reliability, 2007. **47**(12): p. 1997-2006.

83. Huang, Z., et al., *Reliability issues in Pb-free solder joint miniaturization.* Journal of Electronic Materials, 2006. **35**(9): p. 1761-1772.

84. Amalu, E.H., Ekere, N.N., *Damage of lead-free solder joints in flip chip assemblies subjected to high-temperature thermal cycling.* Computational Materials Science, 2012. **65**: p. 470-484.

85. Liu, P., Yao, P., and Liu, J., *Evolutions of the interface and shear strength between SnAgCu-xNi solder and Cu substrate during isothermal aging at 150 degrees C.* Journal of Alloys and Compounds, 2009. **486**(1-2): p. 474-479.

86. Lim, G.-T., et al., *Temperature Effect on Intermetallic Compound Growth Kinetics of Cu Pillar/Sn Bumps.* Journal of Electronic Materials, 2009. **38**(11): p. 2228-2233.

87. Cho, M.G., et al., *Interfacial Reactions and Microstructures of Sn-0.7Cu-xZn Solders with Ni-P UBM During Thermal Aging.* Journal of Electronic Materials, 2009. **38**(11): p. 2242-2250.

88. Yao, P., Liu, P., and Liu, J., *Interfacial reaction and shear strength of SnAgCu-xNi/Ni solder joints during aging at 150 degrees C.* Microelectronic Engineering, 2009. **86**(10): p. 1969-1974.

89. Wu, M., et al., *Effect of various Ni plating layers and aging on microstructure and shear strength of Sn-2.5Ag-2.0Ni solder joint.* Surface & Coatings Technology, 2009. **203**(20-21): p. 3011-3018.

90. Xu, R.L., et al., *The formation and evolution of intermetallic compounds formed between Sn-Ag-Zn-In lead-free solder and Ni/Cu substrate.* Journal of Materials Science-Materials in Electronics, 2009. **20**(7): p. 675-679.

91. Alam, M.O., et al., *Fracture mechanics analysis of solder joint intermetallic compounds in shear test.* Computational Materials Science, 2009. **45**(2): p. 576-583.

92. Laurila, T., et al., *Effect of Ag, Fe, Au and Ni on the growth kinetics of Sn-Cu intermetallic compound layers.* Microelectronics Reliability, 2009. **49**(3): p. 242-247.

93. Chen, X., et al., *Effect of a trace of Cr on intermetallic compound layer for tin-zinc lead-free solder joint during aging.* Journal of Alloys and Compounds, 2009. **470**(1-2): p. 429-433.

94. Wei, C., et al., *Effects of Thermal Aging on Microstructure and Microhardness of Sn-3.7Ag-0.9Zn-1In Solder.* Journal of Electronic Materials, 2009. **38**(2): p. 345-350.

95. Ngoh, S.L., Zhou, W., and Pang, J.H.L., *Effect of Stress State on Growth of Interfacial Intermetallic Compounds Between Sn-Ag-Cu Solder and Cu*

Substrates Coated with Electroless Ni Immersion Au. Journal of Electronic Materials, 2008. **37**(12): p. 1843-1850.

96. Choubey, A., et al., *Intermetallics characterization of lead-free solder joints under isothermal aging.* Journal of Electronic Materials, 2008. **37**(8): p. 1130-1138.

97. Abbaschian, R., Reed-Hill, R., *Physical Metallurgy Principles* 3rd ed1992, Boston: PWS-KENT Publishing Company.

98. Raeder, C.H., Messler, R.W., and Coffin, L.F., *Partially-constrained thermomechanical fatigue of eutectic tin-bismuth/copper solder joints.* Journal of Electronic Materials, 1999. **28**(9): p. 1045-1054.

99. Callister, W.D.J., *Materials Science and engineering : An Introduction*. 6th ed2003: Wiley.

100. Mavoori, H., et al., *Creep, stress relaxation, and plastic deformation in Sn-Ag and Sn-Zn eutectic solders.* Journal of Electronic Materials, 1997. **26**(7): p. 783-790.

101. Lau, J.H., *Thermal Stress and Strain in Microelectronics Packaging*1993, New York: Van Nostrand Reinhold.

102. Huang, M.L., Wu, C.M.L., and Wang, L.,*Creep resistance of tin-based lead-free solder alloys.* Journal of Electronic Materials, 2005. **34**(11): p. 1373-1377.

103. Huang, M.L., Wang, L., and Wu, C.M.L., *Creep behavior of eutectic Sn-Ag lead-free solder alloy.* Journal of Materials Research, 2002. **17**(11): p. 2897-2903.

104. Lin, D.C., et al., *An investigation of nanoparticles addition on solidification kinetics and microstructure development of tin-lead solder.* Materials Science and Engineering a-Structural Materials Properties Microstructure and Processing, 2003. **360**(1-2): p. 285-292.

105. Liu, P., Yao, P., and Liu, J., *Effect of SiC nanoparticle additions on microstructure and microhardness of Sn-Ag-Cu solder alloy.* Journal of Electronic Materials, 2008. **37**(6): p. 874-879.

106. Guo, F., *Composite lead-free electronic solders.* Journal of Materials Science-Materials in Electronics, 2007. **18**(1-3): p. 129-145.

107. Mavoori, H. and Jin, S., *New, creep-resistant, low melting point solders with ultrafine oxide dispersions.* Journal of Electronic Materials, 1998. **27**(11): p. 1216-1222.

108. Shi, Y.W., et al., *Creep property of composite solders reinforced by nano-sized particles.* Journal of Materials Science-Materials in Electronics, 2008. **19**(4): p. 349-356.

109. Gain, A.K., et al., *The influence of addition of Al nano-particles on the microstructure and shear strength of eutectic Sn-Ag-Cu solder on Au/Ni metallized Cu pads.* Journal of Alloys and Compounds. **506**(1): p. 216-223.

110. Wiese, S. and Wolter, K.J., *Microstructure and creep behaviour of eutectic SnAg and SnAgCu solders.* Microelectronics Reliability, 2004. **44**(12): p. 1923-1931.

111. Vanherpe, L., et al., *Pinning effect of spheroid second-phase particles on grain growth studied by three-dimensional phase-field simulations.* Computational Materials Science. **49**(2): p. 340-350.

112. Dennis, J., Bate, P.S., and Humphreys, F.J., *Abnormal grain growth in Al-3.5Cu.* Acta Materialia, 2009. **57**(15): p. 4539-4547.

113. Tsao, L.C. and Chang, S.Y., *Effects of Nano-TiO(2) additions on thermal analysis, microstructure and tensile properties of Sn3.5Ag0.25Cu solder.* Materials & Design. **31**(2): p. 990-993.

114. Song, K. and Aindow, M., *Grain growth and particle pinning in a model Ni-based superalloy.* Materials Science and Engineering a-Structural Materials Properties Microstructure and Processing, 2008. **479**(1-2): p. 365-372.

115. Chang, K.N., Feng, W.M., and Chen, L.Q., *Effect of second-phase particle morphology on grain growth kinetics.* Acta Materialia, 2009. **57**(17): p. 5229-5236.

116. Liu, Y.X. and Patterson, B.R., *Stereological analysis of Zener pinning.* Acta Materialia, 1996. **44**(11): p. 4327-4335.

117. Shi, X.Q., et al., *A new creep constitutive model for eutectic solder alloy.* Journal of Electronic Packaging, 2002. **124**(2): p. 85-90.

118. Che, F.X., et al., *Creep Properties of Sn-1.0Ag-0.5Cu Lead-Free Solder with Ni Addition.* Journal of Electronic Materials. **40**(3): p. 344-354.

119. Xun, Y.W. and Mohamed, F.A., *Superplastic behavior of Zn-22%Al containing nano-scale dispersion particles.* Acta Materialia, 2004. **52**(15): p. 4401-4412.

120. Qiang, X. and Armstrong, W.D., *Tensile creep and microstructural characterization of bulk Sn 3.9Ag 0.6Cu lead-free solder.* Journal of Electronic Materials, 2005. **34**(2).

121. Shi, Y.W., et al., *Constitutive Relations for Creep in a SnCu-Based Composite Solder Reinforced with Ag Particles.* Journal of Electronic Materials, 2009. **38**(9): p. 1866-1873.

122. Gore, M.J., et al., *Thermally activated grain-boundary unpinning.* Acta Metallurgica, 1989. **37**(11): p. 2849-2854.

123. Kawabata, K., Sato, E., and Kuribayashi, K., *Creep deformation behavior of spherical Al2O3 particle-reinforced Al-Mg matrix composites at high temperatures.* Acta Materialia, 2002. **50**(13): p. 3465-3474.

124. Kaibyshev, R., et al., *Deformation behavior of a modified 5083 aluminum alloy.* Materials Science and Engineering a-Structural Materials Properties Microstructure and Processing, 2005. **392**(1-2): p. 373-379.

125. Solhjoo, S., *Analysis of flow stress up to the peak at hot deformation.* Materials & Design, 2009. **30**(8): p. 3036-3040.

126. El-Danaf, E.A., AlMajid, A.A., and Soliman, M.S., *Hot deformation of AA6082-T4 aluminum alloy.* Journal of Materials Science, 2008. **43**(18): p. 6324-6330.

127. Shen, J. and Chan, Y.C., *Research advances in nano-composite solders.* Microelectronics Reliability, 2009. **49**(3): p. 223-234.

128. Mohankumar, K. and Tay, A.A.O., *Nano-particle reinforced solders for fine pitch applications.* 6th Electronics Packaging Technology Conference, Proceedings (Eptc 2004), 2004: p. 455-461.

129. Yu, K.O., et al., *Toxicity of amorphous silica nanoparticles in mouse keratinocytes.* Journal of Nanoparticle Research, 2009. **11**(1): p. 15-24.

130. Tsai, C.-J., and Pui, D.Y.H., *Recent advances and new challenges of occupational and environmental health of nanotechnology*. journal of Nanoparticle Research, 2009. **11**: p. 1-4.

131. Boverhof, D.R. and David, R.M., *Nanomaterial characterization: considerations and needs for hazard assessment and safety evaluation.* Analytical and Bioanalytical Chemistry. **396**(3): p. 953-961.

132. *EEC Material Safety Data Sheet*, in *91/155/EEC*, n. AG, Editor 2006.

133. Takahashi, H., et al., *A new method of surface preparation for high spatial resolution EPMA/SEM with an argon ion beam.* Microchimica Acta, 2006. **155**(1-2): p. 295-300.

134. Ogura K., et al., *New Methods for Cross-Section Sample Preparation Using Broad Argon Ion Beam Microsc microanal.* 2007.

135. Tseng, A.A., *Recent developments in nanofabrication using focused ion beams.* Small, 2005. **1**(10): p. 924-939.

136. Sezen, M., et al., *An investigation on focused electron/ion beam induced degradation mechanisms of conjugated polymers.* Physical Chemistry Chemical Physics. **13**(45): p. 20235-20240.

137. Erdman, N., Campbell, R., and Asahina, S., *Precise SEM Cross Section Polishing via Argon Beam Milling.* Microscopy Today, 2006. **14**(3): p. 22-25.

138. Jee Y.-K., Xia, Y.-H., Yu J., Kang H.-W., and Lee T.-Y., *Effect of Al addition in Sn-Ag solder on the interfacial reactions with Cu and ENIG metallization*, in *Electronic Components and Technology Conference*2008. p. 491-494.

139. Scheel, W., Wittke, K., and Nowottnick M., *TLSD–Temporary Liquid Solder Design* 2004.

140. Nowottnick, M., Pape, U., Wittke, K., and Scheel, W., *Solder joints for high temperature electronics*, in *SMTA International Conference Proceedings*2003: Chicago. p. 693.

141. Kotadia, H.R., et al., *Reactions of Sn-3.5Ag-Based Solders Containing Zn and Al Additions on Cu and Ni(P) Substrates.* Journal of Electronic Materials, 2010. **39**(12): p. 2720-2731.

142. Li, J.F., et al., *Interfacial reactions between molten Sn-Bi-X solders and Cu substrates for liquid solder interconnects.* Acta Materialia, 2006. **54**(11): p. 2907-2922.

143. Xia, Y.H., et al., *Effect of Aluminum Concentration on the Interfacial Reactions of Sn-3.0Ag-xAl Solders with Copper and ENIG Metallizations.* Journal of Electronic Materials, 2008. **37**(12): p. 1858-1862.

144. McAlister, A.J., Kahan, D.J., *The Al-Sn (Aluminium-Tin) System.* Bulletin of Alloy Phase Diagrams, 1983. **4**(4).

145. Mannan, S.H., and M.P. Clode, *Dissolution of solids in contact with liquid solder.* Soldering & Surface Mount Technology, 2004. **16**(3): p. 31-33.

146. Dybkov, V.I., *Growth Kinetics of Chemical compound Layers*1998, Cambridge: Cambridge International Science Publishing.

147. Eremenko, V.N., and Natanzon, Y.V., *Kinetics of External Dissolution of Metals in Metallic Melts.* Poroshkovaya Metallurgiya, 1970. **92**(8): p. 39-54.

148. Crank, J., *The Mathematics of Diffusion*. 2nd ed1975, Oxford: Oxford University Press.

149. Rizvi, M.J., Lu, H., and Bailey, C., *Modeling the diffusion of solid copper into liquid solder alloys.* Thin Solid Films, 2009. **517**(5): p. 1686-1689.

150. Fawzy, A., *Effect of Zn addition, strain rate and deformation temperature on the tensile properties of Sn-3.3 wt.% Ag solder alloy.* Materials Characterization, 2007. **58**(4): p. 323-331.

151. Wu, C.M.L., et al., *Properties of lead-free solder alloys with rare earth element additions.* Materials Science & Engineering R-Reports, 2004. **44**(1): p. 1-44.

152. Jee, Y.K., Ko, Y.H., and Yu, J., *Effect of Zn on the intermetallics formation and reliability of Sn-3.5Ag solder on a Cu pad.* Journal of Materials Research, 2007. **22**(7): p. 1879-1887.

153. McCormack, M. and Jin, S.H., *Progress in the design of new lead-free solder alloys.* Jom-Journal of the Minerals Metals & Materials Society, 1993. **45**(7): p. 36-40.

154. McCormack, M. and Jin, S., *New lead-free solders.* Journal of Electronic Materials, 1994. **23**(7): p. 635-640.

155. Kang, S.K., et al., *Interfacial reactions of Sn-Ag-Cu solders modified by minor Zn alloying addition.* Journal of Electronic Materials, 2006. **35**(3): p. 479-485.

156. Cho, M.G., et al., *Effects of minor additions of Zn on interfacial reactions of Sn-Ag-Cu and Sn-Cu solders with various Cu substrates during thermal aging.* Journal of Electronic Materials, 2007. **36**(11): p. 1501-1509.

157. Yu, C., Lu, H., and Li, S., *Effect of Zn addition on the formation and growth of intermetallic compound at Sn-3.5 wt% Ag/Cu interface.* Journal of Alloys and Compounds, 2008. **460**(1-2): p. 594-598.

158. Yu, C.-Y., Wang, K.-J., and Duh, J.-G., *Interfacial Reaction of Sn and Cu-xZn Substrates After Reflow and Thermal Aging.* Journal of Electronic Materials, 2010. **39**(2): p. 230-237.

159. Takamatsu, Y., Esaka, H., and Shinozuka, K., *Liquid-Phase Separation in the Interdendritic Region After Growth of Primary beta-Sn in Undercooled Sn-2.8Ag-0.3Cu Melt.* Journal of Electronic Materials, 2012. **41**(8): p. 2035-2044.

160. Takamatsu, Y., Esaka, H., and Shinozuka, K., *Formation Mechanism of Eutectic Cu6Sn5 and Ag3Sn after Growth of Primary beta-Sn in Sn-Ag-Cu Alloy.* Materials Transactions, 2011. **52**(2): p. 189-195.

161. Ochoa, F., Williams, J.J., and Chawla, N., *Effects of cooling rate on the microstructure and tensile behavior of a Sn-3.5wt.%Ag solder.* Journal of Electronic Materials, 2003. **32**(12): p. 1414-1420.

162. Anderson, I.E., *Development of Sn-Ag-Cu and Sn-Ag-Cu-X alloys for Pb-free electronic solder applications.* Journal of Materials Science-Materials in Electronics, 2007. **18**(1-3): p. 55-76.

163. Hao, H., et al., *Properties of Sn3.8AgO.7Cu solder alloy with trace rare earth element Y additions.* Journal of Electronic Materials, 2007. **36**(7): p. 766-774.

164. Chen, S.W. and Chang, C.A., *Phase equilibria of the Sn-Ag-Cu-Ni quaternary system at the Sn-rich corner.* Journal of Electronic Materials, 2004. **33**(10): p. 1071-1079.

165. Hwang, C.W., Kim, K.S., and Suganuma, K., *Interfaces in lead-free soldering.* Journal of Electronic Materials, 2003. **32**(11): p. 1249-1256.

166. Chang, K., Feng, W., and Chen, L.-Q., *Effect of second-phase particle morphology on grain growth kinetics.* Acta Materialia, 2009. **57**(17): p. 5229-5236.

167. Ashayer, R., Mannan, S.H., and Sajjadi, S., *Synthesis and characterization of gold nanoshells using poly (diallyldimethyl ammonium chloride).* Colloids and Surfaces a-Physicochemical and Engineering Aspects, 2008. **329**(3): p. 134-141.

168. Jackson, J.B., et al., *Controlling the surface enhanced Raman effect via the nanoshell geometry.* Applied Physics Letters, 2003. **82**(2): p. 257-259.

169. Prodan, E., Lee, A., and Nordlander, P., *The effect of a dielectric core and embedding medium on the polarizability of metallic nanoshells.* Chemical Physics Letters, 2002. **360**(3-4): p. 325-332.

170. Westcott, S.L., et al., *Relative contributions to the plasmon line shape of metal nanoshells.* Physical Review B, 2002. **66**(15).

171. Bradley, J.S., et al., *Preparation and Characterization of organosols of monodispersed nanoscale palladium – particle-size effects in the binding geometry of adsorbed carbon-monoxide.* Chemistry of Materials, 1992. **4**(6): p. 1234-1239.

172. Singler, T., et al., *Solder research in the physicochemical hydrodynamics laboratory.* IEEC Research Highlights.

173. Lee, H.Y. and Duh, J.G., *Influence of Ni concentration and Ni3Sn4 nanoparticles on morphology of Sn-Ag-Ni solders by mechanical alloying.* Journal of Electronic Materials, 2006. **35**(3): p. 494-503.

174. Shen, J., Liu, Y.C., and Gao, H.X., *In situ nanoparticulate-reinforced lead-free Sn-Ag composite prepared by rapid solidification.* Journal of Materials Science-Materials in Electronics, 2007. **18**(4): p. 463-468.

175. Gancarz T., Pstrus, J., Gasior, W., and Henein, H., *Physicochemical Properties of Sn-Zn and SAC + Bi Alloys.* Journal of Electronic Materials, 2013. **42**(2): p. 288-293.

176. Ma, H. and Suhling, J.C., *A review of mechanical properties of lead-free solders for electronic packaging.* Journal of Materials Science, 2009. **44**(5): p. 1141-1158.

177. Evans, R.W., Wilshire, B., *Creep of metals and alloys*1985, New York: The Institute of Metals.

178. Long, X., et al., *Deformation behavior of Sn-3.8Ag-0.7Cu solder at intermediate strain rates: Effect of microstructure and test conditions.* Journal of Electronic Materials, 2008. **37**(2): p. 189-200.

179. Shohji, I., et al., *Tensile properties of Sn-Ag based lead-free solders and strain rate sensitivity.* Materials Science and Engineering a-Structural Materials Properties Microstructure and Processing, 2004. **366**(1): p. 50-55.

180. Lang, F.Q., et al., *The effect of strain rate and temperature on the tensile properties of Sn-3.5Ag solder.* Materials Characterization, 2005. **54**(3): p. 223-229.

181. Plumbridge, W.J., and Gagg, C.R., *Effects of strain rate and temperature on the stress-strain response of solder alloys.* Journal of Materials Science-Materials in Electronics, 1999. **10**(5-6): p. 461-468.

182. Vianco, P.T., and Rejent, J., *Compression deformation response of 95.5Sn-3.9Ag-0.6Cu solder.* presented at the UCLA Lead-Free Workshop 2002.

183. Pang, J.H.L., and Xiong, B.S.,*Mechanical properties for 95.5Sn-3.8Ag-0.7Cu lead-free solder alloy.* Ieee Transactions on Components and Packaging Technologies, 2005. **28**(4): p. 830-840.

184. Vianco, P.T., Rejent, J.A., and Martin, J.J., *The compression stress-strain behavior of Sn-Ag-Cu solder.* Jom-Journal of the Minerals Metals & Materials Society, 2003. **55**(6): p. 50-55.

185. Vianco, P.T., Rejent, J.A., and Kilgo, A.C., *Time-independent mechanical and physical properties of the ternary 95.5Sn-3.9Ag-0.6Cu solder.* Journal of Electronic Materials, 2003. **32**(3): p. 142-151.

186. *ASTM E9-89A*, 1995, West Conshohoken, PA. p. 101-103.

187. Suganuma, K., *Advances in lead-free electronics soldering.* Current Opinion in Solid State & Materials Science, 2001. **5**(1): p. 55-64.

188. Ogura, H., et al., *Carboxylate-Passivated Silver Nanoparticles and Their Application to Sintered Interconnection: A Replacement for High Temperature Lead-Rich Solders.* Journal of Electronic Materials, 2010. **39**(8): p. 1233-1240.

189. Li, D.Z., Liu, C.Q., and Conway, P.P., *Characteristics of intermetallics and micromechanical properties during thermal ageing of Sn-Ag-Cu flip-chip solder*

interconnects. Materials Science and Engineering a-Structural Materials Properties Microstructure and Processing, 2005. **391**(1-2): p. 95-103.

190. Wright, S.I. and Field, D.P., *Recent studies of local texture and its influence on failure.* Materials Science and Engineering a-Structural Materials Properties Microstructure and Processing, 1998. **257**(1): p. 165-170.

191. Zhou, W., and Zhong, L.W., *Scanning Microscopy for Nanotechnology: Techniques and Appilcations,* 2007, New York: Springer.

192. Telang, A.U., et al., *Grain-boundary character and grain growth in bulk tin and bulk lead-free solder alloys.* Journal of Electronic Materials, 2004. **33**(12): p. 1412-1423.

193. Ashayer, R., et al., *Nanoparticle synthesis and formation of composite solder for harsh environments.* Estc 2008: 2nd Electronics System-Integration Technology Conference, Vols 1 and 2, Proceedings, 2008: p. 929-933.

194. Bate, P., *The effect of deformation on grain growth in Zener pinned systems.* Acta Materialia, 2001. **49**(8): p. 1453-1461.

195. Miodownik, M., Martin, J.W., and Cerezo, A., *Mesoscale simulations of particle pinning.* Philosophical Magazine a-Physics of Condensed Matter Structure Defects and Mechanical Properties, 1999. **79**(1): p. 203-222.

196. Smith, C.S., *Grains, phases, and interfaces - An interpretation of microstructure.* Transactions of the American Institute of Mining and Metallurgical Engineers, 1948. **175**: p. 15-51.

197. Nai, S.M.L., Wei, J., and Gupta, M., *Using carbon nanotubes to enhance creep performance of lead free solder.* Materials Science and Technology, 2008. **24**(4): p. 443-448.

198. Lee, J.A. and Raynor, G.V., *The lattice spacing of binary tin-rich alloys.* Proceedings of the Physical Society of London Section B, 1954. **67**(418): p. 737-747.

199. Köhler M., Fritzsche, W., *Nanotechnology*. 2nd ed., 2007, Weinheim: Wiley-VCH.

200. Snugovsky, P., Arrowsmith, P., and Romansky, M., *Electroless Ni/immersion Au interconnects: Investigation of Black Pad in wire bonds and solder joints.* Journal of Electronic Materials, 2001. **30**(9): p. 1262-1270.

201. *Specification for Electroless Nickel/Immersion Gold (ENIG) Plating for Printed Circuit Boards*, 2002, Association Connection Electronics Industries: Northbrook.

202. Malucci, R.D., *Accelerated testing of tin-plated copper alloy contacts.* Ieee Transactions on Components and Packaging Technologies, 1999. **22**(1): p. 53-60.

203. Kim, D.G., Kim, J.W., and Jung, S.B., *Effect of aging conditions on interfacial reaction and mechanical joint strength between Sn-3.0Ag-0.5Cu solder and Ni-PUBM.* Materials Science and Engineering B-Solid State Materials for Advanced Technology, 2005. **121**(3): p. 204-210.

204. Smithells, C.J., Brandes, E.A., Brook, G.B., *Smithells Metals Reference Book*. 7th ed1992, Oxford: Butterworth-Heinemann.

205. Stephenson, G., *Mathematical Methods for Science Students*. 2nd ed1973, London: Longman.

206. Kotadia, H.R., et al., *Massive spalling of Cu-Zn and Cu-Al intermetallic compounds at the interface between solders and Cu substrate during liquid state reaction.* Journal of Applied Physics, 2012. **111**(7).

207. Anderson, I.E., and Harringa, J.L., *Suppression of void coalescence in thermal aging of tin-silver-copper-X solder joints.* Journal of Electronic Materials, 2006. **35**(1): p. 94-106.